Stony Brook University

Imaging Markers of Cognitive Deficits in RRMS using a Multimodal MR Approach

A Dissertation Presented

by

Hui Jing Yu

to

The Graduate School

in Partial Fulfillment of the

Requirements

for the Degree of

Doctor of Philosophy

in

Biomedical Engineering

Stony Brook University

December 2011

Stony Brook University

The Graduate School

Hui Jing Yu

We, the dissertation committee for the above candidate for the

Doctor of Philosophy degree, hereby recommend

acceptance of this dissertation.

Mark E. Wagshul, Ph.D. – Dissertation Advisor
Associate Professor, Department of Radiology, Stony Brook University

Terry Button, Ph.D. – Chairperson of Defense
Associate Professor, Department of Radiology, Stony Brook University

Helene Benveniste, M.D., Ph.D.
Professor, Department of Anesthesiology, Stony Brook University

Christopher Christodoulou, Ph.D.
Assistant Professor, Department of Neurology, Stony Brook University

This dissertation is accepted by the Graduate School

Lawrence Martin
Dean of the Graduate School

Abstract of the Dissertation

Imaging Markers of Cognitive Deficits in RRMS using a Multimodal MR Approach

by

Hui Jing Yu

Doctor of Philosophy

in

Biomedical Engineering

Stony Brook University

2011

Magnetic resonance imaging (MRI) has made important contributions to the understanding of the dynamics of the disease process of multiple sclerosis (MS) *in vivo* and has an established role in the diagnosis of MS. Despite this, conventional MRI is only partially helpful in understanding the disease and predicting ultimate clinical outcomes. The lack of imaging biomarkers in MS also limits the development of therapeutic interventions that can eventually help treat the various symptoms of MS, including the common finding of cognitive impairment. In this dissertation, multi-modal MR imaging acquisition and analysis techniques were applied with the goal of attaining more sensitive methods for the quantitative characterization of the MS disease processes, especially those that might reflect the underlying pathological mechanisms related to cognitive decline in relapsing-remitting multiple sclerosis. Using advanced volumetric analysis techniques, significant gray matter (GM) atrophy in both cortical and subcortical regions was found in MS brains, where selective patterns of GM atrophy correlated with cognitive decline. Through diffusion tensor imaging (DTI), white matter (WM)

integrity was examined, and the advanced DTI analysis methods employed allowed for the identification of widespread WM alterations in MS. With magnetic resonance spectroscopy (MRS), evidence of metabolic abnormalities was demonstrated in normal-appearing WM and GM in MS. Overall, this body of work advances our knowledge in relating MR metrics to underlying disease processes, and improving image-based characterization of cognitive decline over what is seen with conventional imaging. The results of this work may contribute towards developing future clinical metrics that comprehensively evaluate disease accumulation in patients, facilitating therapy development and monitoring, and thus improving quality of life for people with MS.

Dedication Page

I would like to take this opportunity and dedicate this dissertation to all the people in my life, especially to my family, that have been there every step of the way.

Table of Contents

List of Figures

List of Tables

List of Abbreviations

AD: Axial diffusivity
ADC: Apparent diffusion coefficient
BBB: blood-brain barrier
CGM: Cortical gray matter
CHESS: CHEmical-Shift Selective
Cho: Choline
CNS: Central Nervous System
Cr: Creatine
CSF: Cerebrospinal Fluid
CSI: Chemical shift imaging
CTh: Cortical Thickness
DIR: dual inversion recovery
DMT: Disease Modifying Treatment
DTI: Diffusion Tensor Imaging
DWI: Diffusion weighted imaging
EDSS: Expanded Disability Status Scale
FA: Fractional anisotropy
FLAIR: Fluid-Attenuated Inversion Recovery
Gd: Gadolinium
Glu/Gln or Glx: glutamate and glutamine
GM: Gray Matter
GPC: glycerophosphocholine
Ins or mI: myoinositol
LTHIP: Left Hippocampus
MD: Mean diffusivity
MM: Macromolecule
MRI: Magnetic Resonance Imaging
MRS: Magnetic Resonance Spectroscopy
MS: Multiple Sclerosis
MTR: magnetization transfer ratio
NAA: N-acetylaspartate
NAAG: N-acetyl aspartyle glutamate
NAGM: normal appearing gray matter
NAWM: normal appearing white matter
PCr: Phosphocreatine
PPM: parts-per-million
PRESS: Point Resolved Spectroscopy
RD: radial diffusivity
RRMS: Relapsing-Remitting Multiple Sclerosis
SNR: Signal-to-noise ratio
SPGR: SPoiled Gradient echo-Recalled
SVS: single voxel spectroscopy
T2LV: T2 Lesion Volume/Burden
TBSS: tract based spatial statistics
TE: Echo Time

TFCE: threshold free cluster enhancement
TR: Repetition Time
VOI: volume of interest
WM: White Matter

Acknowledgments

I would like to thank all the individuals who have contributed to this work and offered their guidance.

I am especially grateful to my research supervisor, *Dr. Mark Wagshul*. Throughout my pursuit of this doctorate degree, I was always able to rely on Dr. Wagshul for support, guidance, mentorship, and unfailing dedication to my professional development.

My work would not have been possible without *Dr. Lauren Krupp*, who was closely involved in every aspect of this thesis. I would like to thank her for her kind support and encouragement.

I am also grateful of all my committee members: *Dr. Terry Button, Dr. Helene Benveniste, and Dr. Christopher Christodoulou*. Thank you all for taking an interest in my research and for dedicating your time and effort towards my training.I was fortunate to work with many brilliant scientists to whom I would like to extend my gratefulness, especially *Dr. Mirjana Maletic-Savatic, Dr. Istvan Pelczer, Dr. Peter Djuric, Dr. Yao Li, and Dr. Lisa Vingara* for providing their insights in MRS and *Dr. Robert Peyster* for his review on hippocampal volumetry.

I also thank all of the faculty and staff in the Neurology and Radiology department, especially: *Ms. Dana Serafin, Dr. Yashma Patel, Dr. Vikram Bhise, Dr. Daniel Greenblatt, Dr. Sachin Jambawalikar,* and *Dr. Haifang Li*.

I would especially point that I could not have completed this experience without the advice provided by *Dr. Emilia Entcheva*, my undergraduate research advisor, and *Dr. Irene Solomon*, my Master's degree research advisor. They have helped shape my career in science.

Thank you to all the anonymous study participants for their altruism. Without these individuals this study would not have been possible.

Special thanks to the financial support provided by our funding agencies: Lourie Foundation Incorporated, the National Multiple Sclerosis Society, the National Center for Research Resources, EMD Serono, Pfizer Inc, and Biogen Idec.

Finally, I would like to express my deepest gratitude to my friends and family. You all have provided me with tremendous support throughout the ups and downs of this journey. Thank you for believing in me.

Vita, Publications and/or Fields of Study

Yu HJ, Christodoulou C, Bhise V, Greenblatt D, Patel Y, Serafin D, Maletic-Savatic M, Krupp LB, Wagshul ME. Multiple White Matter Tract Abnormalities underlie Cognitive Impairment in RRMS. *(Submitted to NeuroImage)*

Vingara LK, Li Y, **Yu HJ**, Wagshul ME, Pelczer I, Krupp LB, Maletic-Savatic M. *In Vivo* Magnetic Resonance Spectroscopy-Based Metabonomics of the Human Brain in Multiple Sclerosis. *(In preparation)*

Li Y, **Yu HJ**, Wagshul ME, Krupp LB, Maletic-Savatic M, Djuric PM. The Limits of Detection and Estimation of a Biomarker from Magnetic Resonance Spectroscopy Data. *(In preparation)*

Wagshul ME, Kelly EJ, **Yu HJ**, Garlick B, Zimmerman T, Egnor MR. Resonant and Notch Behavior in Intracranial Pressure Dynamics. *J Neurosurg Pediatr. 2009 May;3(5):354-64.*

Yu HJ, Chen X, Foglyano RM, Wilson CG, and Solomon IC. Respiratory Network Complexity in Neonatal Rat *In Vivo* and *In Vitro*. Adv. Exp. Biol. Med. 2008;605:393-8.

Dissertation Outline

The goal of this thesis was to utilize non-conventional MR acquisition techniques and apply advanced post-processing methods to improve the understanding of the underlying pathophysiology in multiple sclerosis, and its correlates to cognitive dysfunction in MS.

This dissertation comprises a series of multiple studies designed to address the overall hypothesis, that is, biomarkers extracted from multimodality neuroimaging reflect the underlying neuropathological changes responsible for cognitive impairment in individuals with relapsing remitting multiple sclerosis. It is organized into the following chapters, each of which focuses on a specific (or individual) study:

Chapters 1-3 provide a brief overview of the background information relevant to the work completed for this dissertation. Chapter 1 briefly describes multiple sclerosis. Chapter 2 provides an overview of conventional MR imaging methods and quantification techniques in MS. Chapter 3 introduces advanced MR acquisition and analysis techniques that lead to the individual studies included in this dissertation.

Chapter 4 describes the clinical and imaging data acquisition methods.

Chapter 5 describes experiments in which advanced image processing techniques such as SPM and FreeSurfer were utilized to characterize volume loss, particularly GM atrophy in MS, and its link to cognitive dysfunction.

In Chapter 6, we examined white matter tract pathology and its association with cognitive dysfunction using diffusion tensor imaging and advanced DTI analysis techniques.

In Chapter 7, we aimed to identify and quantify metabolic changes in MS using MR spectroscopy, thus providing additional insights into the underlying pathological mechanisms association with cognitive impairment.

Chapter 8 summarizes the major results in the thesis, discusses the clinical relevance of the work, and offers possible directions for future studies.

Chapter 1

Multiple Sclerosis

1.1. Overview

Multiple sclerosis (MS) is a chronic, progressive disease of the central nervous system (CNS), characterized by inflammation, demyelination, and axonal loss. It affects an estimated 500,000 people in the United States with women twice as susceptible as men (*1*). It is the leading cause of neurological disability that strikes predominately in young adults with onset usually occurring between the ages of 20 and 40 (*1*), thus creating a major health care burden. Although the disease was described as early as 1868 through pathological studies by Charcot (*2*), it wasn't until the introduction of magnetic resonance imaging (MRI) in the early 1980s that understanding of the nature of disease was improved. Yet to date, the exact mechanisms underlying disease initiation and progression remain unclear.

1.2. Pathogenesis of Multiple Sclerosis

Nerve cells communicate by sending signals down nerve fibers called axons (Figure 1). Nerve fibers are coated by fatty substance or myelin that permits the fast and effective transmission of electrical signals between the brain, the spinal cord, and the rest of the body. In multiple sclerosis, destruction occurs in the myelin sheath that covers nerve fibers, which is followed by the formation of scar tissue (or sclerotic plaques) at the demyelinated sites. Sclerotic plaques disrupt the ability of nerves to conduct electrical impulses to and from the brain, leading to the various symptoms of MS. These plaques are characterized by a very well

defined edge and their size can vary from 1.0 mm to several centimeters in diameter. Although the sclerotic plaques are randomly distributed throughout the CNS, they seem to have a preference for the periventricular areas, optic nerve, brain stem, cerebellum and spinal cord (*3*). The majority of MS plaques are generally found in the white matter (WM).

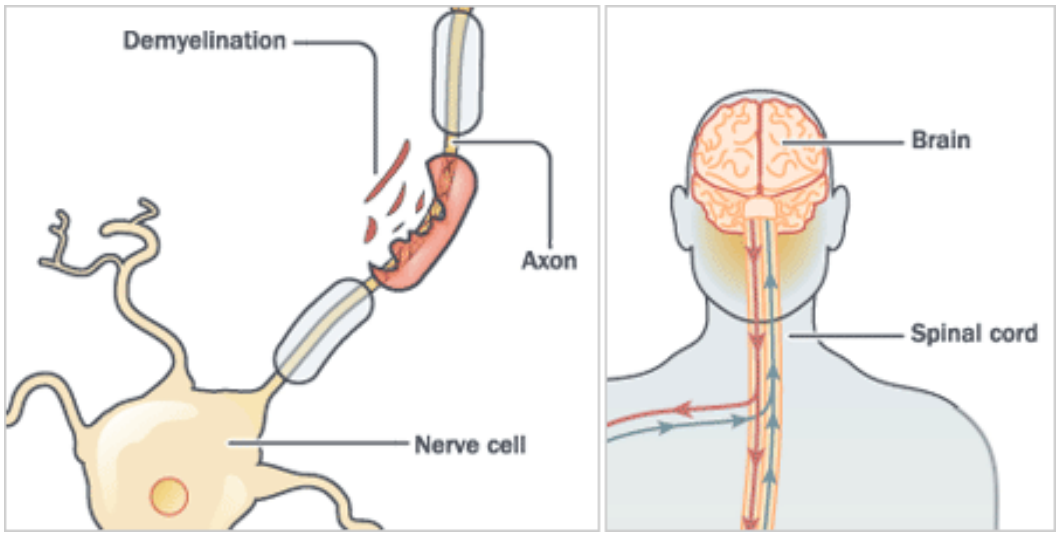

Figure 1. Schematic showing damaged myelin in multiple sclerosis. In multiple sclerosis, destruction occurs in the myelin sheath that covers nerve fibers, disrupting the ability of nerves to conduct electrical impulses to and from the brain. Image source: http://images.agoramedia.com/everydayhealth/gcms/conditionguide_10_key_questions_about_multiple_sclerosis_01.gif

However, observations in histopathological studies suggest that MS pathology is much more complicated than the white matter plaque centered theory (*4, 5*). These investigations showed that the CNS of MS patients is affected not only by WM plaques, but also by changes in the gray matter (GM). Demyelination can be found in the cortical GM as well as deep GM areas such as thalamus, basal ganglia, hypothalamus, hippocampus, and cerebellum (*4*). Furthermore, GM is involved early and significantly in MS (*6*). The GM pathology seems to differ from WM pathology in that inflammation is sparse within abnormal GM, with less macrophage and lymphocyte infiltration. The pathogenic processes leading to GM damage could either be arising

within GM regions or resulting from continuing damage in the cerebral WM. It is important to be able to detect any subtle tissue changes that may precede clinical manifestation of the disease. Indeed, evidence is accumulating to suggest that GM pathology is as important in determining long-term clinical outcomes as WM damage in MS (*7*). The role of GM pathology in the association with the heterogeneity in the phenotypic expression of MS still needs to be elucidated.

1.3. Disease Course and Classifications

There are four generally accepted MS subtypes: relapsing-remitting, secondary-progressive, primary-progressive, and progressive-relapsing (Figure 2). Clinically, MS begins most commonly with episodic neurological deficits or relapses separated by periods of remission. About 85% of patients experience this relapsing-remitting course of MS (RRMS) (*1*), which is characterized by defined acute attacks, lasting from days to weeks. After a relapse, the person may experience full recovery, partial recovery or residual deficits. In RRMS, the illness does not progress between relapses or during remissions. Within 10 to 15 years, 50% of RRMS patients begin to experience gradual worsening and transition into the secondary-progressive form of MS (SPMS) (*1*). Approximately 10-15% of MS patients have a primary-progressive disease course (PPMS), which is characterized by a gradually progressive clinical course directly from onset (*1*). The least common of all subtypes is progressive-relapsing, where MS patients have a steady neurologic decline from onset, superimposed with attacks.

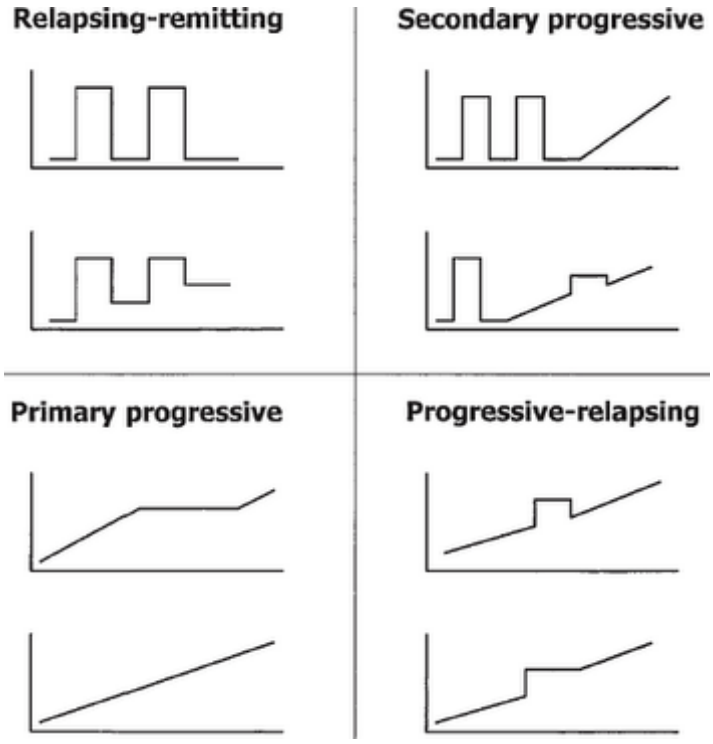

Figure 2. Four classifications of multiple sclerosis. The progressive types of MS include relapsing-remitting (unpredictable attacks which may or may not leave permanent deficits, followed by periods of remission), primary-progressive (steady increase in disability without attacks), secondary-progressive (initial relapsing-remitting multiple sclerosis that suddenly declines without periods of remission), and progressive-relapsing (steady decline since onset with superimposed attacks). For each plot, the x-axis indicates increasing time, and y-axis increasing disability. Image source: Semin Neurol @ 2003 Thieme Medical Publishers (www.medscape.com)

1.4. Diagnosis and Treatment

The diagnosis of MS has included a combination of both clinical and paraclinical studies, such as imaging and CSF analysis, since no single clinical feature or diagnostic test is sufficient for diagnosis. The Poser´s criteria (*8*), introduced in 1983 and used until 2001, require at least two attacks of neurological symptoms and clinical evidence of two separate lesion sites (*i.e.,* MRI-visible MS lesions at separate sites in the CNS), or two attacks and clinical evidence of one lesion with paraclinical evidence of another (*i.e.,* two lesions each supported by MRI and CSF

findings). The new diagnostic criteria of McDonald were introduced in 2001 (*9*), and were revised in 2005 to simplify and speed the diagnosis, while maintaining adequate sensitivity and specificity (*10*). Table 1 provides a summary of the revised McDonald diagnostic criteria for MS. The core concept in MS diagnosis is to determine dissemination of MS lesions in time (*i.e.*, time of appearance) and space (*i.e.*, location in brain and/or spinal cord), with the role of MRI emphasized.

MRI **Dissemination in time**	1) Detection of Gd enhancement at least 3 months after the onset of initial clinical symptoms, if not at the site corresponding to the initial event or 2) detection of new T 2 lesion if it appears at any time compared with reference scan done at least 30 days after the onset of clinical event
MRI **Dissemination in space**	**Three of the following:** 1) At least one Gd+ lesion or nine T2 hyperintense lesions if there is no Gd+ lesion 2) At least one infratentorial lesion 3) At least one juxtacortical lesion 4) At least three periventricular lesions A spinal cord lesion can be considered equivalent to a brain infratenorial lesion.
Clinical Presentation: – Two or more attacks, objective clinical evidence of two of more lesions – Two or more attacks, objective clinical evidence of one lesion – One attack, objective clinical evidence of two or more lesions – One attack, objective clinical evidence of one lesion (CIS)	**Additional data needed for MS diagnosis:** None Dissemination in space in – MRI or – Two or more MRI-detected lesions consistent with MS and positive CSF (oligoclonal bands or increased IqG index) or – New clinical attack implicating a different site Dissemination in time demonstrated by – MRI or – Second clinical attack Dissemination in time demonstrated by – MRI or – Second clinical attack and Dissemination in space demonstrated by – MRI or – Two or more MRI-detected lesions consistent with MS and positive CSF
Insidious neurological progression suggestive of MS	One year disease progression (retrospectively or prospectively determined) and Two of the following: – Positive brain MRI (nine T2 lesions or four or more T2 lesions with positive VEP) – Positive spinal cord MRI (two focal T2 lesions) – Positive CSF

Table 1. Revised McDonald diagnostic criteria for multiple sclerosis

The disease results in a wide range of symptoms including fatigue, motor and sensory disturbances, pain, cognitive impairment, mood disturbance, bladder, bowel and sexual dysfunction (*11*). The Kurtzke's Expanded Disability Status Scale (EDSS) is the most widely used clinical evaluation in MS (*12*). It measures disability in pyramidal, cerebellar, brainstem, sensory, bower/bladder, visual, cerebral, and other functional systems. This method compiles disability in eight functional systems into a single numerical value ranging from 0 to 10 with increments of 0.5. A score of 0 indicates a normal neurological exam, and a score of 10 is defined as death due to MS. Some weaknesses with the EDSS include that it is not linear, some of the subtests require self-reporting that might be subjective, and it is focused on ambulation but is insensitive to cognitive problems.

Although there is no known cure for multiple sclerosis, several therapies have proven helpful. To date, FDA-approved disease modifying treatments (DMTs) available for MS include interferon-beta (Avonex, Betaseron, Extavia, and Rebif), glatiramer acetate (Copaxone), mitoxantrone (Novantrone), natalizumab (Tysabri), and fingolimod (Gilenya). The primary aims of therapy are returning function after an attack, preventing new attacks, and preventing disability. Beginning treatment early has been shown to reduce relapses and slow disease progression both clinically (*i.e.*, disability) and radiologically (*i.e.*, presence of MS lesions) (*13*). However, the accumulation of irreversible tissue damage limits the potential for benefit from DMT as the disease progresses and becomes a degenerative process. Thus, it is important to find imaging biomarkers with a relationship to cognitive decline which can be used to predict impending disease activity prior the onset of symptoms and pathology.

1.5. Cognitive Function in Multiple Sclerosis

Tissue pathology in MS can result in motor, cognitive, and neuropsychiatric symptoms. While demyelination in WM has been used to explain physical disability (usually measured by EDSS) (*14*), specific cognitive deficits might be better explained by gray matter pathology. Impaired cognitive function presents in 40-60% of MS patients (*15*) which can occur with relatively mild physical disability, and may be detectable even before a definitive diagnosis of MS is made (*16*).

Various aspects of cognitive dysfunction are observed in MS, including memory impairment, attention deficits, worsened performance in information processing and executive function (*15*). Memory disturbances are one of the most frequent cognitive impairments in MS and are seen in 40-60% of patients. Earlier work on memory impairment indicated that these may be caused by disturbances in information retrieval from long-term storage. Recent studies suggest that memory deficits might be due to impaired encoding and information storing processes. In other words, the initial learning difficulties are responsible for the differences in the test performance rather than the recalling of information. Information processing is another impaired cognitive domain in MS. Information processing efficiency refers to the ability to maintain and manipulate information in the brain for a short period of time (*i.e.*, working memory), and to the speed with which one can process that information (*i.e.*, processing speed). Slowing of processing in MS patients can present as only motor processing slowness, or mental processing slowness, or both combined. It is also likely that impairments in information processing affect performance on tasks of attention (focused, divided and sustained) and executive functions because those tasks often involve multiple processing steps and the integration of information. Lastly, visual perceptual abilities are also impaired in MS, mainly

from optic neuritis (inflammation and demyelination of the optic nerve) which is common for MS patients. Although relatively little has been investigated in visual perceptual processing, visual problems are likely to contribute to difficulties on other cognitive tasks that have visual demands.

To evaluate the cognitive status of MS patients, the Rao's Brief Repeatable Battery (BRB) of neuropsychological tests are often administered (*17*). The BRB includes five subtests: the Selective Reminding Test (SRT), Selective Reminding Test (SRT), a measure of verbal learning and delayed recall of a 12 paired word list; the Spatial Recall Test which measures visual-spatial learning & delayed recall; the Symbol Digit Modalities Test (SDMT), which is a measure of sustained attention, working memory, and information processing speed; and the Word List Generation (WLG), a verbal fluency test; and the Paced Auditory Serial Addition Test (PASAT), a test of sustained attention, working memory and information processing speed. The PASAT is also one of three components of the Multiple Sclerosis Functional Composite (MSFC) (*18*), which has been used as an outcome measure in clinical trials in MS.

Cognitive dysfunction encompasses all phases of the disease and all types of disease course, and the prevalence and the cognitive profile may vary in people with MS (*19*). In general, deficits are most severe in people with SPMS, followed by PPMS, and then RRMS (*20*). Males with MS have proved to perform more poorly than females with MS in several tests (*21*). Lower education level as well as limitations in person's work and social activities is correlated with the extent of cognitive decline (*22*). Some studies also show an association between cognitive impairment and poor health-related quality of life (*23*). Cognitive deficits may also be related to other secondary factors such as depression and fatigue (*24, 25*). Relatively little is known about the evolution of cognitive dysfunction in MS (*26, 27*). However, a 10 year follow-

up study suggests that (*26*) once cognitive dysfunction occurs it may sometimes remain stable but is more often progressive. The detection of cognitive impairment usually occurs through neuropsychological (NP) testing. However, NP tests are generally complicated and most often require a trained specialist to administer. Moreover, while there are pharmacological disease-modifying-treatments for MS, there is no specific symptomatic treatment for symptoms such as cognitive impairment. Furthermore, whether the approved disease modifying treatments for MS can prevent or slow cognitive decline is yet to be understood. Therefore, improving the understanding of the pathophysiology of cognitive impairment in MS and the mechanisms responsible for its evolution might contribute to the development of better outcome measures for therapeutic strategies.

Chapter 2

The Role of Conventional MRI in Multiple Sclerosis

Magnetic resonance (MR) techniques have had a major impact in the last decades in understanding and managing multiple sclerosis. Conventional MR imaging, including T1 (with and without contrast agents) and T2-weighted sequences, offer the most sensitive way to detect MS lesions and their changes, and play a dominant role in confirming or ruling out MS. Despite this, conventional MRI is only partially helpful in distinguishing the heterogeneous features of MS pathology. The development of modern, quantitative MR techniques, such as diffusion tensor imaging (DTI) and magnetic resonance spectroscopy (MRS) have shown great potential to improve our ability to diagnose and monitor the disease. A brief description of each of these methods will be given in this chapter. Further information on each topic can be found in resources such as Magnetic Resonance Imaging (*28*).

2.1. Overview of MR Physics

Magnetic resonance imaging (MRI) is an imaging technique used in medical settings to produce high quality images of the inside of the human body. The principles of MRI rely on the spinning motion of specific nuclei known as MR active nuclei. However, the majority of clinical MRI focuses on imaging hydrogen nuclei (^{1}H) which are abundant in the human body and have a relatively large magnetic moment, resulting in a detectable signal. In the absence of an external magnetic field, the magnetic moments of the hydrogen nuclei in the body are randomly oriented, and the net macroscopic magnetic moment is zero. In the presence of an external magnetic field

(*i.e.*, a patient placed in a MR scanner), water becomes polarized such that hydrogen nuclei are oriented in the direction of the applied magnetic field. The protons or spins exhibit resonance at the so-called Larmor frequency, which is proportional to the strength of the main magnetic field. To obtain a MR signal, a radiofrequency or RF pulse is applied. Protons absorb energy from RF excitation that brings them out of equilibrium. When the RF pulse is turned off, the system of protons relaxes back to its equilibrium while dissipating the absorbed energy to their surroundings.

The spins return to their equilibrium usually by two spin relaxation mechanisms known as T1 or longitudinal relaxation and T2 or transverse relaxation. T1 relaxation is caused by the protons giving up their energy to the surrounding environment. The T1 relaxation time describes the time constant for restoring the net magnetization to 63% of its original strength in the direction parallel to the applied field (*i.e.*, longitudinal magnetization). T2 relaxation is caused by protons exchanging energy with their neighbors, resulting in the loss of magnetization perpendicular to the external field (*i.e.*, transverse magnetization). The T2 relaxation time represents the time it takes for the transverse magnetization to decay to 63% of its original strength. Since the physical properties of the tissue affect the T1 and T2 relaxation times, tissue contrast can be generated. Within the MRI pulse sequence, the echo time (TE, the period between the start of the RF pulse and the echo) and the repetition time (TR, the period between two RF pulses) are used to determine how the resulting image is weighted. A short TE and a short TR will give a T1-weighted image, whereas a long TE and a long TR will give a T2-weighted image.

2.2. Conventional MRI in MS

T1-weighted, gadolinium-enhanced T1-weighted, and T2-weighted (particularly T2-weighted fluid attenuated inversion recovery or T2-FLAIR for its excellent delineation of MS lesions as distinct from the nearby cerebrospinal fluid) MR images are the conventional MR modalities frequently used for MS evaluation and outcome measures.

2.2.1. Lesion-Based Assessment

2.2.1.1. T2 Lesions

T2-weighted MRI is a conventional imaging modality in which the contrast is due to differences in the T2 relaxation time. The highest intensities correspond to tissues with relatively long T2 relaxation times (*e.g.*, CSF), and the lowest intensities correspond to relatively short T2 relaxation times (*e.g.*, normal WM). MS plaques often appear as bright areas on conventional T2-weighted fluid-attenuated inversion recovery (FLAIR) brain images and are often referred to as T2 lesions. A lesion (or plaque) containing more free water will have longer T2, thus will appear brighter on a T2-weighted image. FLAIR is a T2-weighted sequence that uses an inversion pulse to null the signal from CSF for discriminating similarly bright hyperintense lesions commonly found in periventricular white matter. Such lesions can also be found in the inner surface of the corpus callosum, the juxtacortical gray-white junction, the infratentorial brain regions, and the spinal cord. Most T2 lesions are discrete on conventional MRI, but some with poorly defined borders, so called dirty appearing white matter, are also seen around the ventricles. T2-weighted hyperintensities reflect overall increase in water content, which can accompany edema, demyelination, remyelination, reactive gliosis and axonal loss (*29-33*). All of these histopathological changes are known to occur in MS lesions, but are not uniformly represented across patient populations and thus contribute to disease heterogeneity

(*34*). Overall, T2-weighted MRI is sensitive to white matter abnormalities and is therefore useful for diagnosis, but can be nonspecific for the underlying pathology.

2.2.1.2. T1 Lesions

While T2-weighted MRI gives limited explanation about the pathophysiological heterogeneity of MS lesions, T1-weighted images extend the understanding of tissue destruction in MS. In T1-weighted images, tissues with relatively short T1 relaxation times (*e.g.* WM) have higher intensities than tissues with relatively longer relaxation times (*e.g.* CSF). T1-weighted images reveal hypointense abnormalities, also known as "black holes" that may correspond to all or only a portion of the T2 hyperintense plaque. About half of the T1 hypointense lesions disappear during the natural disease course, and these are called transient lesions usually lasting 6 to 12 months. However, some of the T1 hypointense lesions persist indefinitely, and are known as chronic black holes. Unlike T2 lesions, T1 lesions reflect underlying pathology. Those that show profound hypointensity (increased T1) are attributed to demyelination and loss of glial and neuronal cells, whereas transient ones (gradual T1 recovery with time) reflect edema and partial remyelination.

2.2.1.3. Gadolinium Enhanced Lesions

T1-weighted techniques are often used with paramagnetic contrast agents, typically gadolinium (Gd). Gadolinium ions are toxic, so ions are encapsulated, and because of their size, these complexes cannot pass through the cell layers that comprise the blood-brain barrier (BBB). However, when the BBB is compromised, the contrast agent can leak from the blood into the brain. MS lesion formation is thought to occur by infiltration and activation of various T-lymphocytes and microglia (*35*), which recognize myelin as a foreign element and attacks it; this

autoimmune response damages the BBB. Gd-enhanced MRI reveals leakage through the BBB, which probably reflects the earliest stage of MS lesion development. These contrast agents markedly shorten the T1 of neighboring water protons. As a result, after intravenous bolus administration, they locally increase the signal from brain tissue where there is normally no BBB, or where the barrier is significantly compromised. Lesions that appear hyperintense on T1 contrast-enhanced images are called "enhancing lesions". The enhancing lesions, which may vary in shape and size, usually start with homogeneous enhancement and subsequently progress to ring-like enhancement. This likely reflects edema and partial remyelination of affected tissue in the center of the lesion.

2.2.1.4. Lesion Findings and Limitations

T2 hyperintense lesion number/volume is one of the most commonly used MRI measures for disease severity and clinical trial efficacy. In general, the distribution and extent of T2 hyperintense lesions correlate well with histopathological abnormalities in the CNS of patients with MS (*29, 36*). However, T2 lesion load (either total T2 lesion volume or normalized to brain volume) can show no or only modest correlation with clinical disability as measured by EDSS (*37*). While it might be a limitation of EDSS as an appropriate functional measure of disability (i.e., insensitive to cognitive deficits), one reason for this weak correlation could be due to the inability of T2-weighted images to detect diffuse pathology in the normal appearing white matter (NAWM) regions. In addition, a major limiting factor in using lesion load as a longitudinal surrogate measure is its plateauing relationship with clinical disability (*38*), which suggests that MR metrics other than T2 lesion loads should be considered when assessing the more advanced phases of the disease.

Measurement of T1 hypointense lesion load correlates better with physical disability than measurement of T2 lesion burden (*37*). Evidence from histopathology shows that T1 hypointensity predicts axonal loss, and that a lesion with less axonal loss and demyelination shows a tendency to become isointense (*39*). However, the study of T1 hypointense lesions may only benefit a limited number of patients since it is not a common feature in MS patients. T1 hypointense lesions are also rarely seen in the spinal cord where axonal loss is commonly found (*40-42*). For T1-weighted Gd-enhancing lesions, although the presence of gadolinium enhancement has been shown to predict the onset and severity of clinical relapses, Gd-enhancing lesions may not correlate with clinical disability at baseline (*30, 37, 43*). While T1 lesions provided additional information to that obtained from T2 lesions, it still lacks specificity about the underlying disease processes and diffuse changes which occur in the MS disease. Moreover, the identification of T1 hypointensity is arbitrary, and highly dependent on image contrast and the technique used. Until a standardized definition for the measurement of T1 hypointensities is established, the use of the T1 hypointense lesion as a surrogate imaging biomarker for MS disability will be limited.

In summary, conventional MRI based lesion measures have contributed to the understanding of MS pathophysiology, but they have limited sensitivity and specificity for the underlying tissue damage. There are different and possibly concurrent processes inside lesions, such as demyelination and remyelination that cannot be recognized on conventional MRI. In addition, evidence suggests that there are changes in the normal appearing tissue which precedes the appearance of visible T1 and T2 MS lesions (*31*). While both T2 and Gd-enhancing lesions are still mainly used in the diagnostic criteria of MS, the presence of lesion heterogeneity, as shown in our data (Figure 3), suggest that pathologic heterogeneity might have implications for

disease diagnosis and therapy development. It is likely that future improvements in diagnostic criteria will include more MRI markers of disease as imaging technology develops and the disease processes and markers are better understood.

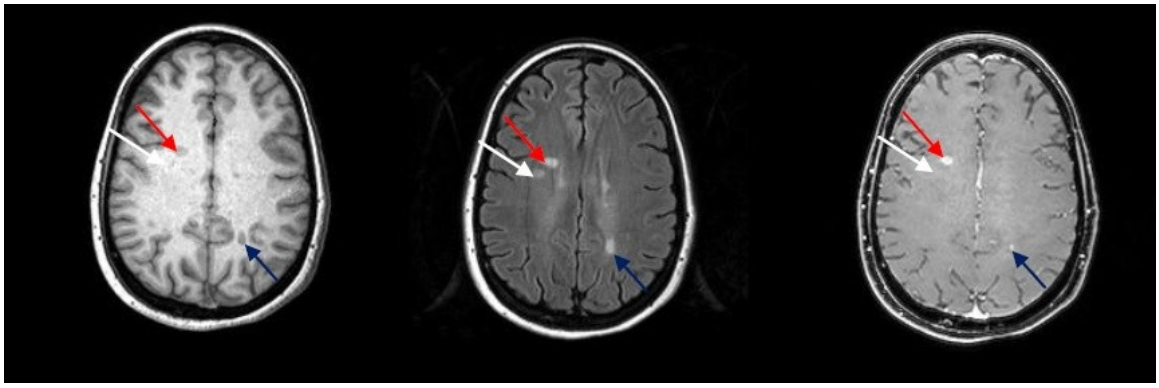

Figure 3. Example images showing the heterogeneity of the MRI-appearance of lesions. Axial images were obtained from a RRMS patient with SPGR (left), FLAIR (middle), and T1-weighted post-contrast (right), demonstrating heterogeneity of MRI appearance of MS lesions. T2 lesions are hyperintense on FLAIR (indicated by all arrows), but may be hypointense (indicated by red and blue arrows, known as black holes) or isointense on the T1 SPGR image. Some MS lesions are enhanced by gadolinium (indicated by red and blue arrows) due to the compromise of the blood-brain barrier. There are also marked differences in the appearance of lesion size based on technique.

2.2.2. Atrophy in MS

In addition to MS lesions, another imaging hallmark of MS is brain atrophy or irreversible tissue loss. The exact mechanism leading to atrophy in MS is unclear, but it could be the result of all types of pathologic processes in MS (*44*). Overall, there is global and regional atrophy present in MS. Global atrophy can be defined as a measure of global brain volume loss, or global loss of a particular tissue class (*e.g.*, WM or GM). Regional atrophy measures tissue loss at the structural or voxel level. With the advancement of structural image analysis

techniques, the study of regional atrophy is of great interest since different brain regions may be affected differently in MS, thus reflecting different clinical disabilities.

In general, longitudinal studies showed that MS patients typically have brain volume loss at rates around 0.5% to 1% per year where annual age-related atrophy rates in age-matched healthy subjects is about 0.1% to 0.3% per year (*45-47*). Brain atrophy appears to proceed throughout the course of MS, even at the earliest stages (*48*), and atrophy rate seems to be independent of subtype (*49*). Atrophy correlates weakly-to-moderately with lesion burden, and can progress irrespective of lesion load. This suggests that there might be other mechanistic changes, which are independent of lesion pathogenesis.

Although MS is a demyelinating disease and brain atrophy would likely reflect tissue loss mostly from myelin and axonal damage in WM, GM pathology is also present and demonstrated in atrophy measures. Several studies have shown that GM atrophy begins early in the MS course (*50-53*), and it may evolve progressively (*54, 55*). However, GM atrophy is not necessarily dependent on WM changes, and the extent of GM atrophy can be greater than that of WM atrophy (*56*). In fact, atrophy in cortical and deep GM regions can be involved earlier and more strongly in the pathological process than in other brain regions (*57-62*). Interestingly, decreases in WM volumes are rarely reported in cross-sectional or longitudinal studies compared with decreases in GM volumes (*51, 53, 63*).

The clinical correlation between atrophy and clinical disability has been found to be stronger than the correlation between lesion load and clinical disability (*64-69*). Atrophy was shown to be a relevant marker for disease progression and may even precede the development of measurable disability (*70*). The quantitative measure of atrophy has also been included as an

index of efficacy in clinical trials (*71-74*). However, brain atrophy estimation still remains an issue in terms of the ability for the various automatic algorithms to measure small disease-related changes (*75-77*). Therefore, we should also take advantage of the continuing effort to develop image acquisition and image analysis techniques for better quantitative characterization of regional volume changes in MS.

2.2.3. Conventional MRI and Cognitive Impairment in MS

Conventional MRI has been applied to identify the extent and the severity of pathological processes underlying cognitive dysfunction. A number of studies have focused on the relationship between cognitive parameters and the extent of damage detected with conventional MRI to help further pinpoint the causal mechanisms.

The notion that white matter damage has an effect on neural functioning is supported by studies investigating the correlations between T2 lesion burden and cognition (*78, 79*). The location of MS lesions can have a regional effect on cognitive function (*78, 80*). For example, frontal lobe lesions are associated with impaired executive function, and lesions of the corpus callosum cause information processing speed deficits (*81*). Several studies have also investigated the correlations between atrophy and MS-related neuropsychological dysfunctions. Significantly smaller brain volumes have been observed in MS subjects with cognitive impairments according to neuropsychological tests of verbal memory, verbal fluency, and attention as compared to the unimpaired patients (*73, 82-84*). In longitudinal studies, subjects who worsened on neuropsychological tests had greater brain atrophy than those with stable or improved cognition (*84*). Overall, brain atrophy accounts for more variance than lesion burden in predicting cognitive impairment in MS (*68, 69, 85*). Both lesion load and brain atrophy have

greater degrees of correlations with cognitive function than with physical disability measured by EDSS (*68, 69, 86*).

The associations between specific cognitive functions and regional atrophy are worth exploring in MS as suggested by evidence from a study where GM volumes were found to be correlated with cognitive function but not motor disability (*87*). Indeed, regional GM atrophy in areas such as the cortex, neocortex, thalamus, and hippocampus, has been found to correlate with cognitive measures in MS patients (*88-92*). Some more specific cognitive deficits, such as memory impairment, might be better explained by pathological processes (*i.e.*, demyelination and possible resultant damage to the neurons) within GM structures. It remains to be determined exactly how cognitive dysfunction evolves from disease onset, and how it relates to GM and WM pathology on a global and regional basis. Since pathology in MS is diffuse and diverse, the use of a multi-modal MR approach would likely increase the amount of information derived that can be used to predict and examine cognitive functions.

2.3. Summary

Numerous pathological processes contribute to onset and progression of multiple sclerosis. Although conventional MRI (T1- and T2-weighted images) provides a direct measure of the extent of macroscopic pathology in MS, such as lesion plaques and atrophy, it suffers with poor pathological specificity and sensitivity. It has become increasingly evident that MS is a disease that affects the brain globally, and the disease processes do not occur only within lesion plaques, but also in white matter and gray matter distant to the lesions that appear macroscopically normal on conventional MRI. Pathological changes outside of lesions visible on conventional MRI may also contribute to the weak correlations between clinical MRI techniques and neurological symptoms. Advanced MRI techniques have the ability to detect

changes in the normal appearing brain tissues, and have the ability to improve the characterization of MS pathology *in vivo*, thus improving MRI-clinical associations. These advanced MRI techniques will be discussed in Chapter 3.

Chapter 3

Role of Advanced MRI in Multiple Sclerosis

While conventional MRI techniques have proven to be useful in monitoring multiple sclerosis activity and evolution, the development and clinical application of non-conventional MR techniques such as diffusion tensor imaging, magnetic resonance spectroscopy, magnetization transfer imaging, functional MRI, and myelin water imaging has the potential to further increase the importance of MR in the evaluation of MS by improving sensitivity and increasing the pathological specificity of the abnormalities detected. These measures are particularly useful in revealing subtle changes in normal appearing white and gray matter and therefore may help resolve the dissociation between clinical and conventional T2-weighted and T1-weighted MRI findings.

3.1. Diffusion Tensor Imaging

Axonal injury is the major component of the pathophysiology of MS; therefore any technique that sensitively captures axonal fiber architecture would be useful in understanding the disease. MR diffusion imaging is of growing interest as a tool to detect and quantify MS-related tissue damage, as well as to detect remote damage not apparent on conventional MRI (*93-95*).

3.1.1. Basic Principles of DTI

Diffusion imaging is based on Brownian movement or the random motion of molecules in a fluid system. In water, individual molecules are in constant random motion in all directions,

resulting in isotropic diffusion. However, in brain tissue, diffusion is restricted in direction by structural components such as cell membranes and axonal cytoskeletons, resulting in anisotropic diffusion (*96*). Diffusion imaging allows quantitative measurement of this molecular motion of water, and thus detects alterations in mobility of water due to changes in the directional restriction of tissue structures. With disease, this directional restriction can be altered due to pathological processes such as demyelination (*97*).

Diffusion contrast in MR is achieved by applying a set of high amplitude magnetic gradients or diffusion gradients, which can dephase and rephase spins in the magnetic field. For stationary protons, there is no net change in phase because spins dephased by the first gradient pulse are completely rephased by a second gradient pulse of equal area but with opposite polarity. In contrast, if diffusion occurs, the "diffusing" spins will not be completely rephased by the second gradient pulse, resulting in a decrease in signal. The degree of signal loss then provides information on the amount of diffusion occurring in the corresponding tissues. In basic diffusion weighted imaging (DWI), the amount of water diffusion in tissue is usually quantified by the apparent diffusion coefficient or ADC. The measured diffusion described by ADC is a measure of magnitude and provides no indication of diffusion direction.

However, diffusion can occur in any direction in the three-dimensional space, so that for any given measurement, the degree of diffusion weighting will be highly dependent to the relationship between the direction of the applied diffusion gradients and the preferred direction of the diffusion. This is important when diffusion is anisotropic in tissues such as white matter tracts, where molecular movement is not the same in all directions due to the structural barrier within the fiber tracts. Diffusion along different axes can be fitted using a 3D ellipsoid and the

full characteristics of diffusion can be described by the use of a tensor. The diffusion tensor D is a 3x3 symmetric matrix:

$$\overline{\boldsymbol{D}} = \begin{vmatrix} \boldsymbol{D_{xx}} \boldsymbol{D_{xy}} \boldsymbol{D_{xz}} \\ \boldsymbol{D_{yx}} \boldsymbol{D_{yy}} \boldsymbol{D_{yz}} \\ \boldsymbol{D_{zx}} \boldsymbol{D_{zy}} \boldsymbol{D_{zz}} \end{vmatrix}$$

where each element of the matrix is associated with a pair of diffusion axes annotated by its subscript. Since Dxy = Dyx, Dxz = Dzx, and Dyz = Dzy, leaving six independent elements required to solve this tensor, thus in DTI, at least 6 diffusion gradients along non-collinear and no-coplanar (or independent) directions are applied to the volume of interest. Each tensor can then be diagonalized through matrix multiplication to obtain the properties of this diffusion ellipsoid, namely, eigenvectors and eigenvalues (λ_1, λ_2, λ_3), which define the direction and magnitude of diffusion, respectively. In completely isotropic diffusion, all eigenvalues are equal (*i.e.*, $\lambda_1=\lambda_2=\lambda_3$). If diffusion is highly anisotropic, the eigenvalue corresponding to the primary diffusion direction will be much greater than the eigenvalues corresponding to other directions (*i.e.*, $\lambda_1>>\lambda_2\geq\lambda_3$). From a DTI tensor, it is possible to derive scalar metrics that help to describe diffusion; the most commonly used are mean diffusivity (MD) and fractional anisotropy (FA). MD is a measure of the amount of water diffusion in tissue, which is affected by cell size and integrity, and is also closely related to ADC. It can be calculated as:

$$\overline{\lambda} = \frac{\lambda_1 + \lambda_2 + \lambda_3}{3}$$

FA is a measure of the anisotropy of diffusion ($0 < FA < 1$), which indicates the structural integrity and degree of structural alignment within fiber tracts, and is calculated as:

$$FA = \sqrt{\frac{3}{2}\frac{(\lambda_1 - \overline{\lambda})^2 + (\lambda_2 - \overline{\lambda})^2 + (\lambda_3 - \overline{\lambda})^2}{\lambda_1^2 + \lambda_2^2 + \lambda_3^2}}$$

In addition to MD and FA, other measures can be also derived from diffusion data including axial diffusivity, radial diffusivity, relative anisotropy, volume ratio, etc., and the details on how to derive these measures can be found in resources elsewhere (*98-100*).

3.1.2. DTI in MS

Diffusion imaging provides additional insights into the underlying pathology in MS patients as compared to conventional MRI. Overall, MS patients exhibit increased diffusion and decreased anisotropy in MS lesions when compared with control white matter or remote normal appearing tissue. These might be the result of damage or removal of highly aligned cellular structures or replacement of axonal fibers with amorphous cells. Differentiation of lesion types is also possible through MS-DTI studies. Mean diffusivity was found to be the largest in T1 hypointense lesions amongst conventional MRI visible WM lesions (*101*). Mean diffusivity is also greater in T1 non-enhancing lesions than in enhancing lesions (*102*). Similarly, FA is lowest in enhancing lesions amongst lesions (*103*).

Aside from lesions, an overall increase in diffusivity and decrease in anisotropy have also been observed in normal appearing white matter in MS patients when compared to white matter in healthy controls (*104*), although the degree of differences is not as great as in lesions. Furthermore, in longitudinal studies, alterations in tissue integrity were detected with DTI (*105, 106*), even before the formation of MR visible MS lesions. Changes in diffusion, however, are not exclusive to MS lesions and NAWM; increased diffusion and decreased anisotropy are also found in normal appearing gray matter (NAGM) as compared to control gray matter (*107-110*),

once again suggesting GM involvement in MS pathogenesis. Altogether, this evidence demonstrates DTI as a valuable technique enabling assessment of tissue abnormalities that are not apparent using conventional MRI, providing increased specificity and sensitivity to MS pathology.

Since conventional lesion and atrophy quantification may underestimate the degree of tissue connectivity and the cumulative effects of tissue damage in functional tracts (*94, 101, 111*), DTI can provide some improvement in the correlation and specificity with clinical severity as compared to conventional MRI studies. Recent studies have investigated the role of DTI-derived measures in explaining the DTI correlates of physical disability, fatigue, depression, and cognitive impairment (*112-115*). Findings from these studies showed improved correlation with DTI derived metrics and clinical measure than those derived from conventional MR , suggesting the potential of DTI as a predictive indicator of clinical outcome and as a tool for evaluating treatment efficacy (*116, 117*). DTI methods are likely to provide increased specificity linking a domain of impairment to white matter tract(s), thus giving a more comprehensive picture of the underlying mechanisms of pathology. Lastly, the integration of DTI with conventional MRI and/or other advanced MR techniques (*118, 119*), holds great potential that will enable the explanation of a large part of the variance of clinical symptoms.

3.2. Proton MR Spectroscopy

3.2.1. Basic Principles of MRS

MR spectroscopy is a method to obtain metabolic information from tissues in vivo. Since biochemical changes precede anatomical changes, MRS can help detect tissue pathologic changes even before the appearance of lesions. Proton MRS (^{1}H-MRS) is most commonly used

for neurological studies, providing access to a large number of biomolecules or metabolites. The metabolic information is based on differences in resonance frequency of nuclei (shift in frequency) depending on their chemical environment, a phenomenon known as chemical shift. MRS signals (free induction decays) are acquired in the time domain; although data processing can be done in the time domain, signals are usually converted to the frequency domain via Fourier transform and analyzed in the frequency domain. Chemical shift determines the resonance frequency position of each peak on a MR spectrum, which is expressed as the shift in frequency in parts-per-million (ppm) relative to a standard (for historical reasons, this is typically the resonant frequency of tetramethylsilane at 0 ppm). The resulting spectrum can then be quantified through analytical methods, and either the absolute quantification or normalized signal intensity to an internal reference will be provided through these methods. The type of metabolites that can be quantified depends on whether long or short echo times (TE) were used. With long TE (> 60 ms, typically 144 or 288 ms), metabolites such as N-acetylaspartate (NAA), choline (Cho), and creatine (Cr) can be resolved. With shorter TE (< 35 ms), although the method is more susceptible to artifacts, it is possible to detect more metabolites such as myoinositol (mI), glutamate and glutamine (Glu/Gln), macromolecules, lipids, and lactate (Lac). Figure 4 provides an MRS spectrum of the brain along with molecular assignment of resonances.

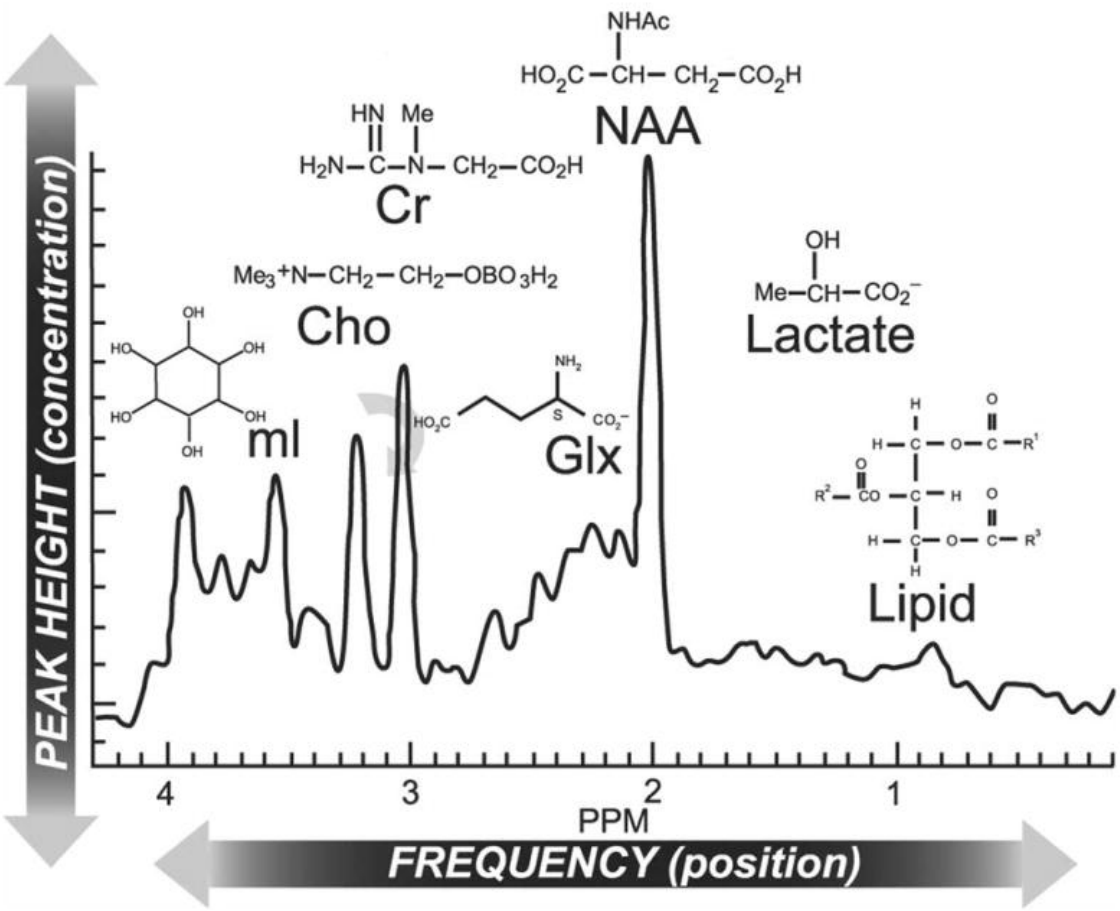

Figure 4. Magnetic resonance spectroscopy (MRS) spectrum of brain along with molecular assignment of resonances. The normal 1H-MRS spectrum is dominated by an *N*-acetylaspartate (NAA) resonance, flanked at the left by peaks for glutamate/glutamine (Glx), creatine (Cr)/phosphocreatine, choline (Cho)-containing phospholipids, and myoinositol (mI) and at the right by peaks for lactate and free lipids. Figure adapted from Lin et al. (*120*)

For spectroscopic data to be clinically useful, it is important to localize the source of the signals. Localization techniques such as PRESS (Point Resolved Spectroscopy) or STEAM (Stimulated Echo Acquisition Mode), allow the definition of tissue volume(s) of interest (VOIs) using anatomical images as reference. Both techniques use frequency selective RF pulses to excite three orthogonal planes, thus a spectrum can be obtained from a small volume of tissue defined by the intersection of the three orthogonal planes, as in single voxel spectroscopy (SVS).

Since water concentration is much higher as compared to the metabolite concentrations, the localization techniques are usually accompanied with water suppression techniques such as CHESS (CHEmical-Shift Selective). MRS data can be also derived from multiple voxels at one time (*i.e.*, multi-voxel spectroscopy) using a chemical shift imaging (CSI) technique. By spatially encoding the chemical information, CSI data (usually 2D CSI) can be obtained as spectral maps or metabolite images, and can be superimposed on anatomical images where the distribution of metabolites across a slice of tissue can be examined. However, the signal-to-noise ratio (SNR) from a multi-voxel spectral signal is usually lower than that from a SVS due to smaller voxel size typically used in CSI, and shimming for field inhomogeneity is more challenging for CSI than for SVS. Therefore, SVS is commonly used in the clinical setting.

3.2.2. MRS in MS

The dominant peak in a normal brain spectrum is at 2.02 ppm. This peak is N-acetylaspartate (NAA) and has overlapping contributions from other N-acetyle compounds such as N-acetyl aspartyle glutamate (NAAG at 2.05 ppm). NAA is a specific marker for neurons, axons, and dendrites, thus it has a high SNR due to its high concentration in the brain. As early as 1990, MRS detection of NAA deficiency was proposed for quantifying MS-related axonal dysfunction or loss (*121, 122*). Since then NAA is often reported to be reduced in acute and chronic lesions, as well as in normal appearing white and gray matters (*123-127*). The diminished NAA level has been correlated with neuronal/axonal dysfunction or loss in postmortem studies (*39, 128*), as well as the degree of neurological disability and cognitive impairment (*85, 123, 127, 129-132*).

Choline and Creatine are two other major brain metabolites studied in MS. The Cr peak occurs at 3.02 ppm and has contributions from creatine (Cr) and phosphocreatine (PCr).

Although its concentration in the brain is relatively stable (hence its frequent use as an internal reference), elevated Cr can be observed in MS lesions and normal appearing tissues, possibly due to gliosis (*133-136*). Choline (Cho) occurs at 3.24 ppm, a composite of glycerophosphocholine GPC, phosphocholine, and free choline. Increased levels of Cho have also been found in MS lesions, NAWM and NAGM (*133, 136-139*), suggesting gliosis and membrane turnover due to de- and remyelination. Other metabolites such as mI, Glu/Gln, and lipid were also found to be altered in brains of MS patients as compared to control subjects'(*140-145*).

However, metabolite changes might not be uniform in NAWM or NAGM within the same brain. A few studies showed that the extent of NAA reduction varied with distance from lesions, and that some regions even showed little or no change in NAA levels (*109, 139, 146*). Moreover, changes in metabolites could be region specific; MRS abnormalities were found in areas such as the corpus callosum, thalamus, hippocampus (*57, 147, 148*), but may or may not be found in cortical GM (*141, 146, 149-151*). These findings might reflect the heterogeneity in the degree of inflammation, axonal loss, neuronal loss, gliosis, or even remyelination in different regions of the brain. Indeed, spectroscopic findings in hippocampus suggested a possible biomarker for neurogenesis that might not be present in other GM areas such as the cortex (*152*). Thus, MRS could be a valuable tool to provide more detailed and region-specific pathologic information, which may be associated with the differences in the disease phenotype for each individual.

MRS findings and conventional MRI findings correlate with each other, and they both also correlate with clinical findings. However, MRS markers seem to yield a stronger clinical correlation than conventional MRI findings (*85, 119, 153-156*). It was shown that whole brain NAA level, when compared with brain parenchymal fraction, as functions of disease duration,

decreased 3.6 times faster than atrophy , suggesting that metabolites measured by MRS might be a more sensitive metric of ongoing disease activity than atrophy (*157*). Strong correlation was also found between reduced cerebral NAA/Cr ratios and increased clinical disability (*158*). In other studies with RRMS patients, cerebral NAA/Cr ratio, combined with other MR measures, accounted for a large portion of cognitive variability (*85*). Furthermore, longitudinal studies demonstrated that MRS measures hold promise in the prediction of disease development and progression (*132, 142, 153, 159*).

Despite its increased specificity to disease pathology and its ability to detect pathological changes prior to the appearance of clinical disability, MRS is not yet part of routine clinical care for MS. To date, there are no standardized procedures for data collection, making it impossible to establish norms that can be used on an individual basis in clinical settings. Additional improvements are needed in terms of SNR, spatial resolution, scan time, and reproducibility for any voxel position and size. The variety of methods associated with analysis of MRS data could also yield somewhat different results. Metabolite quantification is influenced by partial volume contamination of the voxel with different tissue types, and the accuracy of scanner calibration, etc (*160, 161*). Furthermore, while changes in metabolite concentrations may be indicative of cellular pathology, the link between regional MRS pathology and selective functional deficits has yet to be established. Therefore, further research is necessary to identify and assess metabolites that can be used as biomarkers for different MS impairments that would eventually be standardized and extended to clinical trials.

3.3. Other MR Findings in MS

Besides DTI and MRS, magnetization transfer imaging (MT-MRI) and functional MR imaging (fMRI) are also two advanced MR techniques with increasing interest of use in MS

studies. These techniques are all aimed to increase the sensitivity and specificity in the quantification and understanding of MS.

MT-MRI is based on the comparison of the protons of free mobile tissue water with protons in a motion restricted environment. In the brain, the liquid or mobile protons and macromolecular or bound protons have distinctly different MR properties, where the liquid protons have a relatively long T2 and the bound protons have a very short T2. MT-MRI has the ability to capture the very short T2 protons indirectly via magnetization transfer, where the typical MR images have no contribution from bound protons. When the two proton pools are in contact with each other after a saturation pulse, magnetization is transferred from bound protons to mobile protons, resulting in a reduction of MR signal. The amount of magnetization transferred is characterized by the magnetization transfer ratio (MTR). Low MTR may be caused by an increase in mobile protons, which may be a result of inflammation and edema, or the decrease in MTR may be due to a decrease in the bound protons, which can be interpreted as an indication of damage to myelin and other cellular structures (*162, 163*). MT-MRI was able to reveal subtle changes in normal appearing gray and white matters that showed moderate to strong correlations with physical disability (*164, 165*) and cognitive dysfunction (*166-168*) in MS. In addition, changes in MTR values in clinically-relevant regions such as the corpus callosum and hippocampus were seen in MS patients (*169*), further demonstrating the ability of advanced MR techniques to provide insights into different tissue and functional pathological changes underlying the clinical variability in MS.

Functional MRI is one of the most important developed techniques for noninvasive spatial localization of brain function. The signal changes seen on fMRI indicate changes in the blood oxygenation level dependent (BOLD) signal intensity, which is due to changes in neuronal

activity. BOLD fMRI has been used to assess brain function in MS. Altered patterns of cortical activation were seen in MS patients due to brain injury (*170-172*), which may be associated with functional deficits. Studies have also shown altered patterns of connectivity (*i.e.*, functional reorganization) in response to brain injury and consequently lead to recruitment of widespread brain networks engaged in tasks as functional compensation (*173-178*). Overall, these studies suggest that fMRI holds great promise as an assessment tool for MS because it has the potential to relate MS disabilities to changes in the brain's functional anatomy.

While we will not be focusing on these two valuable techniques in this thesis, MT-MRI and fMRI studies provide additional evidence of pathological changes outside of MS lesions. These abnormalities occur in normal appearing white and gray matter, and are associated with impaired motor and cognitive functions. Like all other advanced techniques, these MR approaches need to be standardized in order to be used in everyday clinical practice.

3.4. Summary

This chapter provided a brief overview of advanced MRI applications in MS, describing many, but not all, of the techniques currently available to aid in diagnostic and monitoring disease activity. Conventional MRI methods have had great success in the diagnostic and visualization of MS disease, yet there exists a paradox wherein the conventional MR images do not reflect the clinical disability of patients in many cases. The use of advanced techniques such as DTI and MRS has significantly furthered the understanding of the underlying pathophysiology, and has helped to predict patient outcome. Although much work has been done, many holes remain, especially as to how these MR acquisition and analysis techniques can help us understand the cognitive symptoms seen in MS patients. Thus, the research done for this dissertation was aimed to address these issues.

Chapter 4

Methods Overview

4.1. Summary

Thirty-eight individuals with RRMS and 20 healthy controls participated in this thesis. The control group consisted of healthy subjects from the general population with no history or signs of neurological defect. The multiple sclerosis subjects all had clinically definite relapsing-remitting multiple sclerosis, and were clinically stable for at least three months following relapse. The clinical information for each RRMS subject is summarized in Table 2. The study was approved by the Stony Brook University Institutional Review Board and written informed consent was obtained from all participants.

Subject ID	Age	Handedness	Gender	DurationOfMS	EDSS	DMT
07x-2	31	R	M	11.00	1.5	none
11x-2	46	R	F	7.50	3.0	Betaseron
27x	49	N/A	F	2.00	2.0	Rebif
29x	40	N/A	F	10.00	4.0	Copaxone
31x	30	N/A	F	10.00	3.5	Rebif
32x	37	L	F	10.00	3.5	Rebif/Methotrexate
34x	42	N/A	F	14.00	0.0	none
36x	44	N/A	M	2.00	2.5	none
37x	46	N/A	F	16.00	2.5	Rebif
40x	42	R	F	1.00	2.5	none
42x	52	N/A	F	2.00	2.0	Rebif
45x	43	N/A	F	20.00	2.0	Rebif
46x	29	R	F	0.75	3.5	none
48x	47	R	F	12.00	2.0	Copaxone
49x	39	R	F	5.00	3.5	none
51x	23	R	F	11.00	4.0	none
52x	49	R	F	18.00	1.0	none
54x	39	R	F	0.20	3.5	none
56x	62	R	F	40.00	3.0	none
58x	32	R	F	0.08	2.0	none
59x	62	N/A	F	14.00	4.0	Copaxone/Cellcept
61x	50	R	F	25.00	2.5	none
62x	32	R	M	0.60	2.0	Avonex
63x	36	R	F	8.00	2.0	none
64x	26	L	F	1.00	0.0	none
70x	38	R	F	5.00	2.0	Rebif
71x	36	R	F	8.00	1.5	none
72x	25	R	F	6.00	0.0	prior Copaxone
74x	40	R	F	0.25	1.0	none
76x	35	R	F	0.17	1.5	None
82x	27	R	F	5.00	3.5	None
83x	43	R	M	0.17	0.0	None
Affect-52	61	N/A	F	23.00	2.0	N/A
Affect-49	49	N/A	F	28.00	N/A	N/A
Affect-51	30	N/A	F	1.00	4.0	N/A
Affect-47	50	N/A	F	2.00	3.0	N/A
Affect-46	43	N/A	M	14.00	2.0	N/A
Affect-45	47	N/A	M	22.00	2.5	N/A

Table 2. Subject information for RRMS patients included in this dissertation. Age and Duration of MS measured in years. Numbered ID and Affect ID indicated patient ID from two separate neuropsychological protocols (which does not affect cognition results presented here). N/A: Not available; DMT: Disease modifying treatment at the time of scan.

4.2. Neurological and Cognitive Assessments

All MS participants underwent neurological assessment using the Expanded Disability Status Scale (EDSS) (*12*) at the time of participation. All MS subjects and fifteen healthy controls underwent cognitive assessments exploring commonly affected cognitive domains in MS, including: the Single Digit Modality Test (SDMT) to assess sustained concentration and cognitive processing speed (*179, 180*), the Rey Auditory Verbal Learning Test (RAVLT) to assess short term auditory-verbal learning and memory (*181*), and the 3 second-Paced Auditory Serial Attention Test (PASAT), a timed task that assesses sustained attention and working memory (*179, 182*). All three tests are widely accepted as reliable and sensitive measures of cognitive function in MS (*25*). Due to logistic issues, 9 of 38 RRMS participants received the Selective Reminding Test (SRT) (*179, 183, 184*) rather than the RAVLT as a measure of verbal memory; since both tasks assess the same domain (*181*), the SRT scores were used to estimate RAVLT scores via a *Z* score transformation using scores from a separate MS sample who received both tasks (*185*). Details of each cognitive test are as follows:

Symbol-Digit Modalities Test (SDMT) (*179, 180*): This is a test which measures sustained concentration, and visual information processing speed without a motor component. The subject must orally match, as quickly as possible, a randomly presented series of novel symbols, each to a specific number from 1 to 9, according to a key. The score reported and used for statistical analyses was the total number of correct matches attained during the task.

Rey Auditory Verbal Learning Test (RAVLT) (*181*): This test measures episodic verbal learning and memory. The examiner reads a list of 15 unrelated words to the subject, who tries to recall as many as possible. The examiner then rereads the list to the subject and asks them again to recall

as many words as possible. A total of 5 trials are administered. The score reported and used for statistical analyses was the total number of words recalled over the 5 trials.

Paced Auditory Serial Addition Test (PASAT) (*179, 182*): This task assesses working memory, sustained concentration, and information processing speed. The subject is presented with a series of digits, from 1 to 9, one at a time. The subject's goal is to continually sum the last two numbers that have been presented. The score reported and used for statistical analyses was the total number of correct responses across the 3 second form of the task.

4.3. MRI Acquisition Protocols

All scans (both MRI and MRS) for this thesis were conducted on a 3T Phillips Achieva MR Scanner (Philips Medical Systems, Best, The Netherlands) with an 8-channel SENSE head coil.

4.3.1. SPGR Data Acquisition

Three dimensional (3D) T1-weighted, inversion-recovery prepared, spoiled gradient echo-recalled (SPGR) images were acquired for volumetric analysis and for MRS voxel localization. 3D imaging techniques allow saving scan time, and enable the reformatting of acquired images in any spatial orientation using multiplanar image reconstruction. Images were acquired with the following parameters: TE/TR/TI = 4.6/8.0/400 ms, flip angle 18˚, 1mm slice thickness with no slice gap, field of view (FOV) was 250x250 mm, acquisition matrix was 256x256, which resulted in 1 mm isotropic resolution. All subjects included in this thesis had SPGR images acquired.

4.3.2. FLAIR Data Acquisition

T2-weighted fluid-attenuation inversion recovery (FLAIR) images (fast spin echo images with TE/TR/TI = 125/7600/2320 ms, 15 ETL, 1 x 1 x 3 mm resolution) were acquired for lesion identification. All MS subjects included in this thesis had FLAIR images acquired.

4.3.3. DIR Data Acquisition

Dual/Double Inversion recovery (DIR) images were acquired for suppressing CSF and WM, thus allowing for examination of possible GM abnormalities (*i.e.*, GM lesions). The sequence was acquired with the following parameters: $TE/TR/TI_1/TI_2$ = 25/9500/3130/305 ms, 1 x 1 x 3 mm resolution. Only 21 MS subjects included in this thesis had DIR images acquired. DIR images were used in the qualitative assessment of GM. Figure 5 shows an example DIR image.

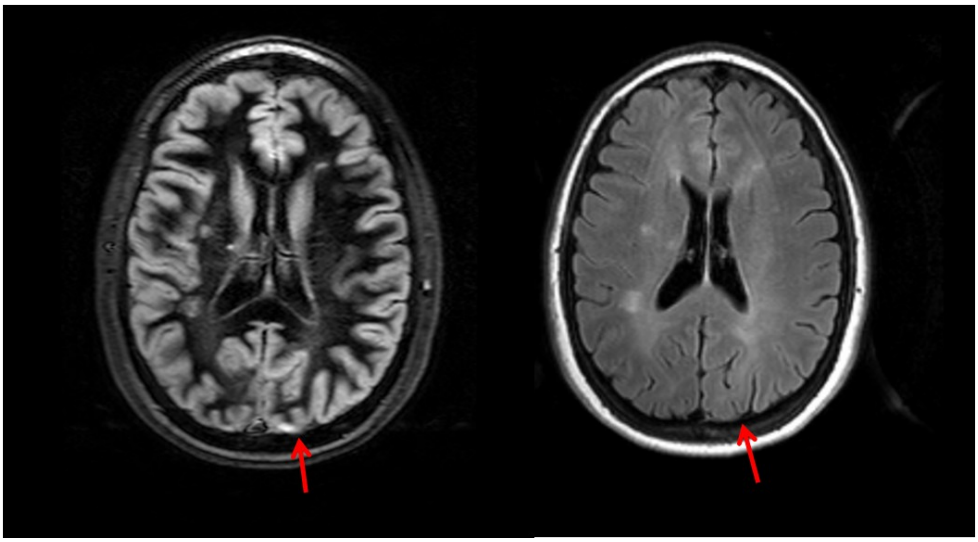

Figure 5. Example DIR image from a RRMS patient showing GM lesion not visible on FLAIR. Double inversion recovery sequence allows the visualization of GM lesions providing evidence of GM pathology beyond conventional imaging. Here, Arrows indicate cerebellar cortical lesions in a patient with relapsing remitting MS that is hyperintense compared to cerebellar gray matter on the DIR image (left), but that is isointense on the T2 FLAIR image (right).

4.3.4. T1-Post Contrast Data Acquisition

3D T1-weighted images were acquired 10 minutes after intravenous gadolinium injection for MS subjects. This is to identify enhancing lesions, and to confirm that lesions used for the MRS study were in fact non-enhancing. Post contrast sequence was collected using the following parameters: TE/TR= 4/7 ms, flip angle 10˚, 1mm slice thickness.

4.3.5. DTI Data Acquisition

DTI images were collected using an echo planar imaging (EPI) spin echo sequence with a SENSE factor of 2.4 (TE/TR = 62/5400 ms, 2x2x3 mm resolution). DTI scans at B-factor of 800s/mm^2 were obtained with 15 encoding directions. All participants but one MS subject had DTI images acquired. This subject who did not have a DTI image acquired had diffusion image collected instead, and was not included in data analysis.

4.3.6. MRS Data Acquisition

MR Spectroscopy data (both unsuppressed and water suppressed spectra) were acquired using a Point Resolved Spectroscopy (PRESS) sequence with the following acquisition parameters: TE/TR = 32/2000 ms, spectral width 2 kHz, 1024 points, NEX 128, and CHEmical-Shift Selective (CHESS) water suppression. Single voxel spectra were obtained in the 1) normal appearing white matter region of control subjects (CTWM, n=20) and MS subjects (NAWM, n=34), 2) non-enhancing lesion (NELES) of MS subjects (n=30), 3) left hippocampus (LTHIP) of control (n=19) and MS (n=34) subjects, and 4) cortical GM (CGM) of control (n=5) and MS (n=7) subjects. Each CTWM, NAWM, NELES, and CGM voxel size was 14x14x14mm. Each LTHIP voxel size as 27.5x10x10 mm with the long axis placed obliquely in the anterior-posterior direction along the main axis of the hippocampus. Pre-scan calibrations included a

second-order shimming procedure to obtain minimal line-width and maximal separation of metabolic components, and an adiabatic, hyperbolic secant CHESS water suppression pulse for obtaining complete water suppression and minimal baseline deviation. The voxels of interest (VOIs) were planned using reconstructed 3D SPGR images, and FLAIR or T1-post contrast images were used for lesion identification when needed. Air-tissue interface and ventricle was avoided when positioning VOIs. For control subjects, CTWM were placed in the periventricular white matter located predominately in the left frontal lobe. For MS subjects, the NAWM and NELES were obtained contralaterally when possible. Since NELES can be located in various regions of the brain, the NAWM and NELES voxels were not restricted to one brain region: a total of twenty-six NAWM voxels were acquired in the frontal lobe, three NAWM voxels in the parietal lobe; eighteen NELES voxels were acquired in the frontal lobe, eight in the parietal lobe and one in the temporal lobe. Examples of VOI placement are shown in Figure 6.

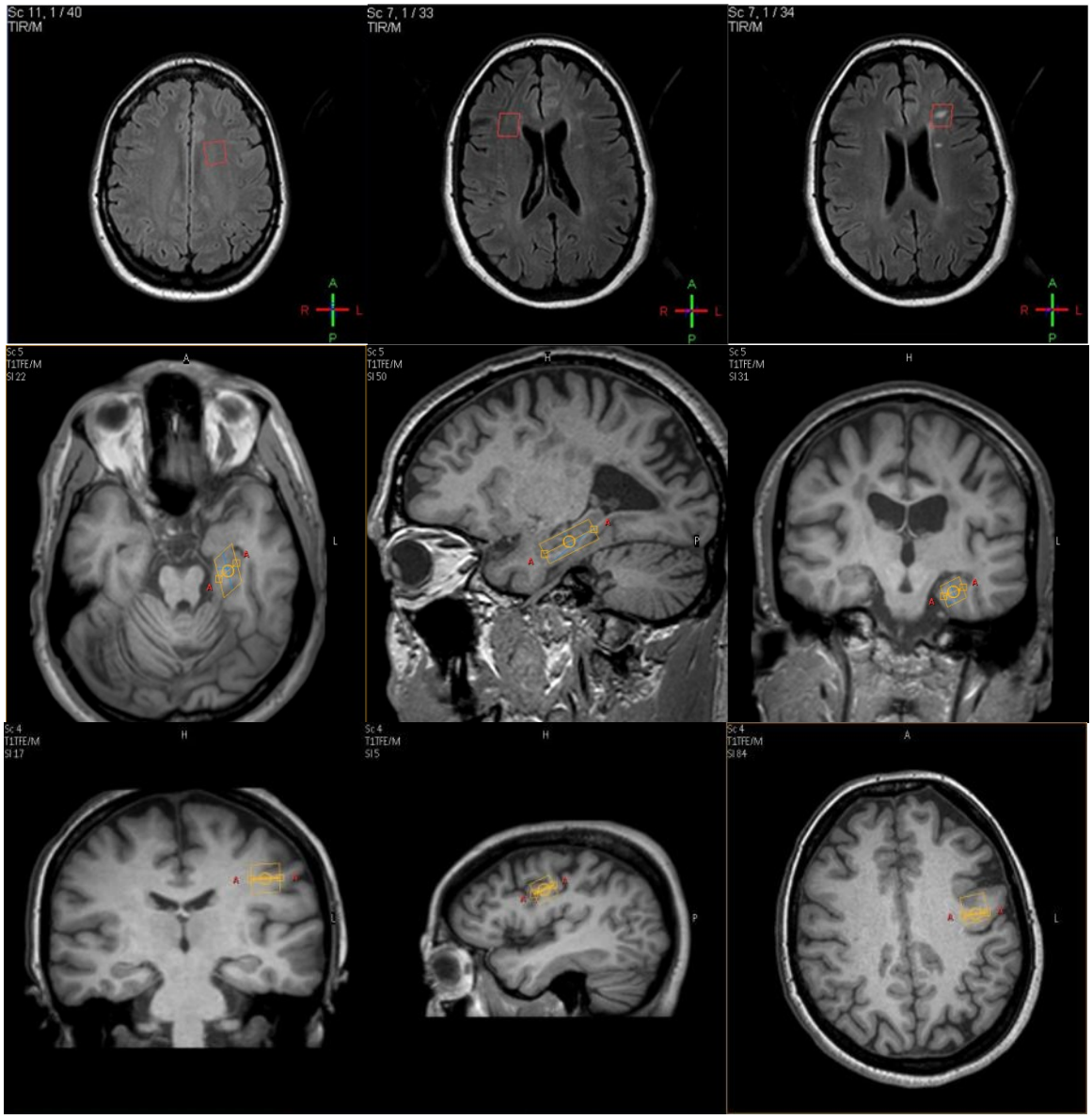

Figure 6. Examples of MRS voxel placement. The MRS voxels of interest (VOIs) were planned using reconstructed 3D SPGR images (middle and bottom row), and FLAIR (top row) or T1-post contrast images. The CTWM voxel (top-left) was located in the left-frontal lobe; whereas the NAWM (top-middle) is located at the contralateral side of the NELES (top-right) voxel. The LTHIP voxel (middle row) is positioned based on SPGR images with multi-planar views (left: axial; middle: sagittal; right: coronal) where the long axis was placed obliquely in the anterior-posterior direction along the main axis of the hippocampus. The CGM voxel (bottom row) was also positioned based on SPGR images with a multi-planar view, usually in cortical regions anterior to the central sulcus.

Chapter 5

Characterization of Volume Loss in MS and Its Link to Cognition

5.1. Introduction

Multiple sclerosis (MS) is an inflammatory demyelinating disease of the central nervous system (CNS), and is the most common disabling neurological disorder in young adults. It was originally defined by the presence of focal white matter lesions, and has been classically thought of as a white matter (WM) disorder. Most therapeutic, diagnostic, and research efforts have been therefore concentrated on the WM pathology in MS. However, as noted in Chapter 1, there is growing evidence from magnetic resonance imaging (MRI) and histopathology studies suggesting that the effects of multiple sclerosis on brain tissues are not limited to focal WM lesions or even white matter *per se*. It is now well acknowledged that gray matter (GM) is also extensively involved in MS, and could be relevant to the understanding of the clinical-radiological dissociation in patients with MS, where WM lesions observed in conventional MRI cannot fully explain the clinical status such as cognitive impairment. Although a large effort has been devoted to quantify the degree of GM involvement through assessing GM atrophy and GM lesions, the clinical relevance and predictive value of these GM measures are not fully evaluated. Given the complexity of the GM anatomy, it is difficult to quantify the extent of regional atrophy. The evaluation is generally done using manual segmentation, but it leads to significant variability in voxel labeling between readers, and it is extremely time consuming. Several automated

volumetric methods have been developed with high reproducibility, have been compared to manual tracings and have showed high accuracy to the goal standard; these may potentially be more efficient than manual volumetry. Amongst them, FreeSurfer is an automated tool (*186, 187*) that segments the brain into cortical and subcortical structures and labels each image voxel based on image intensity, probabilistic atlas location, and local spatial relationships between subcortical structures. It then calculates brain subvolumes, including subcortical volume and cortical thickness, thus allowing the characterization of regional GM atrophy in MS.

The goal was therefore to investigate the existence and extent of volume loss, in particular subcortical and cortical atrophy, in relapsing-remitting multiple sclerosis (RRMS) patients compared to healthy controls, using FreeSurfer. The performance of FreeSurfer was evaluated and compared to results from manual segmentation. We also examined whether cognitive impairment in the different cognitive domains assessed by three cognitive tests is associated with involvement of different GM regions.

5.2. Methods

5.2.1. Subjects and clinical assessments

Thirty-eight individuals with RRMS and 20 healthy controls participated in this study. Please refer to Chapter 4 for details on subject information, neurological and cognitive assessments.

5.2.2. MR data acquisition

3D T1-weighted SPGR, T2-weighted FLAIR, and DIR images were acquired for this study. 3D T1-weighted SPGR images were used for tissue segmentation and volumetric analysis.

T2-weighted FLAIR images were used for lesion quantification. DIR images were used to identify possible GM lesions. Please refer to Chapter 4 for details on MR data acquisition.

5.2.3. MR data analysis

5.2.3.1. SPM quantification

Individual DICOM files were converted into nifti format using MRIcro software (www.cla.sc.edu/psyc/faculty/rorden/mricro.html). Statistical Parametric Mapping software (SPM, version 8) (Wellcome Department of Cognitive Neurology, London, UK) implemented under Matlab R2007b (The Mathworks, Natick, MA) was used for global atrophy analysis. The unified segmentation algorithm with default settings was used (*188*). Briefly, T1-weighted SPGR images were spatially transformed so that each voxel in the image was mapped to its equivalent location in the default tissue probability maps (modified versions of the ICBM Tissue Probabilistic Atlases, http://www.loni.ucla.edu/ICBM/ICBM_TissueProb.html) of gray matter (GM), white matter (WM), and cerebrospinal fluid (CSF). After registration, these maps represented the prior probability of different tissue classes at each voxel. The Bayes rule was then used to combine these priors with tissue type probabilities derived from voxel intensities to provide the posterior probability or the revised probability. This procedure was iteratively optimized for image segmentation that combined registration, tissue classification, and bias correction. Finally, each voxel was classified as GM, WM, or CSF. The resulting tissue probability maps were further masked by segmented lesion maps (see the following section) for MS patients, and all were then summed to obtain the total partial volume estimates (or number voxels multiplied by voxel volume) of GM, WM, CSF (for all subjects), and lesions (for MS patients). Results were assessed as fractions of the total intracranial volume (ICV) as determined by adding the GM, WM, CSF (and lesion) volumes. Gray matter fraction (GMF) was calculated

as GM volume/ICV, and white matter fraction (WMF) was calculated as WM volume/ICV. Total brain volume was indicated by brain parenchymal volume, which was calculated as GM+WM or GM+WM+lesion volumes/ICV. An example of whole brain segmentation and quantification is shown in Figure 7.

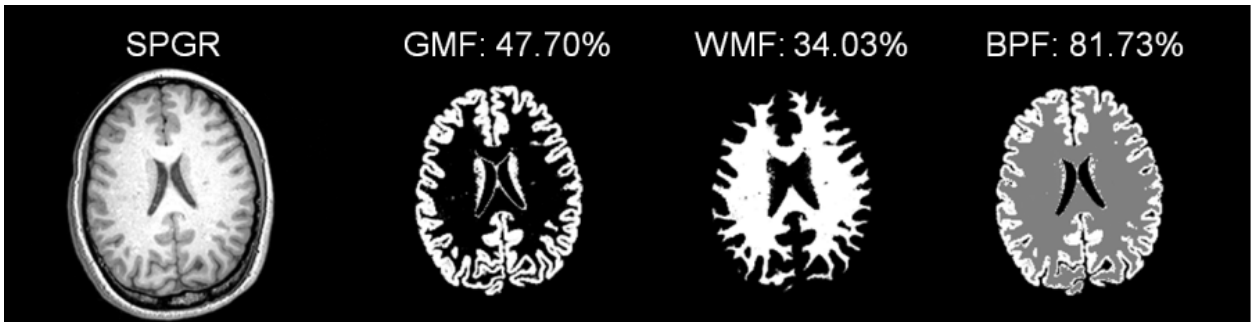

Figure 7. Example of whole brain segmentation and volumetric analysis. SPGR image (with only axial slice showing) from a healthy control (1st left image) was segmented (using SPM) into tissue probability maps of GM (2nd image), WM (3rd image), and CSF. Volumetric index Gray Matter Fraction (GMF) was then derived by normalizing the sum of all GM voxels to total intracranial brain volume (ICV calculated as GM+WM+CSF); White Matter Fraction (WMF) was derived by normalizing WM to ICV, and Brain Parenchymal Fraction (BPF) was derived by normalizing GM+WM to ICV.

5.2.3.2. Lesion segmentation and quantification

MS lesion segmentation has always been a challenge. Here, an in-house developed algorithm was implemented under Matlab R2007b for lesion segmentation and quantification. The algorithm used both T1-weighted SPGR and the co-registered T2-weighted FLAIR images to segment out the hyperintense lesions. First, the skull-stripped FLAIR images were enhanced by an image median filter (for noise reduction), and an erosion/dilation process (for shape/border enhancement). FLAIR images were then thresholded at two standard deviations above mean intensity of GM on FLAIR (for voxels defined as GM by SPM segmentation). This threshold was determined empirically by examining intensity histograms of a subset of FLAIR images (see Figure 8). The initial lesion masks were "cleaned" by filling holes and removing spurious voxels

based on voxel connectivity. Since hyperintensities on FLAIR can also come from bone and flow artifacts, the lesion masks were then further refined by morphological criteria including eccentricity (shape is oval or round) and area (at least 6 mm in one dimension). The final lesion masks were overlaid on FLAIR images and visually inspected on the GUI; the algorithm parameters could be manually adjusted if needed. Finally, the lesion masks were superimposed on SPGR white matter maps to manually correct for occasional misidentification of hypointense white matter lesions as gray matter. Total T2 lesion volume (T2LV) was calculated by summing voxels labeled as lesions, and the total T2 lesion load (%T2LV) was calculated as T2LV/ICV. Example of lesion segmentation and quantification is shown in Figure 8.

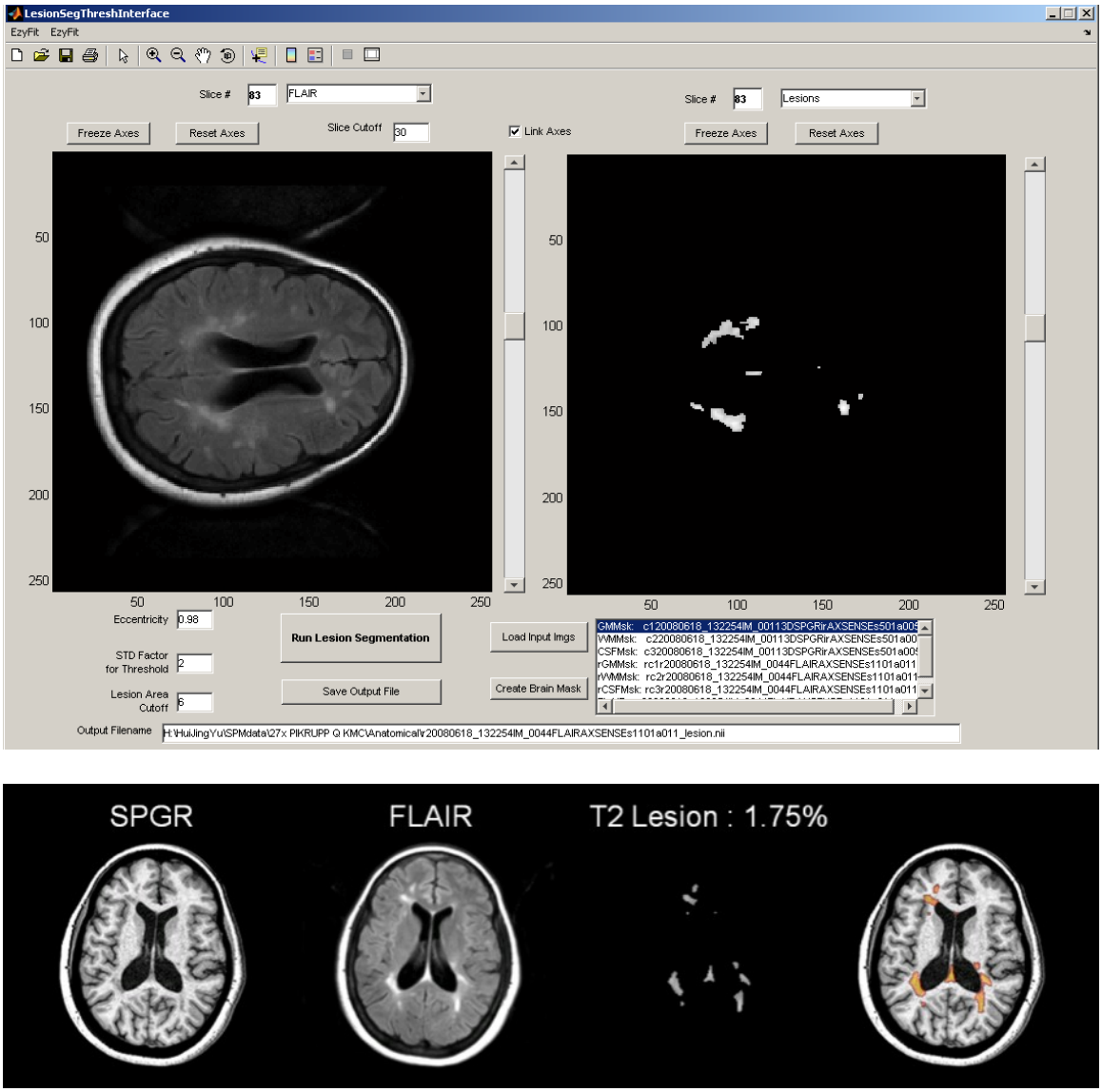

Figure 8. Example of lesion segmentation and volumetric analysis. For a RRMS patient, FLAIR Lesion was segmented from the co-registered FLAIR image using in-house developed automatic lesion segmentation GUI (shown as top screenshot). The parameters, such as eccentricity, standard deviation factor for intensity threshold, lesion area cutoff (on the lower left of GUI) were used for limiting lesion definition, and could be modified if needed. The GUI provides the flexibility for one to limit the brain regions/slices for analysis and the image pull-down panels allow selection of SPGR, FLAIR, brain mask, tissue probability maps, and lesion masks for visualization and comparison. The segmented lesion mask was then used to calculate for T2LV (bottom), and was overlaid on the SPGR image (bottom) to correct for voxel misclassification in SPM segmentation.

5.2.3.3. Manual hippocampal segmentation

As mentioned before, automated GM volumetry is difficult due to its structural complexity. To ensure the validity of automatic segmentation results, one would like to compare such GM volumetry results with manual segmentation results from multiple raters for one or a few representative structures. Due to time and resource limitations, the hippocampus was picked as a representative GM structure for comparison between manual and automatic segmentations for this dissertation. Hippocampus was also picked as an example GM structure since it has been shown to be important for cognitive function in many neurological disorders including MS (*189-193*).

Manual hippocampal segmentation was done using interactive software called ITK-SNAP (http://www.itksnap.org/pmwiki/pmwiki.php). ITK-SNAP provides tools for manual delineation of anatomical structures, and segmentation/labeling was done in all three orthogonal planes of the SPGR images. If necessary, images were magnified and trilinear interpolated to provide better visualization of landmarks. The protocol by Jack et al (*194*) was used for manual tracing since this protocol is often referenced and high rater reliability has been consistently achieved. Details of the protocol are as follows (also see Figure 9 where anatomical landmarks defining each boundary (from top to bottom) for hippocampal segmentation are indicated by crosshairs and arrows):

1. The anterior-most boundary was the level at which the uncal recess of the temporal horn, or the alveus, was visible.
2. The posterior-most boundary of the hippocampus was determined by the oblique coronal anatomic section on which the crura of the fornices were identified in full profile.
3. The medial boundary was the CSF in the uncal and ambient cistern.

4. The lateral boundary was the CSF in the temporal horn.

5. The inferior boundary was the gray/white matter junction between the subiculum and the white matter in the parahippocampal gyrus.

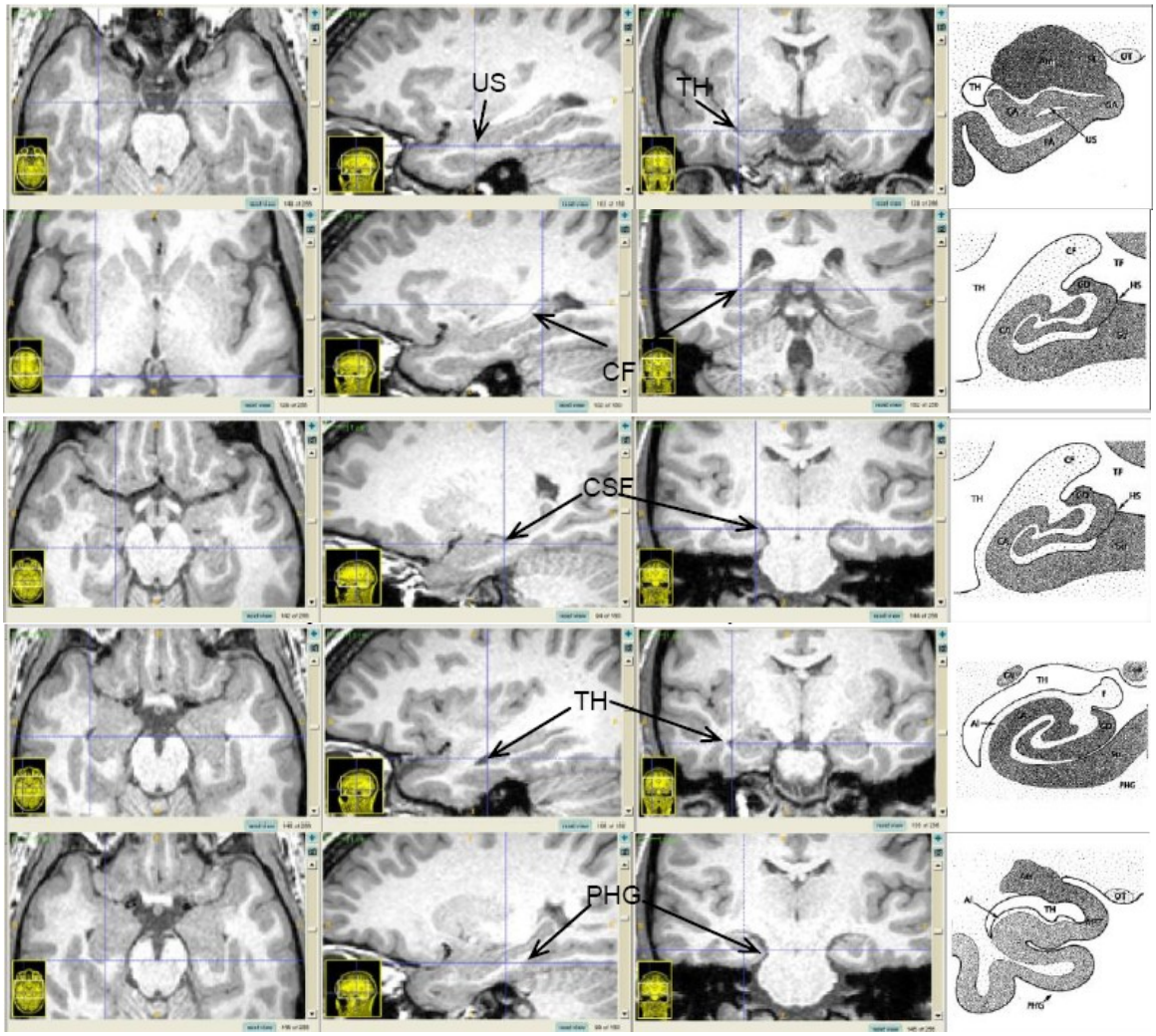

Figure 9. Manual hippocampal segmentation protocol. SPGR images (axial, sagittal, and coronal views) were manually segmented based on the Jack et al (*194*) protocol. Anatomical landmarks defining the anterior limit, posterior limit, medial boundary, lateral boundary, and inferior boundary for hippocampal segmentation are indicated as arrows on SPGR images, along with anatomical drawing showing in coronal view with the following landmarks: *Al* indicates alveus; *Am,* amygdala; *CA*, cornu Ammonis; *CF*, crus fornices; CN, caudate nucleus; *EA*, entorhinal area; F, fimbria; *GA*, gyrus ambiens; *GD*, gyrus dentatus; *HS*, hippocampal sulcus; *LGB*, lateral geniculate body; *OT*, optical tract; *PHG*, parahippocampal gyrus; *SL*, semilunar gyrus; *Su*, subiculum; *TF*, transverse fissure; *TH*, temporal horn; *US*, uncal sulcus

Measurements were performed by a single rater (author of this thesis) who was blinded to the clinical information. The whole procedure took about 45 min for each side. Segmentation results were validated by an expert neuroradiologist. Finally, absolute hippocampal volumes were calculated by multiplying the total labeled voxel count by the volume of each voxel.

5.2.3.4. Cortical volume and thickness measurements

The volume-based subcortical segmentation and surface-based cortical reconstructions were completed using the automated FreeSurfer software (http://surfer.nmr.mgh.harvard.edu/fswiki/FreeSurferWiki). Quantification was done using 3D T1-weighted SPGR images. The technical details of these procedures have been described in previous publications (*186, 187*).

Briefly, the MRI images were registered to the Talairach space and the intensity of the output images was normalized. The skull was then automatically stripped off the 3D anatomical data set by a hybrid method that uses both watershed algorithms and deformable surface models. Visual inspection was done and manual interventional was performed to edit areas of the skull, cortex, or cerebellum as needed. After skull stripping, the output brain mask was labeled using a probabilistic atlas where each voxel in the normalized brain mask volume was assigned one of the following labels: cerebral WM, cerebral cortex, lateral ventricle, inferior lateral ventricle, cerebellum WM, cerebellum cortex, thalamus, caudate, putamen, pallidum, hippocampus, amygdala, accumbens area, third ventricle, fourth ventricle, brainstem, and cerebrospinal fluid (CSF). At this point the volumes of such structures were calculated. For the purpose of this chapter, six subcortical GM structures, thalamus, caudate, putamen, pallidum, hippocampus, and amygdale, were selected for further analysis and normalized by intracranial volume. Examples of FreeSurfer subcortical segmentation are shown in Figure 10.

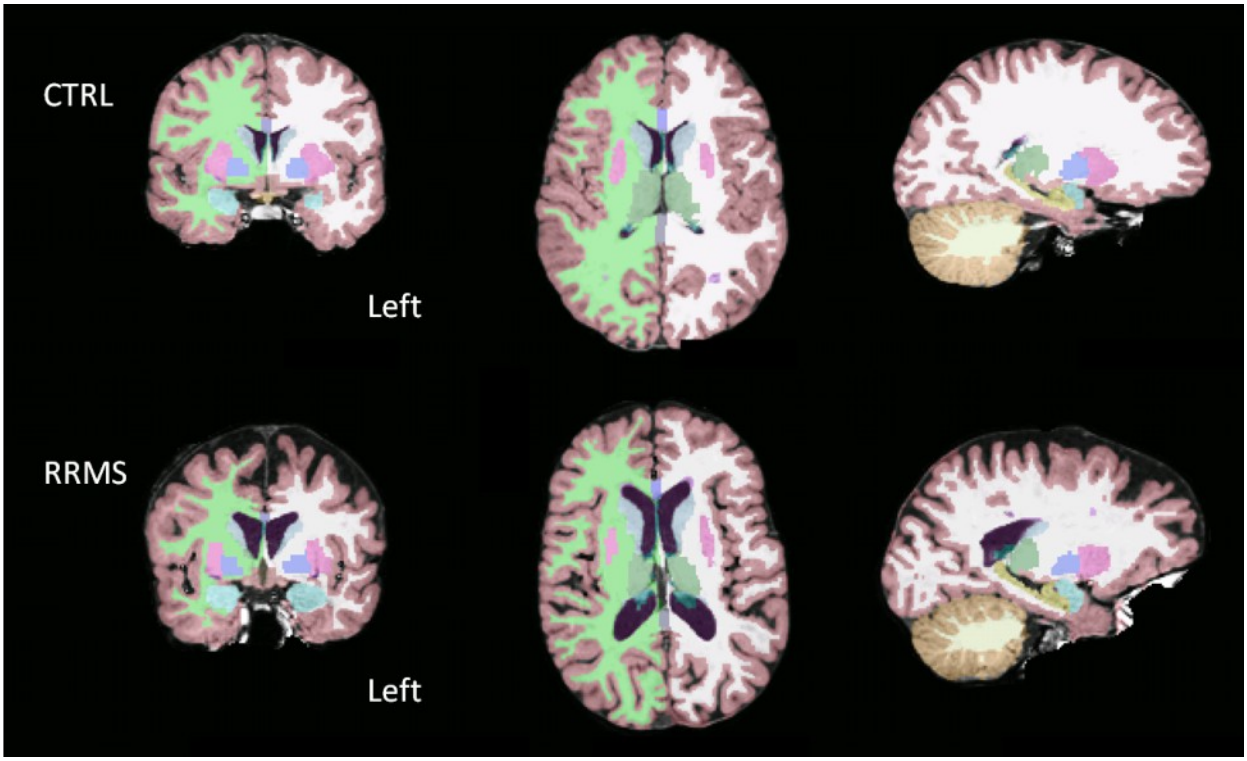

Figure 10. Examples of FreeSurfer subcortical segmentation showing regional brain structures in a patient with multiple sclerosis and a healthy control. Representative 3D T1-weighted SPGR images show regional brain segmentation results in (bottom row) a relapsing remitting multiple sclerosis patient (30 year old female with 10 years of disease duration and an EDSS of 3.5), compared to (top row) a gender and age matched healthy control. Different regions as segmented by FreeSurfer are displayed in coronal (left), axial (middle), and sagittal (right) views. FreeSurfer labeled regions include gray matter (pink), putamen (rose pink), pallidum (blue), thalamus (green), and caudate (light blue), lateral ventricles (violet), cerebellum gray matter (brown), cerebellum white matter (light brown), left cerebral white matter (white), right cerebral white matter (neon green), brainstem (gray), and hippocampus (yellow).

The cortical surfaces from each subject were also reconstructed using the automated FreeSurfer software. This method uses both intensity and continuity of the information from the entire three-dimensional MRI volume in segmentation and deformation procedures, producing representations of cortical thickness (CTh), calculated at each vertex on the tessellated surface as the closest distance from the grey/white boundary to the grey/CSF boundary. The maps produced

are not restricted to the voxel resolution of the original data; consequently, they are capable of detecting sub-millimeter differences between groups.

5.2.4. Statistics

5.2.4.1. Whole brain group comparison and correlation

Statistical analyses were performed using SPSS v18 (SPSS, Chicago, Ill., USA). A *t* test with Bonferroni correction adjusting for age was used to examine group differences in GMF, WMF, and BPF. Partial correlations adjusting for age were used to examine relationships within the volume measurements (GMF, WMF, BPF, and %T2LV), and between volume measurements and cognitive test scores (SDMT, RAVLT, PASAT) in the MS group. All statistical analyses had a two-tailed alpha level of <0.05 for defining significance. Since this is an exploratory study, corrections for multiple comparisons were not made.

5.2.4.2. Manual segmentation versus FreeSurfer segmentation

To compare the manually or FreeSurfer segmented normalized hippocampal volume between controls and RRMS subjects, a *t* test was performed with covariate age. To determine the degree of correlation between manual and automated segmentation methods, Pearson correlation analysis was used.

5.2.4.3. FreeSurfer subcortical volume and cortical thickness

To compare the differences between RRMS and control for subcortical volume, a *t* test followed by Bonferroni's correction, adjusting for age, was applied. To analyze the correlation between subcortical volume and cognitive scores, partial correlations adjusting for age and ICV were performed.

To compare the differences between RRMS and control for cortical thickness, a *t* test followed by Bonferroni's correction, adjusting for age, was applied. Due to the large number of areas included in this exploratory study, cortical regions were also grouped into frontal, occipital, parietal, and temporal lobes for each hemisphere to examine cerebral lobe differences.

Furthermore, a surface-based group analysis using tools within FreeSurfer was performed. First, the subjects' surface was smoothed using a full-width half-maximum Gaussian kernel of 10 mm. This smoothing was done so that all subjects could be displayed on a common template given by FreeSurfer in order to perform and visualize the analysis. FreeSurfer then fitted a general linear model at each vertex in the cortex to perform correlation analysis against each cognitive measure on the cortical surface within the MS group. In order to correct for multiple comparisons, all analyses were thresholded by running Monte Carlo-style simulation (http://surfer.nmr.mgh.harvard.edu/fswiki/FsTutorial/QdecGroupAnalysis) with 10,000 iterations with False Discovery Rate (FDR) set at $p < 0.05$, and finally only significant clusters (with surface area of more than 25 mm^2) at $p < 0.01$ were shown. Localization of anatomical regions was determined using the standard FreeSurfer atlas.

5.3. Results

5.3.1. Demographic and disease characteristics

Table 3 shows the demographic, clinical, and cognitive test performances of the two study groups. The MS group had a relatively low level of neurological impairment as measured by the EDSS consistent with our restriction to RRMS subjects. MS participants relative to controls had worse scores across all cognitive tests. However, likely due to the small sample size of controls with cognitive test results, only differences in RAVLT scores reached statistical significance ($p < 0.01$). However, the SDMT results appeared to be skewed by a single

individual; when this MS outlier with an exceptionally elevated SDMT score (> 2.5SD above the mean) was excluded, the SDMT was also significantly lower compared to controls (p = 0.046). No significant correlation were found between EDSS or disease duration and any of the three cognitive tests, and thus EDSS and disease duration were not included as a variable for MRI-cognition correlation analyses.

	MS Patients	Controls	*p* -value
Sex (M/F)	6/32	4/16	
Age (years)	40.8 ± 10.0	34.0 ± 10.3	0.02
Disease duration (years)	9.4 ± 9.4	--	
Median EDSS (range)	2.00 (0 - 4.0)	--	
SDMT	54.0 ± 12.4	60.7 ± 11.5	0.08
RAVLT	47.2 ± 8.8	56.5 ± 9.2	< 0.01
PASAT	42.1 ± 11.1	48.5 ± 8.8	0.05

Table 3. Demographic, clinical, MRI, and neuropsychological characteristics (mean±SD), except for EDSS (which has median and range). Only 15 of the healthy controls underwent cognitive testing. The cognitive tests are SDMT: Single Digit Modality Test (SDMT); RAVLT: Rey Auditory Verbal Learning Test; PASAT: Paced Auditory Serial Attention Test (3 second version).

5.3.2. Whole brain volume measures

There were significant differences, with and without age correction, between individuals with RRMS and healthy controls in BPF and GMF values, but not WMF (Figure 11). GMF correlated with age within the control group ($r = -0.44$, $p < 0.05$), whereas both GMF and BPF correlated with age within the MS group (GMF: $r = -0.43$, $p < 0.05$; BPF: $r = -0.45$, $p < 0.01$). GMF did not correlate with WMF or T2LV, while WMF correlated with T2LV. As for the associations between cognitive scores and volume measures, all cognitive measures correlated with T2LV (RAVLT $r = -0.398$, $p < 0.05$; SDMT $r = -0.578$, $p< 0.001$; PASAT $r = -0.388$, $p <$

0.05), but only the RAVLT scores correlated with GMF ($r = 0.334$, $p < 0.05$) and only the SDMT scores correlated with WMF ($r = 0.367$, $p < 0.05$).

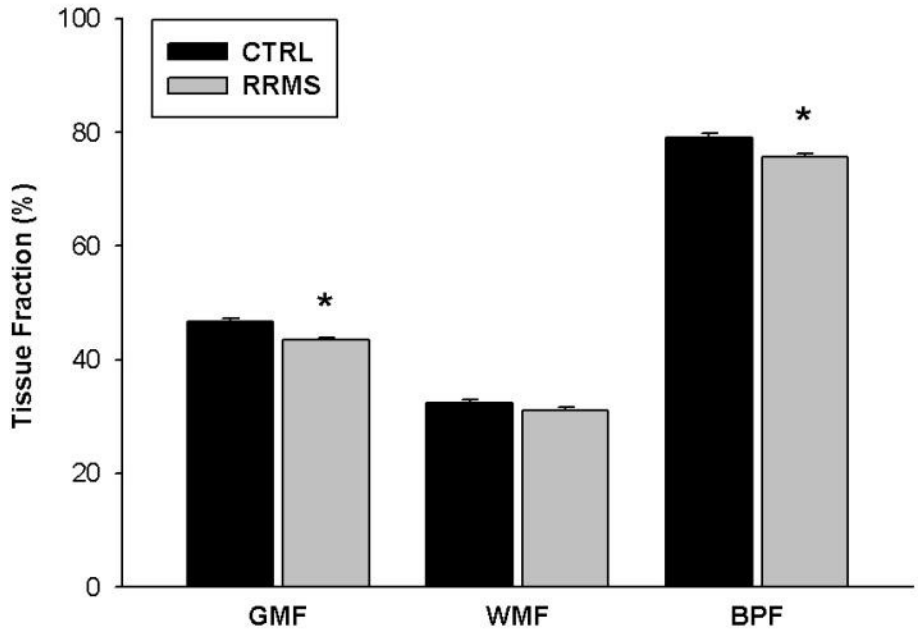

Figure 11. Volumetric features of MS subjects as compared to controls. Adults diagnosed with RRMS (n=38) exhibited GM and whole brain atrophy as compared to healthy control subjects (n=20). While MS is typically thought of as a disease primarily involving WM, the analyses showed no significant WM atrophy in MS subjects. Asterisk (*) indicate statistical significance ($p<0.05$). GMF: Gray matter fraction, WMF: White matter fraction, BPF: brain parenchyma fraction

5.3.3. Manual segmentation and correlation using FreeSurfer

Both manual and automated segmentation (Figure 12), showed trend of reduction in unnormalized hippocampal volume in MS subjects compared to controls (manual: 5.3 ± 0.8 vs 5.4 ± 0.6 and FreeSurfer: 8.4 ± 0.9 vs 8.8 ± 0.7). After correcting for age and ICV, both techniques showed reduction of total hippocampal volume (manual -2% and FreeSurfer -5%) as compared

to healthy controls, though both differences did not reach statistical significance. However, right hippocampus (not normalized) yielded significant atrophy in RRMS with FreeSurfer (Control 4.45±0.36 vs. MS 4.17±0.51, $p < 0.05$). Significant correlations were found between the two methods on both the left hippocampus ($r = 0.625$, $p < 0.001$) and right hippocampus ($r = 0.701$, $p < 0.001$).

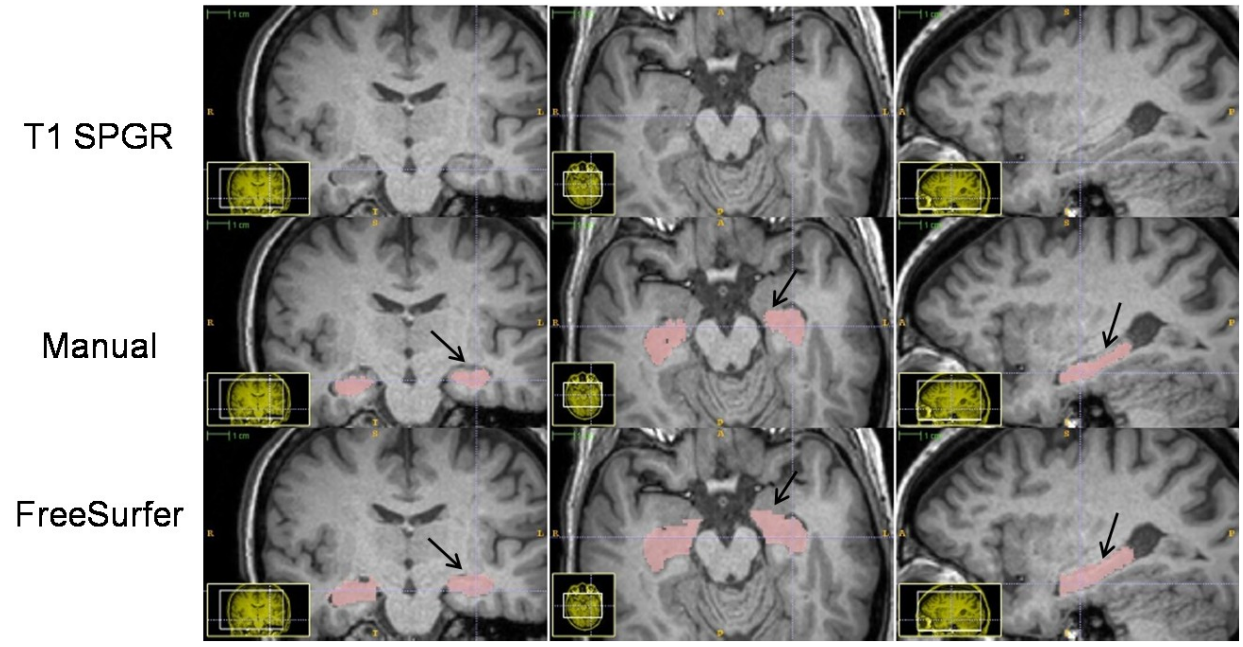

Figure 12. Comparison of manual and automatic FreeSurfer hippocampal segmentation. Multi-planar view of SPGR images (left column: colonal; middle column: axial; right column: sagittal) from a healthy subject showing agreement between manual (middle row) and automated (bottom row) hippocampal segmentation results, except FreeSurfer included the alveus and fimbria which were not included in the manual segmentation (arrows). Both outputs were accepted by an expert neuroradiologist. Note that FreeSurfer hippocampal results were transformed from FreeSurfer space to the native space by nearest neighbor interpolation, thus these results might seem a bit less smooth as compared to manual segmentation.

5.3.4. Subcortical volume measures

Regional subcortical atrophy was found in RRMS individuals compared to controls. Representative examples of FreeSurfer segmentation are shown in Figure 10. The thalamus, caudate, putamen, pallidum, and right hippocampus yielded significant atrophy in RRMS compared to controls with simple *t* test. However, after controlling for age and ICV, only the left thalamus, caudate, putamen, and pallidum showed statistical significance. Figure 13 displays percentage differences between MS patients and healthy controls for mean normalized subcortical gray matter volumes. The greatest percent differences (more than 10% reduction) were for putamen (left: -12.56%, right: 11.15%), caudate (left: -11.47%, right: -12.71%), and right pallidum (-13.50%).

In the MS group, the left putamen, left pallidum, and right caudate significantly correlated with RAVLT and SDMT (Table 4). The PASAT scores, however, did not correlate to any subcortical measures. Putamen and pallidum volumes also correlated with T2LV ($r=-0.50$ and $r=-0.56$, $p<0.01$).

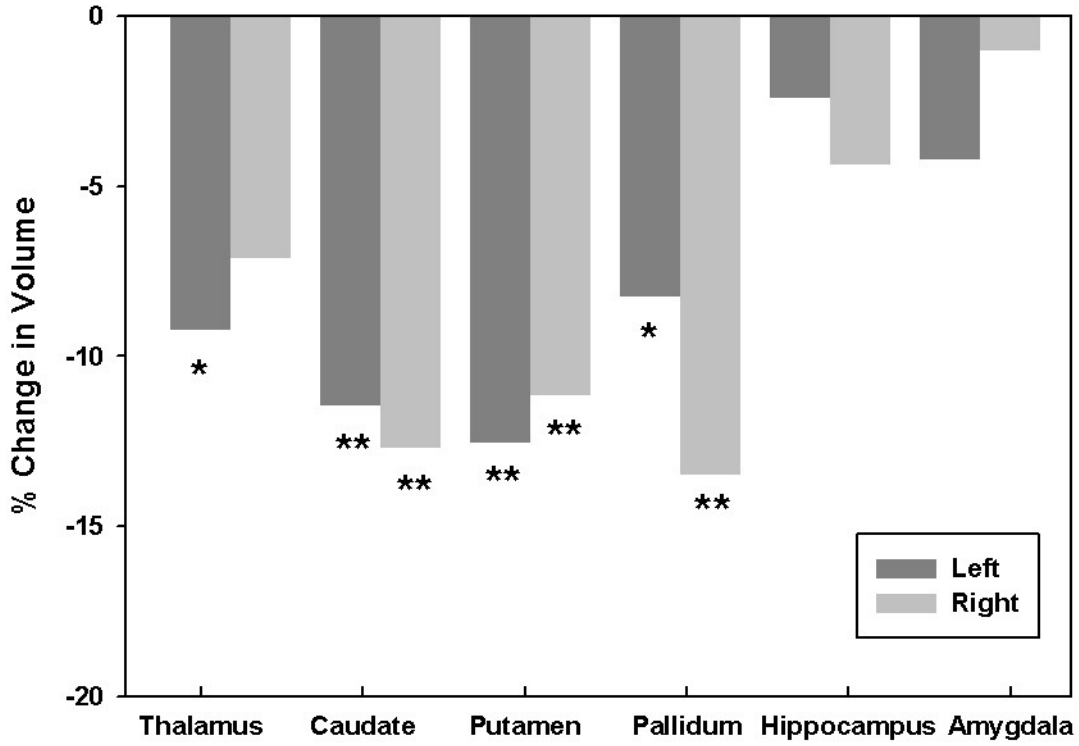

Figure 13. Mean percentage volume difference of deep gray matter structures indicating atrophy in multiple sclerosis patients. The basal ganglia had the largest degree of atrophy amongst structures examined, but no significant volume decrease was found in the hippocampus or amygdala. Percent difference for each structure was calculated as (A – B)/B, where A is the mean normalized volume for MS patients and B is the mean normalized volume for healthy controls. Structures where significant atrophy were found in group comparison are indicated by symbols * for $p < 0.05$, and ** for $p < 0.01$.

	RAVLT	SDMT	PASAT
Left-Thalamus	.051	-.066	-.163
Left-Caudate	.430 **	.283	-.189
Left-Putamen	.450 **	.440 **	.087
Left-Pallidum	.410 *	.416 *	.041
Left-Hippocampus	.093	.104	-.170
Left-Amygdala	.018	.103	-.192
Right-Thalamus	-.037	-.142	-.235
Right-Caudate	.509 **	.368 *	-.134
Right-Putamen	.297	.321	.048
Right-Pallidum	.322	.350 *	.087
Right-Hippocampus	.007	.099	-.254
Right-Amygdala	.143	.150	-.097

Table 4. Partial correlation coefficients between cognitive scores and volume of subcortical GM structures. Significant correlations were found between selective subcortical GM structures and RAVLT and SDMT, but not PASAT. Significant correlations are indicated by symbols * for $p < 0.05$, and ** for $p < 0.01$.

5.3.5. Cortical thickness measures

Most of the cortical areas analyzed were found significantly thinner in RRMS (Figure 14). A significant reduction in global CTh was observed in RRMS compared to control (RRMS vs CTRL: 2.63±0.10 mm vs 2.74±0.07 mm $p < 0.001$). Cortical thinning was observed mainly in the frontal, parietal, and temporal lobes, as shown in Table 5.

FreeSurfer GLM analysis showed clusters with significant correlations between cortical thinning and SDMT, RAVLT, and PASAT scores (Figure 15), however, only a few regions survived cluster-wise correction for multiple comparisons ($p < 0.05$), as followed: 1) for SDMT: right precuneus, left precentral gyrus, 2) for RAVLT: left transverse temporal and left postcentral gyrus, and 3) for PASAT: none of the clusters reached significance after multiple correction.

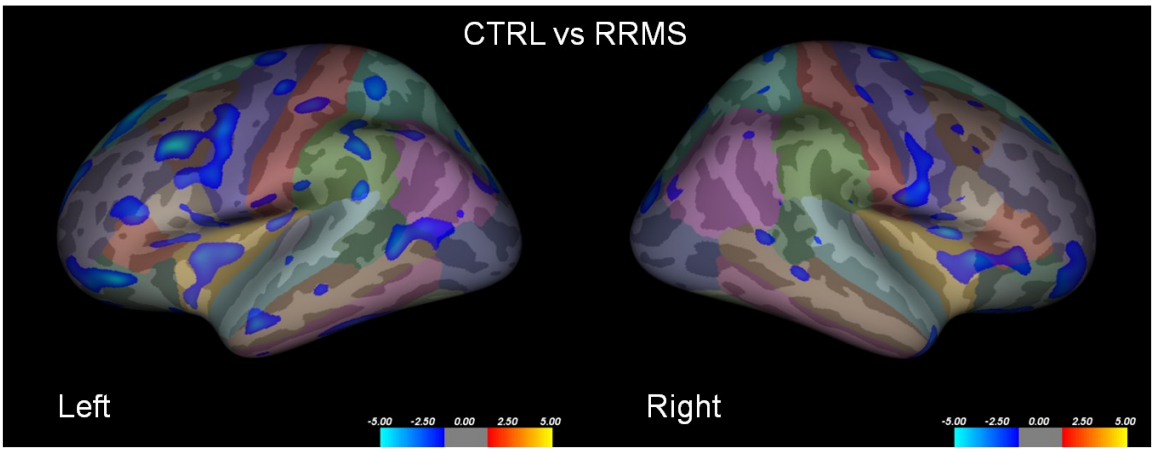

Figure 14. Cortical thinning exists in patients with multiple sclerosis. Displayed are lateral views of the inflated surface 3D representation with cortical thickness map from left and right hemispheres showing regions with cortical thinning in relapsing remitting multiple sclerosis patients compared to healthy controls (blue clusters). The top three cortical regions with largest cluster size of significant thinning for the left hemisphere were pre-central (blue), parahippocampal (not shown), and pars orbitalis (not shown), and for the right hemisphere were middle temporal (light brown), superior frontal (light turquoise), and post-central (crimson red). Other regions shown including caudal middle frontal (dark brown), pars opercularis (skin tone), inferior parietal (light pink), superior parietal (dark turquoise), superior temporal (light blue), rostral middle frontal (violet), lateral orbitofrontal (dark green), pars triangularis (orange), supra-marginal (parrot green), lateral occipital (dark blue), and inferior temporal (dark pink). Color bar indicate significance in –log(10)p value.

Region	Left Hemisphere				Right Hemisphre			
	Control	RRMS	% Change	p value	Control	RRMS	% Change	p value
Frontal	**2.87 ± 0.13**	**2.74 ± 0.10**	**-4.57%**	**0.000**	**2.86 ± 0.09**	**2.77 ± 0.11**	**-3.19%**	**0.002**
Caudal anterior cingulate	2.89 ± 0.32	2.80 ± 0.37	-3.17%	n.s.	2.89 ± 0.22	2.83 ± 0.22	-2.09%	n.s.
Caudal middle frontal	2.73 ± 0.14	2.62 ± 0.13	-4.20%	0.003	2.76 ± 0.11	2.66 ± 0.16	-3.65%	0.016
Frontal pole	3.12 ± 0.36	3.01 ± 0.27	-3.44%	n.s.	3.01 ± 0.23	3.01 ± 0.29	-0.18%	n.s.
Isthmus cingulate	2.77 ± 0.21	2.64 ± 0.22	-4.66%	0.035	2.64 ± 0.16	2.51 ± 0.22	-5.10%	0.019
Lateral orbitofrontal	2.95 ± 0.20	2.87 ± 0.14	-2.49%	n.s.	2.93 ± 0.19	2.83 ± 0.16	-3.54%	0.029
Medial orbitofrontal	2.74 ± 0.18	2.60 ± 0.18	-5.18%	0.006	2.79 ± 0.18	2.71 ± 0.18	-3.07%	n.s.
Pars opercularis	2.83 ± 0.13	2.70 ± 0.16	-4.53%	0.003	2.85 ± 0.14	2.73 ± 0.17	-4.36%	0.008
Pars orbitalis	3.02 ± 0.26	2.89 ± 0.20	-4.31%	0.040	3.09 ± 0.19	2.97 ± 0.22	-3.83%	0.044
Pars triangularis	2.76 ± 0.17	2.60 ± 0.22	-5.69%	0.007	2.79 ± 0.12	2.71 ± 0.25	-2.74%	n.s.
Posterior cingulate	2.68 ± 0.20	2.59 ± 0.22	-3.39%	n.s.	2.71 ± 0.15	2.62 ± 0.16	-3.28%	0.049
Pre-central	2.75 ± 0.09	2.61 ± 0.15	-4.94%	0.001	2.73 ± 0.08	2.64 ± 0.13	-3.28%	0.007
Rostral anterior cingulate	3.24 ± 0.25	3.00 ± 0.37	-7.53%	0.010	3.15 ± 0.27	3.10 ± 0.38	-1.63%	n.s.
Rostral middle frontal	2.62 ± 0.13	2.51 ± 0.12	-4.34%	0.001	2.63 ± 0.14	2.56 ± 0.16	-2.65%	n.s.
Superior frontal	3.03 ± 0.15	2.86 ± 0.13	-5.47%	0.000	3.05 ± 0.11	2.88 ± 0.12	-3.88%	0.000
Occipital	**2.01 ± 0.09**	**1.93 ± 0.15**	**-3.66%**	**0.049**	**2.02 ± 0.09**	**1.92 ± 0.13**	**-4.77%**	**0.005**
Cuneus	1.95 ± 0.13	1.86 ± 0.18	-4.68%	n.s.	1.95 ± 0.13	1.80 ± 0.15	-8.05%	0.000
Lateral occipital	2.35 ± 0.10	2.28 ± 0.17	-3.35%	n.s.	2.43 ± 0.12	2.36 ± 0.15	-2.99%	n.s.
Lingual	2.11 ± 0.11	2.02 ± 0.24	-4.06%	n.s.	2.08 ± 0.11	2.03 ± 0.21	-2.60%	n.s.
Peri-calcarine	1.62 ± 0.12	1.58 ± 0.18	-2.37%	n.s.	1.60 ± 0.14	1.50 ± 0.19	-6.28%	0.038
Parietal	**2.56 ± 0.07**	**2.45 ± 0.13**	**-4.51%**	**0.001**	**2.54 ± 0.08**	**2.44 ± 0.13**	**-3.97%**	**0.003**
Inferior parietal	2.72 ± 0.11	2.60 ± 0.15	-4.33%	0.003	2.71 ± 0.13	2.61 ± 0.13	-3.58%	0.011
Para-central	2.62 ± 0.10	2.45 ± 0.19	-6.18%	0.001	2.61 ± 0.16	2.43 ± 0.22	-6.70%	0.003
Post-central	2.29 ± 0.09	2.25 ± 0.18	-1.79%	n.s.	2.24 ± 0.08	2.23 ± 0.20	-0.86%	n.s.
Pre-cuneus	2.55 ± 0.10	2.41 ± 0.17	-5.59%	0.001	2.54 ± 0.10	2.38 ± 0.19	-6.00%	0.001
Superior parietal	2.42 ± 0.09	2.29 ± 0.14	-5.75%	0.000	2.40 ± 0.11	2.30 ± 0.16	-5.42%	0.026
Supra-marginal	2.78 ± 0.11	2.68 ± 0.15	-3.50%	0.013	2.77 ± 0.10	2.70 ± 0.15	-2.52%	n.s.
Temporal	**3.07 ± 0.10**	**2.97 ± 0.18**	**-3.29%**	**0.026**	**3.12 ± 0.11**	**2.99 ± 0.18**	**-4.10%**	**0.005**
Bank Superior Temporal Sulcus	2.71 ± 0.20	2.59 ± 0.16	-4.55%	0.014	2.73 ± 0.16	2.63 ± 0.22	-3.60%	n.s.
Entorhinal	3.62 ± 0.24	3.48 ± 0.40	-3.89%	n.s.	3.73 ± 0.26	3.51 ± 0.33	-5.88%	0.012
Fusiform	2.87 ± 0.14	2.75 ± 0.20	-3.86%	0.029	2.87 ± 0.12	2.78 ± 0.17	-3.18%	0.039
Inferior temporal	3.09 ± 0.13	2.95 ± 0.20	-4.47%	0.008	3.09 ± 0.16	3.02 ± 0.15	-2.28%	n.s.
Middle temporal	3.11 ± 0.11	3.02 ± 0.16	-2.99%	0.024	3.15 ± 0.10	3.04 ± 0.17	-3.23%	0.020
Para-hippocampal	2.76 ± 0.32	2.79 ± 0.38	0.82%	n.s.	2.84 ± 0.32	2.72 ± 0.32	-4.26%	n.s.
Superior temporal	3.00 ± 0.12	2.89 ± 0.15	-3.69%	0.007	3.02 ± 0.15	2.88 ± 0.16	-4.52%	0.003
Temporal pole	3.94 ± 0.26	3.84 ± 0.53	-2.66%	n.s.	4.09 ± 0.30	3.84 ± 0.57	-6.22%	n.s.
Transverse temporal	2.49 ± 0.20	2.38 ± 0.25	-4.44%	n.s.	2.54 ± 0.24	2.49 ± 0.25	-2.29%	n.s.

Table 5. Summary of cortical thickness (mean±SD) from both hemispheres of MS patients compared to healthy controls. Widespread cortical thinning was found in RRMS subjects compared to control subjects. Percentage (%) change is calculated as (RRMS CTh – CTRL CTh)/CTRL CTh. Significant difference is shown in corresponding p values, otherwise annotated as not significant (n.s.).

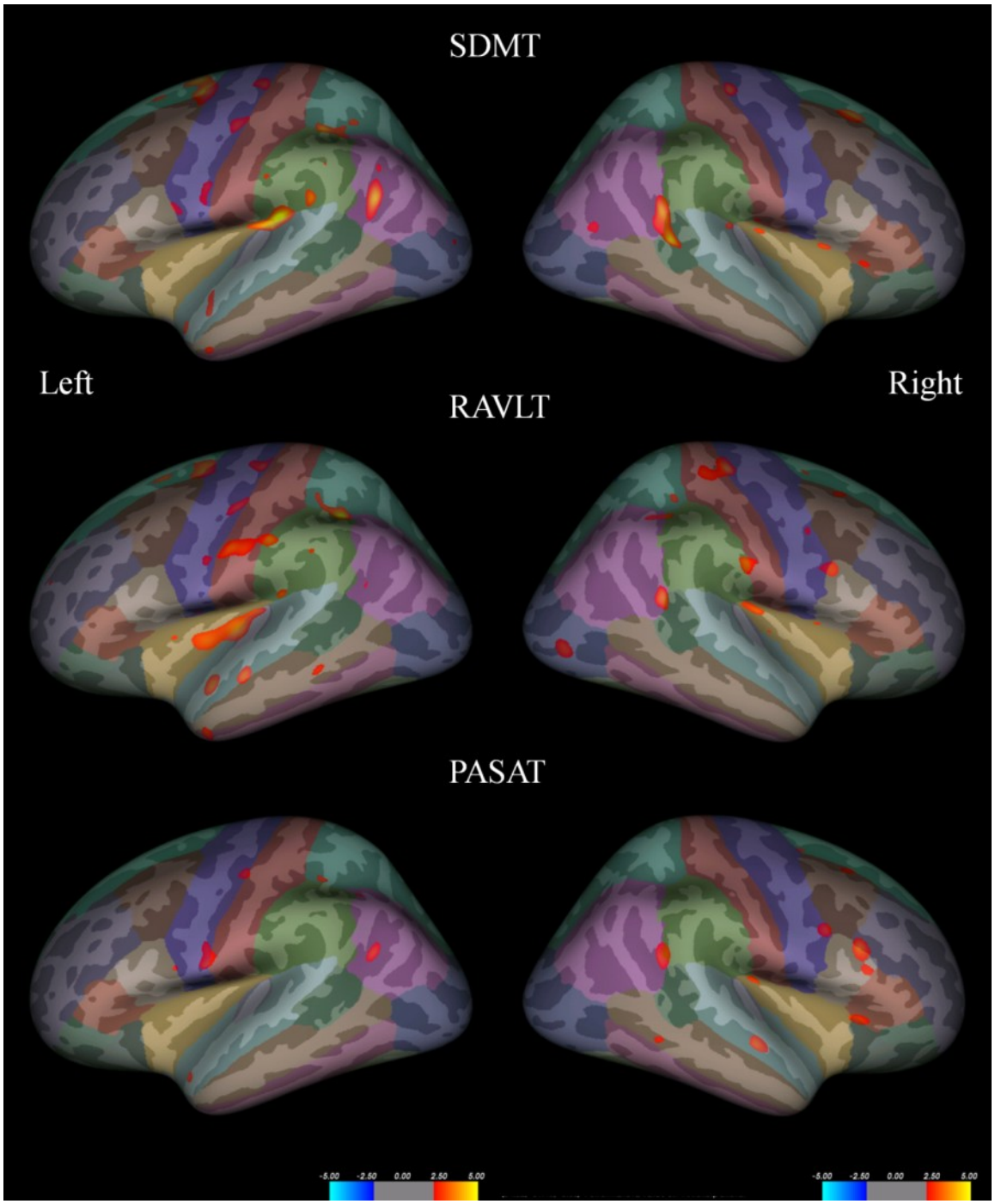

Figure 15. Freesurfer Qdec analysis displaying the statistically significant regions where thickness and each of the cognitive scores are correlated. Correlating clusters are located primarily in the caudal middle frontal (dark brown), pre-central (blue), precuneus (not shown), superior frontal (light turquoise), and supra-marginal (parrot green). Same color annotation as Figure 14.

5.4. Discussion

Multiple Sclerosis is often regarded as a cerebral white matter disease. Studies in recent years have provided evidence of gray matter pathology through histology and imaging. This chapter extended current understanding of the gray matter aspect of this "white matter" disease through quantitative structural imaging. In particular, the correlations between neuropsychological testing and both cortical and subcortical structures were examined. Our results showed widespread atrophy in both subcortical and cortical regions in brains of relapsing remitting multiple sclerosis individuals. Volume loss in selective subcortical gray matter (mostly in the basal ganglia) and widespread cortical regions correlated with worse cognitive performance in RRMS patients. Altogether, this morphological study provided a comprehensive characterization of GM involvement in MS and both cortical and subcortical GM contributions to cognition.

5.4.1. Evidence of gray matter abnormalities in multiple sclerosis

In line with previous reports (*56, 195, 196*), our analysis showed significant atrophy in several subcortical GM structures as well as in cortical regions in the frontal, parietal, and temporal lobes in RRMS patients, and confirmed the presence of global GM atrophy in MS patients compared to healthy controls. Atrophy of the GM reflects the ultimate consequence of tissue injury from various mechanisms. One hypothesized mechanism is that following axonal transection within the MS lesion, the distal segment of the axon undergoes Wallerian degeneration (*197, 198*), and eventually results in apoptotic death of the neuronal cell body. This slow dying-back or anterograde degeneration of the axon with cell shrinkage and/or cell death consequently leads to thinning of the GM. This is supported by studies where cortical thinning

was found to be associated with lesion load (*60, 199, 200*). However, GM atrophy can also be independent from WM pathology (*201, 202*). Direct involvement of GM pathology including demyelination, neuronal loss, inflammation, and iron deposition in the cortical, juxtacortical, and subcortical regions could also result in atrophy of such regions. Although the precise dynamics, incidences and mechanisms of GM pathology still remain unclear, GM lesions are often identified in multiple sclerosis brains (*203, 204*). Indeed, our DIR images (Figure 5) also presented evidence of GM lesions (although this was limited to only 5% of our patients). In addition, like many other studies (*50, 53*), WM atrophy was not observed in RRMS subjects, and global GM volume did not correlate with WM volume or WM lesion burden. These findings suggested that different pathological processes might be taking place in each of the tissue types and that GM pathology could be occurring independent from WM changes. On the other hand, our results also show that subcortical GM volumes of putamen and pallidum correlated with T2LV. The fact that some GM subcortical volume correlated with WM lesion burden could be because GM and WM are related pathological processes or they occur in parallel due to some mechanism which drives both GM and WM changes.

5.4.2. FreeSurfer as a tool for hippocampal volumetry in MS

To characterize GM involvement beyond global changes, a single automated segmentation algorithm called FreeSurfer was used to investigate volume changes in various gray matter structures. FreeSurfer was the choice for automated labeling of subcortical structures, which was validated against manual tracing previously on aged and pathological brains (*205-207*). Here, the performance of FreeSurfer was again compared to manual labeling of one subcortical gray matter structure - hippocampus. Recent imaging research has highlighted the role of hippocampal volume loss and its importance to cognitive functions in many

neurological disorders (*192, 208, 209*). In MS patients, extensive hippocampal demyelination was reported (*210*), which might lead to deficits in cognitive functions. While we have found significant volume reduction in other subcortical structures, we did not find significant hippocampal atrophy in our MS population compared to healthy controls, although lower hippocampal volume was observed. Furthermore, results from our manual tracing of hippocampus according to a standard protocol also did not find hippocampal atrophy, coinciding with results from FreeSurfer. However, hippocampal atrophy has been shown in previous MS studies (*89, 211, 212*). While one study using automatic segmentation technique showed volume loss in the cornu ammonis (CA1) region of the hippocampus in RRMS patients (*89*), the other showed smaller CA 2-3 and dentate gyrus volumes (*212*). The heterogeneity of our patient population (e.g., more variable disease duration and DMT) might have contributed to the variability in the measurements and have diluted the effect of volume change, whereas less variation in patient demographics is seen in other studies (*89, 212*). The differences in results between our study and the two studies may be related to different segmentation techniques utilized. Nevertheless, our results, similar to another MS study utilizing FreeSurfer, showed much greater percent differences in other subcortical structures than in hippocampus (*213*), which suggests that hippocampal atrophy might be less prominent in comparison to other subcortical structures in our RRMS population.

5.4.3. Subcortical atrophy as a cognitive marker in RRMS

Correlation analysis revealed that lower volumes in the putamen, pallidum, and caudate were predictive of MS cognitive measures. Amongst all subcortical GM structure studies, these three structures also had the greatest volume reduction in MS subjects. Atrophy in these subcortical gray matters may result from pathological changes including demyelination,

inflammation, and neurodegeneration that are often seen in *in vitro* studies (*214*), and these pathological changes are particularly frequent in the caudate nucleus. Atrophy of the caudate nucleus was also found using other image analysis techniques such as voxel-based morphormetry (VBM) (*215*) and manual parcellation (*59*). These regional GM losses may help explain cognitive deficits seen in MS patients. For example, the frontal-subcortial circuit, which relays through the caudate nucleus, is known to play a role in informational processing speed (*216*); disruption of this pathway could contribute to worsening cognitive performance in tasks such as the SDMT.

It should be noted that the putamen, pallidum, and caudate are components of the basal ganglia. Abnormalities in basal ganglia are often associated with cognitive deficits. Transcranial brain sonography, an imaging method displaying tissue echogenicity of the brain through the skull, found that abnormality in basal ganglia was associated with cognitive impairment in MS (*217*). Strong association of basal ganglia T2 hypointensity with cognitive dysfunction implies a role for basal ganglia iron deposition in neuropsychological impairment (*79*). Significant impairment of blood flow in the basal ganglia was present in MS patients with fatigue, which also influences cognitive performance (*218*). Moreover, metabolite abnormalities in the basal ganglia were observed in RRMS patients using 3D 1H-MRS when compared to healthy controls (*219*). Our study, along with these studies on basal ganglia, suggests that basal ganglia may be a worthwhile target as a cognitive marker in MS in future studies.

5.4.4. Cortical thinning distribution is associated differently with cognitive functions

Widespread cortical thinning, involving almost all the cortical areas, was observed in RRMS subjects. The widespread cortical atrophy found may lead to a failure of functional organization, which contributes to abnormal activation patterns associated with the disease and

to behavioral impairments, as suggested by functional studies (*178, 220*). Cognitive impairment is one clinical consequence of functionally-relevant pathological changes. Our study included RRMS patients with no restriction in degree of cognitive functions (*i.e.*, cognitively-normal and mildly impaired patients). But one study with a much larger sample size showed differences in the pattern of cortical thinning between cognitively normal and cognitively impaired patients(*221*). This study using FreeSurfer showed frontotemporal bilateral cortical thinning in cognitively normal RRMS compared to healthy controls, while widespread cortical thinning involving almost all cortical areas were observed in mild cognitively impaired RRMS compared to controls. Another study using VBM, however, has demonstrated correlation between the severity of cognitive impairment and GM loss in selective cortical regions such as the prefrontal cortex, superior parietal cortex, and precuneus in RRMS patients (*87*). Our findings also showed similar correlations between MS-related cognitive deficits and cortical atrophy in such areas. For example, the precuneus, part of the superior parietal lobe that is involved in episodic memory, visuospatial processing and consciousness, is correlated to worse performance on the SDMT, a test that measures visual information processing speed and sustained concentration. Correlations between worse performance on the SDMT test and cortical atrophy of the precuneus thus provided the link between this GM abnormality and this particular aspect of cognitive impairment. Similarly, performance on the RAVLT, a test for auditory verbal learning and memory, was associated with cortical thickness in the transverse temporal gyri, located in the primary auditory cortex. Although we have observed correlations between the PASAT, another cognitive test that is frequently used in MS, and cortical thickness, these correlations did not survive after a stricter statistical test of multiple comparison correction.

5.4.5. Limitations

While this study provided a comprehensive characterization of volume loss and its link to cognitive functions, the relatively small sample size for this study prevents a detailed analysis of the potential contribution of subject characteristics to brain atrophy, such as gender and education. The study would also be improved by inclusion of a larger sample with a wider range of domain specific cognitive testing which were not included, such as the continuous visual memory test (CVMT) for non-verbal memory (*222*), and the Wisconsin card sorting test (WCST) for executive function (*25*). Other factors, such as fatigue and depression, which could also affect cognitive performance were collected for some of the subjects in the present study and could be investigated in future analyses.

Another technical difficulty was with lesion segmentation. An underestimation of GM atrophy due to the wrong evaluation of the GM volume may result from WM lesion misclassification. It should be noted that the lesion segmentation results were carefully inspected before inputting to tissue segmentation and volume assessment in SPM. As for FreeSurfer analysis, a manual editing was performed to edit any misclassifications. It is possible that the definition of lesion included edema and inflammation which is difficult to differentiate based on the images we had available.

It should be noted that we did not go in depth in characterizing regional WM atrophy, which could exist in MR patients without global WM atrophy. However, as mentioned in Chapter 2, despite the fact that MS was initially considered a classic WM disease, WM atrophy is relatively rarely reported as compared in GM atrophy (*223*). Moreover, GM atrophy is more often found in patients in earlier stages such as relapsing remitting MS, whereas WM atrophy is

more often found in patients in more severe stages such as secondary progressive and benign MS (*223*).

Finally, the lack of association between MRI and PASAT could be due to the limitations of the PASAT test itself. During the PASAT examination, one needed to quickly perform mathematically calculation, which could be influenced by the subject's IQ, education, and familiarity to the test, which were not controlled for in this thesis. Improvement of test performance due to practice effect, as shown in previous studies (*224*), especially for those patients with longer disease duration, could have obscured the correlation. Indeed, the SDMT (a test that has demonstrated consistent associations with MR modalities) was suggested as an alternative for PASAT (*18, 225*).

5.5. Summary

In this chapter, we presented the volumetric GM aspect of multiple sclerosis, a disease traditionally thought of as a white matter disease. Using several structural imaging and analysis methods, we were able to identify various regions with GM abnormalities as indicated by atrophy and GM lesions in multiple sclerosis, thus advancing our understanding of the disease mechanism. There are also distinct regional patterns of GM atrophy that are associated with different neuropsychological tests that could help toward the prediction of cognitive impairment in MS.

Chapter 6

Diffusion Tensor Imaging and Cognitive Function in MS

While in Chapter 5, we studied GM extensively, WM abnormalities should not be neglected. The functional connection between WM pathology and cognitive impairment will be examined in this chapter using diffusion tensor imaging. It should be noted that some of the results presented in this chapter have been submitted to NeuroImage as an original article.

6.1. Introduction

White matter tissue pathology in MS leads to multiple neurologic deficits including cognitive and neuropsychiatric impairments (*15, 226-229*). A technique that can noninvasively capture subtle changes in the fiber structure would therefore be useful in understanding disease progression, and potentially, in predicting clinical outcome. As discussed in Chapter 3, diffusion tensor imaging (DTI) is a magnetic resonance imaging (MRI) technique that enables the measurement of restricted diffusion of water in tissue (*99*), which is a unique property of tissue water within myelinated white matter axons. Thus, it is possible to derive quantitative metrics related to white matter fiber integrity from DTI. DTI has been used increasingly in MS over the last few years due to its sensitivity to white matter injury (*93-95*), and has helped better delineate the mechanisms underlying tissue injury and that are responsible for neurological dysfunction. For example, MS-associated clinical disability is correlated with DTI measures of reduced

functional connectivity between cortical-cortical or cortical-subcortical regions, implicating disruption of critical white matter tracts as an important part of the pathophysiology (*172, 230*). Moreover, tissue injury in normal appearing white matter regions may only be detectable by advanced techniques such as DTI (*5, 231, 232*). Advanced imaging techniques such as DTI can capture subtle changes in the white matter and improve our understanding of the pathophysiology of cognitive impairment in MS.

In this chapter, we took advantage of advanced DTI analysis methods to identify areas of damaged tract integrity in relapsing remitting multiple sclerosis (RRMS) patients. In contrast to most prior studies using an MS population with mixed subtypes, this chapter focused on RRMS, to avoid differential effects due to pathological heterogeneity and cumulative effects of disability progression. In the current chapter, we also utilized a recently developed DTI analysis method, tract-based spatial statistics (TBSS), which has improved sensitivity to identify areas of disrupted WM tract integrity in RRMS. TBSS is a non-hypothesis driven technique that enables DTI data analysis in a voxelwise fashion (*233*), minimizing multi-subject registration errors by carrying out the analysis in a common skeleton of major WM structures. TBSS has been applied to a few MS DTI studies; however, prior studies utilized cluster-based thresholding for identifying regions with significant cognitive associations (*113, 234*). In contrast, this study used a new, threshold-free technique (TFCE) does not require an (arbitrarily chosen) cluster size threshold or spatial smoothing of the data. The overall goal is to examine DTI abnormalities in individuals with MS compared to healthy controls, as well as the associations between DTI abnormalities and impairments in cognitive function.

6.2. Methods

6.2.1. Subjects and clinical assessments

Thirty-seven individuals with RRMS and 20 healthy controls participated in this study. Please refer to Chapter 4 for details on subject information, neurological and cognitive assessments.

6.2.2. MR data acquisition

3D T1-weighted SPGR, T2-weighted FLAIR, and DTI images were acquired for this study. 3D T1-weighted SPGR images were used for tissue segmentation and volumetrics. T2-weighted FLAIR images were used for lesion quantification. DTI images were used for histogram, fiber tractography, and TBSS analysis. Please refer to Chapter 4 for details on MR data acquisition.

6.2.3. MR data analysis

DTI data were analyzed using three methods: 1) histogram analysis to provide global assessment of diffusion properties for white matter and lesion, 2) fiber tractography to reconstruct cognitively-relevant fibers, and 3) tract-based spatial statistics, a non-hypothesis driven technique that enables the DTI data analysis in a voxelwise fashion (*233*), also minimizing multi-subject registration errors by carrying out the analysis in a common skeleton (shared by all subjects) of major white matter structures.

6.2.3.1. Histogram Analysis

The individual DTI scans were first corrected for eddy current induced image distortions and motion artifacts using a 3D affine registration algorithm from the Automated Image

Registration (AIR) package (*235*). Whole brain DTI maps for the mean diffusivity (MD) and fractional anisotropy (FA) were calculated in DTI Studio 3.0.1 (*236*), and exported for further analysis. DTI maps were then co-registered with the segmented anatomical mask. Whole brain histogram analysis was performed using corresponding voxels from control white matter (CTWM), normal appearing white matter in MS subjects (NAWM), and T2 lesions as derived from FLAIR images. For each subject, histograms containing 200 bins were generated for FA and MD. Each bin was then normalized by the total number of voxels contributing to the histogram. The DTI histograms were smoothed with a 5 point moving average method. The following features of each histogram were extracted: peak location, peak height, and peak width. Mean histograms for each of the DT parameters were also calculated by averaging the individual histograms obtained from each subject group.

6.2.3.2. Fiber Tractography

The pre-processed data were also further analyzed using fiber tractography. Manual inspection of images and the AIR/motion correction matrix did not show differences between the two subject groups. For 3D tract reconstruction, the fiber assignment by continuous tracking or FACT method (*237*) was used with a FA threshold of 0.2, and tracking stopped with angles larger than 40°. The fiber tracking was performed by DTI Studio. A dual-ROI approach was used to reconstruct tracts of interest which exploits existing anatomical knowledge of tract trajectories. Tracking was performed from all pixels inside the brain (brute-force approach). DTI data matrix was zero-filled from 220x220 to a standard matrix of 256x256mm. The posterior portion (hippocampal part) of cingulum (CGH) and the fornix (FX) were examined using the ROI drawing strategy. These two fibers were of interest because they are part of the limbic system that plays an important role in cognitive functioning (*238, 239*). The fiber reconstruction

protocol was as follows: 1) Cingulum (hippocampal part): The inferior segment of the cingulum runs along the ventral aspect of the hippocampus. For the first ROI, a coronal plane in the middle of the splenium of corpus callosum was selected using the mid-sagittal plane, and the cingulum below the corpus callosum was delineated, and the second ROI was drawn to include the cinglum on a coronal slice anterior to the pons using the mid-sagittal plane; 2) Fornix: The first ROI was placed around each crus of the fornix at the level where their fusion is visible, whereas the second ROI was placed at the level of the cerebral peduncles encompassing the hippocampal tail. Examples of ROI placement are shown in Figure 16.

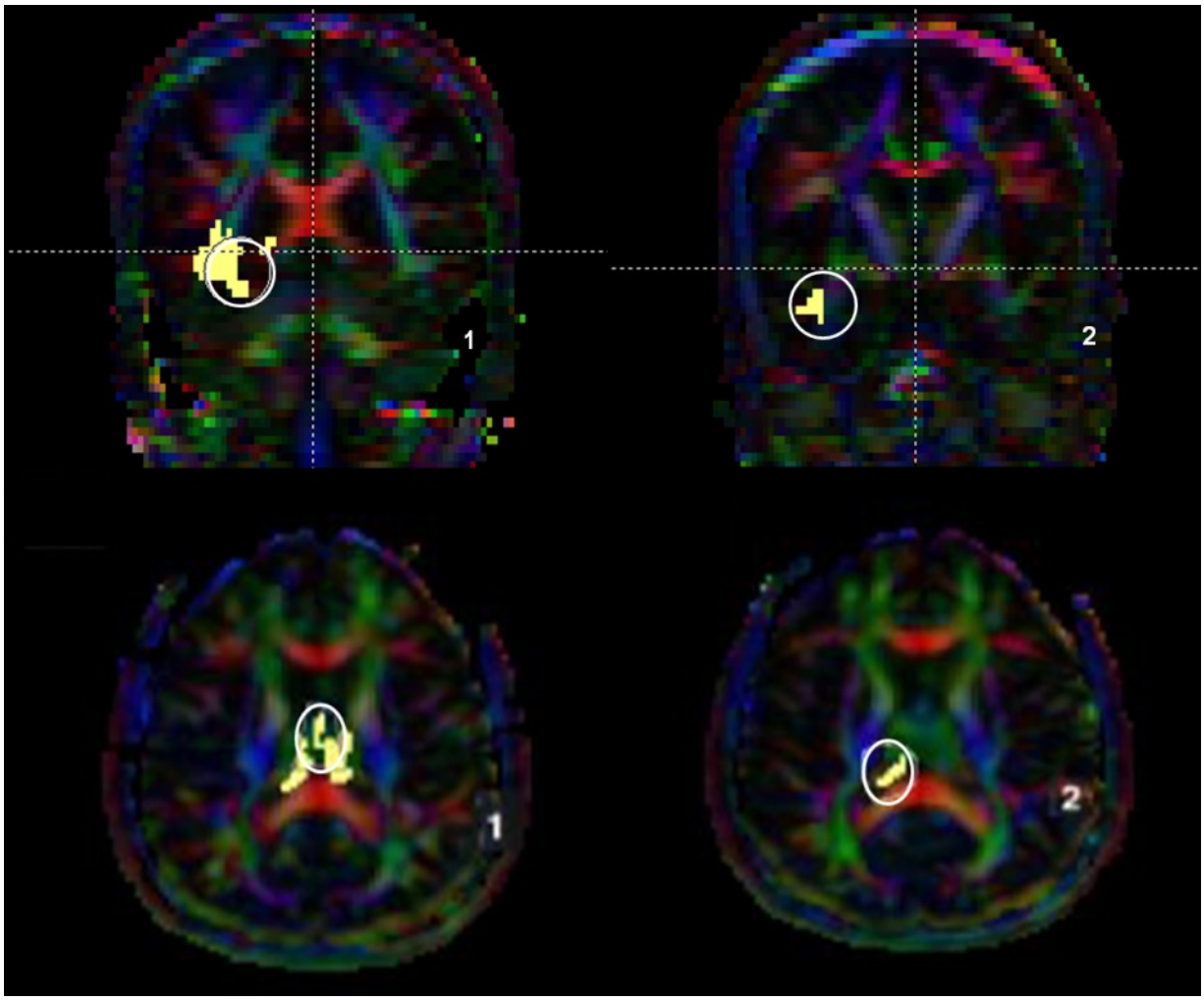

Figure 16. Location of the ROIs for fiber tractography. Both the cingulum in the hippocampal part (CGH) and the fornix (FX) were tracked by two ROIs with "AND" logic (meaning fibers passing through both ROIs). Colormaps showing examples of such ROIs (circles) and fibers tracked with ROIs: first (top-left) and second (top-right) ROI for tracking the cingulum in the hippocampal part (CGH) on two coronal slices; and first (left-bottom) and second (right-bottom) ROI for tracking the fornix (FX) on two axial slices

6.2.3.3. Tract-Based Spatial Statistics

All DTI images were processed following the TBSS pipeline, part of FMRIB Software Library (FSL, http://www.fmrib.ox.ac.uk/fsl). Briefly, images were preprocessed to correct for motion and eddy current distortion, and the diffusion tensors were then fitted to each voxel. The

four primary quantitative DTI measures, fractional anisotropy (FA), mean diffusivity (MD), axial diffusivity (AD), and radial diffusivity (RD), were then derived voxelwise. The TBSS registration then nonlinearly transformed the FA images using the FMRIB58_FA standard-space images (http://www.fmrib.ox.ac.uk/fsl/data/FMRIB58_FA.html) as the target, and the tract skeletonization process was subsequently performed using a lower threshold of FA of 0.2 to exclude non-WM voxels. The final WM skeleton is a representation of the WM tract geometry common to the entire group of subjects, including both patients and controls. Similar processes were applied to non-FA data (*i.e.*, MD, AD and RD maps) using the individual registration and projection vectors obtained in the FA nonlinear registration and skeletonization stages. The effect of white matter lesions on the skeletonization process was investigated by generating additional TBSS skeletons for MS subjects only and for control subjects only, and comparing these skeletons in terms of absolute number of pixels for the presence of missing pixels in the MS group within the major tracts.

To examine whether the distribution of MS lesions overlapped with DTI abnormalities (and the presence of DTI changes in NAWM), a lesion probability map was created to overlay onto the TBSS DTI maps. Volumetric analysis was performed using methods described in Chapter 5. The mean lesion probability maps were created by first registering the SPGR images to MNI 152 space (*240*), then applying this same transformation matrix to each of the co-registered binarized lesion masks. Lesion maps were then averaged to create a single lesion probability map. The threshold for lesions in overlay figures was set at 30%, *i.e.*, identifying those voxels demonstrating lesions in at least 30% of patients.

In the past, there has been a general assumption that white matter injury in MS is mostly associated with T2 lesions and the question of whether or not there is injury within the normal-

appearing white matter and whether or not such injury is independent or secondary to T2 lesions is an ongoing debate in the field. To investigate this matter further, correlation analysis was performed, exploring the association between DTI changes and T2 lesion load. Partial correlations between FA and T2 local lesion load were calculated within each anatomical region, using mean FA either within the entire skeletal region or within NAWM-only (because lesions can occur outside of the skeleton, mean FA in NAWM could not utilize TBSS but was calculated across each anatomical region, as determined by the JHU WM atlas, based on the white matter mask). Similarly, the associations of regional NAWM changes with cognitive performance were investigated by calculating partial correlations between mean FA, within each anatomical region and the three cognitive tasks.

6.2.4. Statistics

Statistical analysis was done for histogram and TBSS measures. For histogram analysis, differences between histogram properties (*i.e.*, peak width, peak height, and peak location) of CTWM, NAWM, and lesion maps were compared using ANOVA, where significance is indicated with $p < 0.05$.

For TBSS analysis, whole brain FA skeletons were compared between patients and controls using a permutation algorithm (*randomise* from the FSL library) (*241*) in a voxelwise fashion. Briefly, a permutation method calculates the value of the statistic for each voxel based on the specified null hypothesis and statistic of interest, builds the permutation (randomized) distribution, and uses the permutation distribution to determine if voxel-level statistic is correctly labeled and the labeling is then used for thresholding statistic maps. The permutation analysis was done with 5000 permutations using threshold-free cluster enhancement (TFCE) ($p \leq 0.01$) (*242*) while treating age as a nuisance covariate, and multiple comparisons were accounted for

by controlling for family-wise error (FWE) rates. TFCE works by using the spatial information inherent in the data to calculate statistical maps which are not only dependent on the height of the signal (e.g., FA), but also on the level of spatial support which the signal has (i.e., how many of the neighboring voxels also have similar signal). So the final TFCE statistic is based on the spatial information in the image itself, and it therefore does not require arbitrary pre-smoothing of the images and does not depend on the initial cluster forming threshold. Group comparison using TFCE was also compared with a cluster-based thresholding method (by using the null distribution of the max cluster size, $t > 2$, $p \leq 0.01$) to examine differences in the two statistical methods in detecting white matter changes in the MS patient group. Mean skeletal FA values were extracted for all subjects. To compare overall group differences in diffusivity in relation to MS-related FA abnormality, mean MD, AD and RD were derived for each subject, restricted to voxels with significant FA reduction compared to controls, as identified above using TFCE. Student's t-test was used for group comparisons when data was normally distributed; otherwise, the Mann-Whitney U test was used. For RRMS patients, voxelwise correlation between FA and cognitive scores was performed within the subgroup of voxels identified as significantly abnormal compared to healthy controls in the initial group comparisons, using *randomise* and TFCE ($p \leq 0.05$). Similar correlation analysis was repeated for the subset of 15 controls who underwent neurocognitive testing, to determine whether correlations are specific to cognitive deficits related to MS or if they are generalizable to normal anatomical/functional pathways.

To quantify the degree of white matter involvement in correlations between DTI and cognitive measures, individual skeletal regions were identified based on anatomical or functional groupings and the percentage of each region with significant DTI-cognitive correlations was then calculated. To accomplish this, the skeletal regions with significant group differences were

located and labeled anatomically by mapping the TBSS statistical map from TFCE to the JHU-ICBM-DTI-81 white matter atlas (*243*). To limit the number of regions reported, the 46 fiber tracts in the original atlas were then grouped into larger fiber bundle categories based on their anatomical and functional associations. The fiber bundles examined were 1) association fibers: cingulum (cingulate gyrus and hippocampal portions), external capsule, fornix (column, body, and cres), sagittal stratum (including inferior longitudinal fasciculus and inferior frontal-occipital fasciculus), superior fronto-occipital fasciculus, and superior longitudinal fasciculus; 2) commissural fibers: corpus callosum (body, genu and splenium), and uncinate fasciculus; 3) projection fibers: corona radiata (anterior, posterior, and superior), internal capsule (anterior limb, posterior limb, and retrolenticular part), and posterior thalamic radiation (including optic radiation); 4) brainstem tracts: cerebellar penduncle (inferior, superior, and middle), cerebral peduncle, corticospinal tract, and medial lemniscus. The degree of fiber involvement within each fiber bundle was examined, by calculating the percentage of voxels with significant correlations to the total number of voxels showing FA reduction. Theoretically, one could transform a t-statistic to a correlation coefficient using the expression $r = t/\sqrt{t^2 + v}$r where v represents the error or degrees of freedom of the raw t-statistic. However, we could not generate such correlation coefficient maps voxelwise since our results were presented using TFCE, which does not define a t-threshold and only provides a corrected p-value map instead of a raw t-statistical map. Instead, partial correlation coefficients between mean abnormal skeletal FA values in each of the fiber bundles and each of the neuropsychological scores were extracted, controlling for age. Finally, to determine the degree to which normal appearing white matter is involved in these processes, correlations between FA and cognitive tests were investigated within the NAWM for each anatomical region.

6.3. Results

6.3.1. Demographic and disease characteristics

Table 3 shows the demographic, clinical, and cognitive test performances of the two study groups. One individual with MS had diffusion rather than diffusion tensor image acquired, and was therefore not included in the DTI study. MS participants relative to controls had global brain atrophy ($p < 0.01$) and worse scores across all cognitive tests, as also shown in Chapter 5.

6.3.2. Whole brain histogram comparisons

Mean diffusivity and fractional anisotropy histograms of CTWM, NAWM, and lesion are reported in Figure 17. Compared with CTWM, the average FA histogram of NAWM was shifted toward lower FA with a higher height (indicating a tighter FA distribution where voxels have lower FA values), while the lesion histogram was shifted toward an even lower FA. For MD, the average MD histograms of CTWM and NAWM were very similar, with NAWM slightly shifted toward higher MD. The average lesion histogram, however, had a lower peak height with broader MD distribution compared to both CTWM and NAWM, and the distribution of voxels was shifted to the right with higher MD values.

All MD and FA histogram-derived features of lesions were significantly different ($p < 0.05$) from CTWM andFA peak height of lesions were significantly different from NAWM. The FA peak width and MD peak height of the average histogram of NAWM were significantly different as compared to CTWM. Figure 18 shows comparisons between the histogram characteristics of healthy control and RRMS patients.

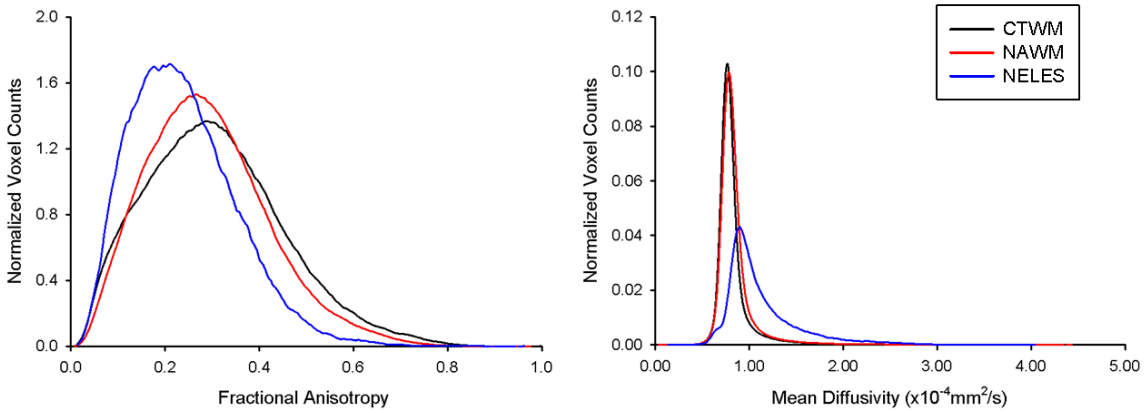

Figure 17. Average fractional anisotropy (left) and mean diffusivity (right) histograms of the non-lesion white matter from control subjects (black) and patients with MS (red), and MS lesions (blue). FA histograms (from CTWM to NAWM to NELES) became narrower and higher as the peak positions shifted to lower values. MD histogram of NELES was wider and had lower peak height and higher peak position than CTWM and NAWM. No obvious difference was observed between the MD histograms of CTWM and NAWM, except a very slight shift of the MD histogram of NAWM to higher values with a lower peak height as compared to CTWM.

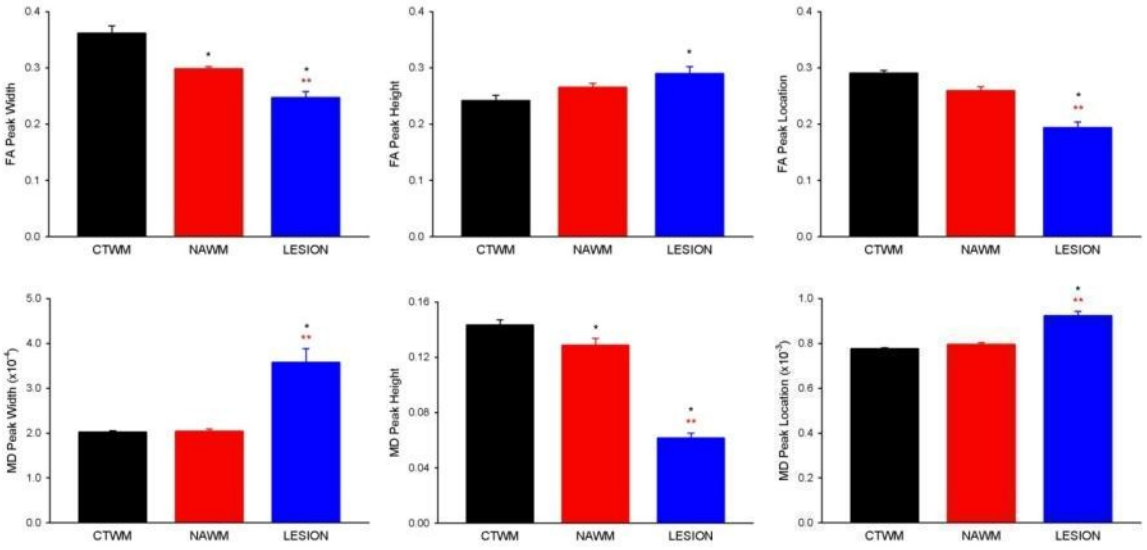

Figure 18. Comparison of DTI histogram characteristics. Summary data showing group averages (mean $\pm$ SE) of individual FA (top) and MD (bottom) histogram characteristics from RRMS (n=37) and control (n=20) subjects. As expected, lesion histogram characteristics are significantly different from CTWM and NAWM. Histogram analysis also revealed altered FA and MD properties in NAWM compared to CTWM. *$p \leq 0.05$ for comparisons versus CTWM, and **$p \leq 0.05$ for comparisons versus NAWM.

6.3.3. Fiber tractography

Another DTI analysis method we used was fiber tractography; however, we were not able to reconstruct a complete CGH through the standard tracking protocol in 20% of control subjects and 20% of MS subjects. For those subjects where CGH were constructed, no statistical significance difference in FA or MD values between the control and the MS groups, though a trend of decreased FA (difference of 0.1) was found in the MS group. Reconstruction was unsuccessful mainly because tracking stopped in the middle of the tractography path resulting in very short fiber bundles and/or an insufficient number of fibers (usually less than 5). Tractography of the FX was even harder, which resulted in unsuccessful reconstruction in 30% of controls and in 60% of MS subjects. Difficulties in reconstruction arose due to the absence of the crus of fornix, and in some cases the column of fornix could not be tracked. Successful examples of CGH and FX tractography are shown in Figure 19

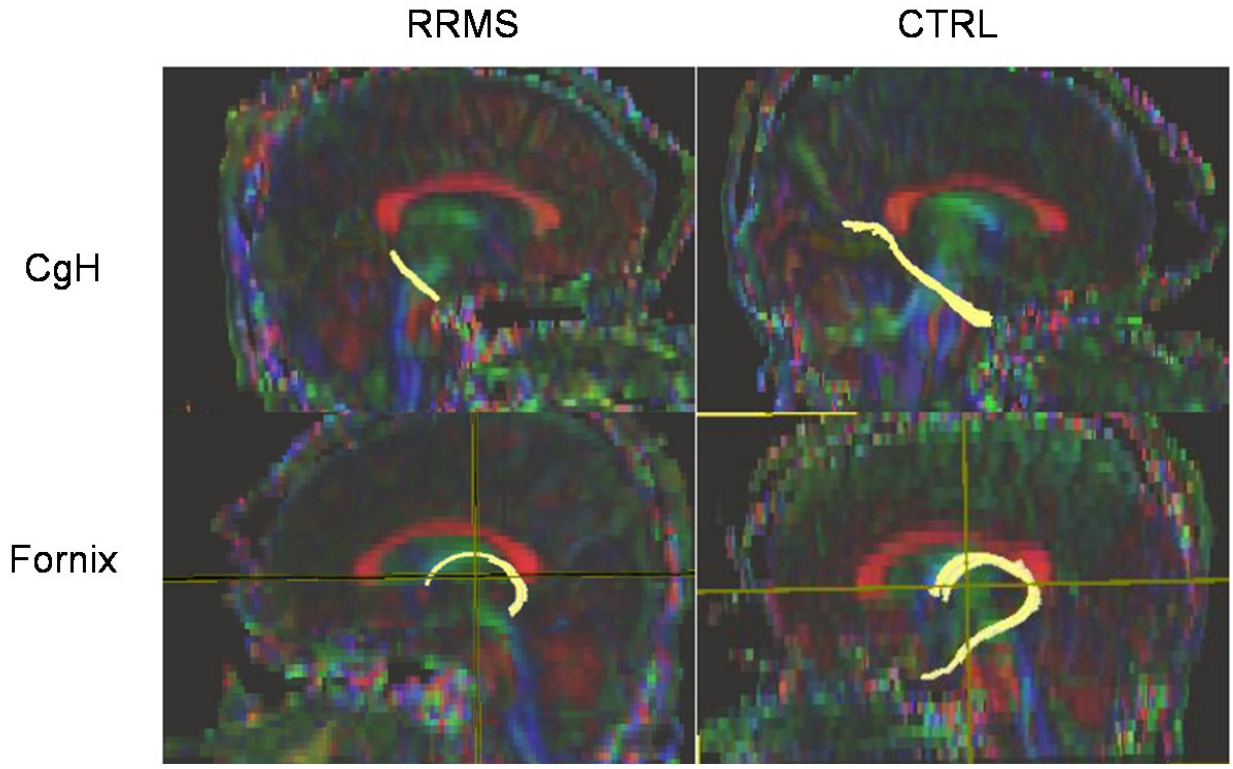

Figure 19. Illustration of fiber tractography results. Using the predefined ROIs, fiber tractography for posterior cingulum (top) and fornix (bottom) were unsuccessful in majority of the RRMS patients, most likely due to a small number of fibers (fiber atrophy), and short fibers (presence of lesion on tracking path). The examples shown here demonstrate very thin and short fibers in the RRMS patients (left) as compared to control subjects (right).

6.3.4. DTI-TBSS group comparisons

The whole brain skeletal FA was significantly reduced in the MS group as compared to the healthy control group (0.40±0.03 versus 0.43±0.01, $p < 0.01$). In the MS group, global FA reduction correlated with EDSS, BPF, and lesion volumes ($p < 0.01$). Widespread reduction in FA among the MS group was noted across the skeleton (Figure 20) using either cluster-based thresholding or threshold-free cluster enhancement, although there were some differences. In particular, TFCE, but not cluster-based thresholding (at the same $p \leq 0.01$ level) detected

reductions in FA among the MS group in the left cingulum (hippocampal portion), right external capsule, right fornix (cres), superior fronto-occipital fasciculus, right uncinate fasciculus, anterior limb of internal capsule, cerebellar peduncle, right cerebral peduncle, corticospinal tract, and medial lemniscus. Figure 20 shows the fiber bundles with reduced FA by TFCE. For those voxels with reduced FA, mean diffusivity was significantly increased in the MS relative to the healthy control group (0.78±0.02 versus 0.82±0.04, $x10^{-3}$ mm^2/s, $p < 0.01$), predominately due to significantly increased radial diffusivity was significantly increased in MS participants as compared to controls (0.62±0.05 versus 0.57±0.02, $x10^{-3}$ mm^2/s, $p < 0.01$), whereas there was no statistically significant difference in axial diffusivity (1.22±0.03 versus 1.21±0.02, $x10^{-3}$ mm^2/s, $p = 0.36$) (Figure 21). No significant regions with increased FA were found in the MS as compared to the control group.

No major differences were found between the TBSS skeletons generated for control subjects alone or for all subjects as compared to that generated for MS subjects alone (Table 6). In particular, all of the major tracts described here were found to have fewer than 6% of its pixels missing in the MS-only skeleton, with the exception for the superior fronto-occipital fasciculus, likely due to the small size of this tract (only 126 pixels total). There was no significant correlation between regional lesion load and regional changes in skeleton size for the MS group, indicating that lesions were not adversely affecting the TBSS skeletonization process.

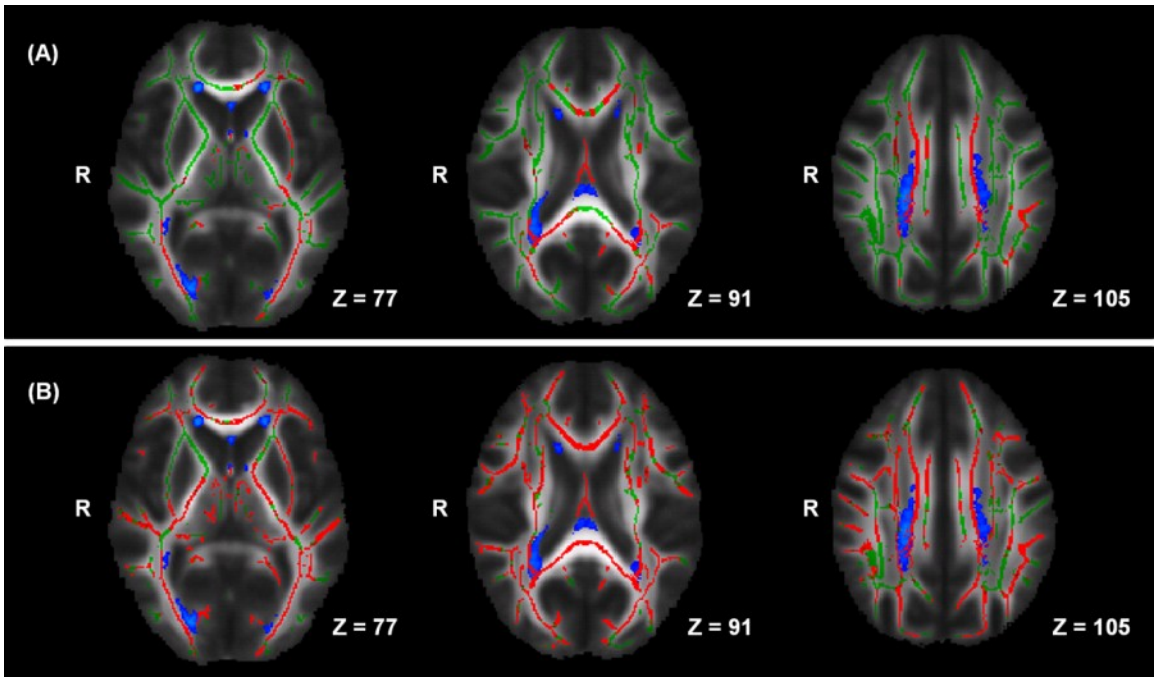

Figure 20. FA reduction in RRMS as demonstrated by TBSS. Axial images showing significantly reduced FA (red) in RRMS patients as compared to control subjects ($p \leq 0.01$), overlaid on the TBSS skeleton mask (green) within which the TBSS analyses were carried out. The lesion probability map (blue) shows the spatial distribution of the regions in which at least 30% of patients had demonstrated lesions on FLAIR. All data is overlaid on the mean FA map across both groups (grayscale). TBSS analyses corrected for multiple comparisons using both the cluster-based thresholding (A) and the threshold-free cluster enhancement (TFCE) (B) methods, illustrating the increased areas of change which can be delimited using the TFCE method. All TBSS analyses treated age as covariate.

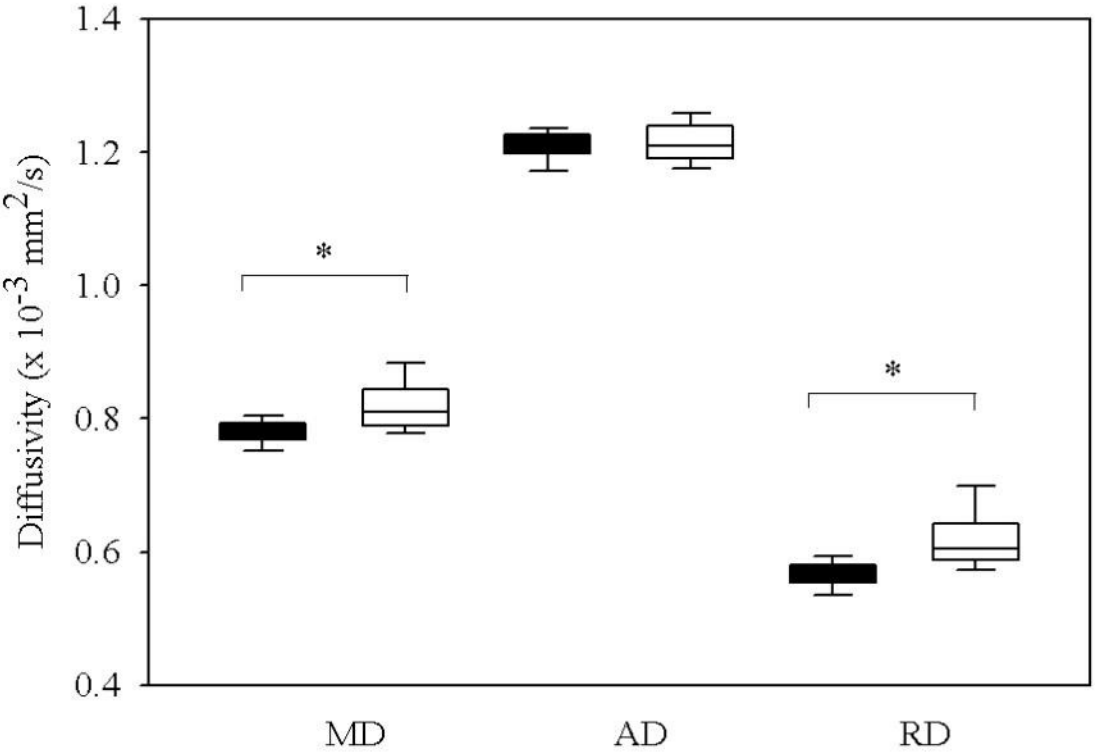

Figure 21. Comparison of diffusion characteristics for voxel with reduced FA. Reduced FA was accompanied by increased mean diffusivity, predominantly due to significant increased radial diffusivity (diffusion across fiber) but not axial diffusivity (diffusion along fiber). Filled bars indicate mean and range of diffusion values (MD: mean diffusivity, AD: axial diffusivity, RD: radial diffusivity) for healthy controls; empty bars indicate mean and range of diffusion values for RRMS patients. Symbol * indicates significance at $p < 0.05$.

Fiber Bundles	All Subjects	MS-only	CTRL-only	MS/CTRL
Superior longitudinal fasciculus	2868	2990	2777	108%
External capsule	1822	1834	1778	103%
Cingulum	1347	1349	1320	102%
Sagittal stratum	1024	1068	962	111%
Fornix	797	786	791	99%
Superior fronto-occipital fasciculus	126	78	169	46%
Corpus callosum	7470	7470	7469	100%
Uncinate fasciculus	136	133	137	97%
Corona radiata	7520	7570	7547	100%
Internal capsule	4891	4923	4834	102%
Posterior thalamic radiation	2291	2251	2307	98%
Cerebellar peduncle	4138	4129	4093	101%
Cerebral peduncle	1256	1282	1171	109%
Corticospinal tract	802	776	828	94%
Medial lemniscus	432	407	429	95%

Table 6. Comparison of TBSS skeleton generated for control subjects only, for MS subjects only, and for all subjects. Numbers indicate the number of voxels making up the tract within the skeleton generated using all subjects, control subjects alone, or MS subjects alone; percentages indicate the fraction of voxels in each tract for the MS subject skeleton compared to number of voxels in the control subject skeleton.

6.3.5. DTI-TBSS correlations with cognitive assessment

As shown in Figure 22, among the MS group, FA reduction was significantly correlated with each of the three cognitive scores in the voxelwise analysis. Among the cognitive tests, reduced FA correlated most strongly and consistently with lower with the SDMT scores, indicating that widespread areas of cerebral dysfunction are associated with deficits in cognitive processing speed and visual working memory. Significant correlations with cognitive scores occurred within all of the association fibers, the commissural fibers, and the projections fibers, but not within tracts in the brainstem (except for the cerebral peduncle). The posterior thalamic radiation, the sagittal stratum, and the corpus callosum had the most extensive FA reduction, and

displayed the strongest correlations with all of the cognitive tests; examples of such correlations are shown in Figure 23.

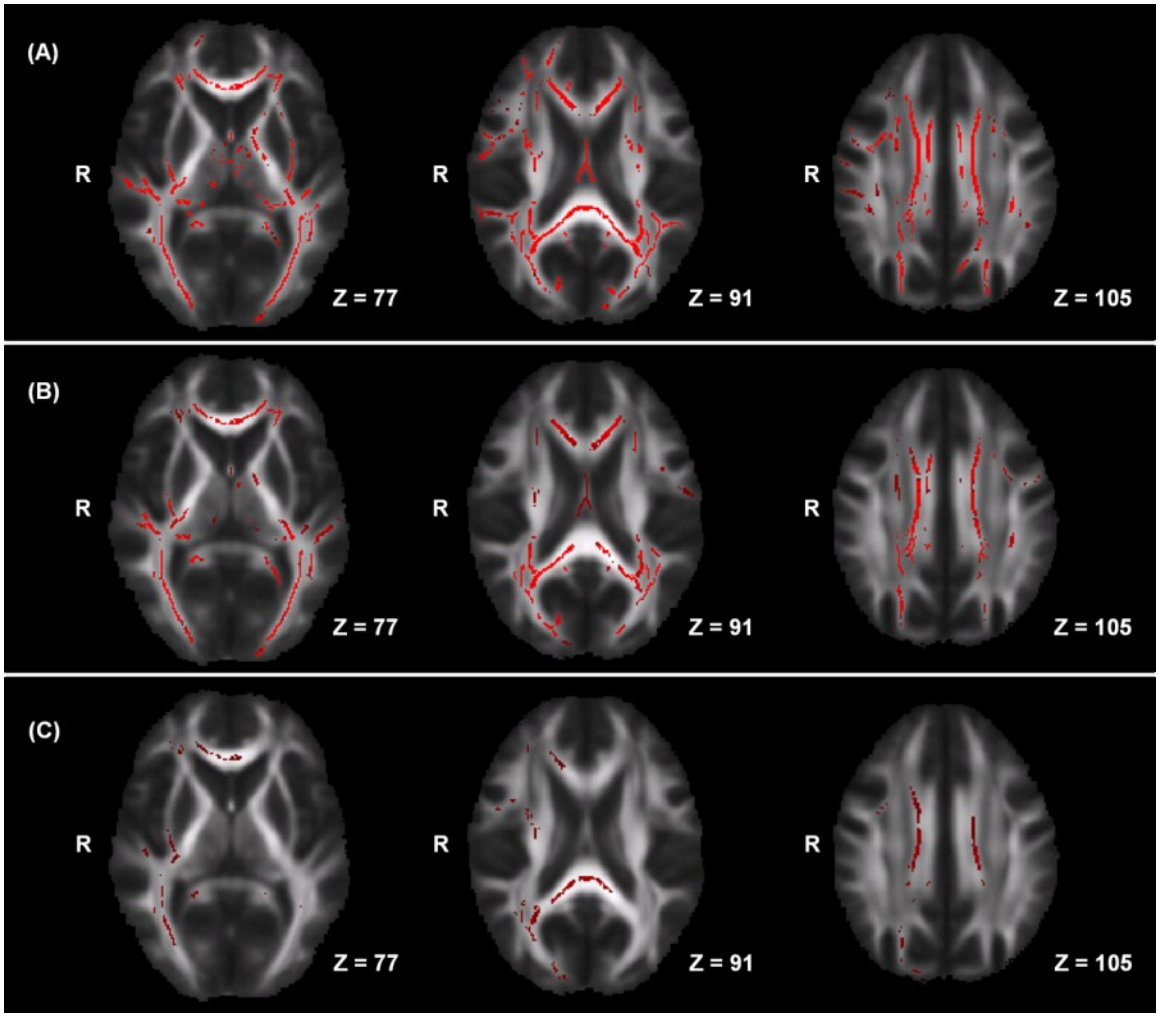

Figure 22. The association between cognitive measures and reduced FA in the TBSS skeleton in RRMS patients. The red voxels in the axial images show those areas of reduced FA in the patients (from Figure 20B) that also significantly correlate with each of the cognitive measures: A: SDMT; B: RAVLT; C: PASAT. The TFCE method was used to correct for multiple comparisons, while treating age as a covariate ($p \leq 0.05$). While PASAT is a widely used technique in clinical practice, the weakest correlations were found between FA and PASAT.

With respect to the degree of white matter involvement, a large number of tracts showed involvement of 50% or more of the voxels within the tract (see Table 7). For SDMT these were: anterior and posterior corona radiata, superior corona radiata (right), corpus callosum (body, genu and splenium), cingulum (cingulated gyrus portion), cingulum (right hippocampal portion),

external capsule (left), fornix (column, body, and cres), posterior thalamic radiation, sagittal stratum, and uncinate fasciculus. The distribution of voxels significantly correlated with the RAVLT overlapped with those correlated with SDMT at the anterior corona radiata (left), corpus callosum, hippocampal cingulum (right), fornix, posterior corona radiata, posterior thalamic radiation, sagittal stratum peduncle. In contrast to the widespread associations between reduced FA in fiber tracts and the SDMT and RAVLT, significant correlations with the PASAT were only present in the posterior thalamic radiation (right), sagittal stratum (right), and in the splenium of corpus callosum (see details in Table 8). Figure 23 are scatter plots showing FA and cognitive correlations for the major tracts. Furthermore, similar patterns of correlations were found between radial diffusivity and cognitive measures (*i.e.*, SDMT and RAVLT) in tracts with reduced FA using TBSS, but no correlations were found with axial diffusivity (Figure 24). Similar analysis in the control group showed significant correlation between FA and RAVLT, however, these correlations were only in a small fraction of pixels and much lower correlation strengths compared to correlation in the MS group. No significant correlations were found between FA and either SDMT or PASAT measures in the control group.

Fibers	Skeletal Size (Voxel)	FA Reduction Size	SDMT %	RAVLT %	PASAT %
Association fibers					
Cingulum (cingulate gyrus) L	402	79%	87%	11%	2%
Cingulum (cingulate gyrus) R	403	78%	98%	57%	11%
Cingulum (hippocampus) L	252	27%	94%	0%	0%
Cingulum (hippocampus) R	290	52%	100%	100%	66%
External capsule L	1419	65%	77%	6%	0%
External capsule R	1330	25%	96%	80%	63%
Fornix (column and body of fornix)	199	100%	99%	85%	0%
Fornix (cres) L	347	95%	97%	75%	0%
Fornix (cres) R	251	95%	99%	91%	11%
Sagittal stratum L	475	85%	95%	83%	15%
Sagittal stratum R	549	79%	99%	89%	69%
Superior fronto-occipital fasciculus L	65	94%	30%	0%	0%
Superior fronto-occipital fasciculus R	61	93%	0%	0%	0%
Superior longitudinal fasciculus L	1384	59%	56%	60%	0%
Superior longitudinal fasciculus R	1484	54%	71%	13%	16%
Commissural fibers					
Corpus callosum (body)	3244	97%	97%	85%	35%
Corpus callosum (genu)	1782	88%	98%	93%	33%
Corpus callosum (splenium)	2444	93%	98%	79%	55%
Uncinate fasciculus L	77	88%	78%	0%	0%
Uncinate fasciculus R	59	51%	100%	0%	0%
Projection fibers					
Anterior corona radiata L	1669	75%	88%	76%	4%
Anterior corona radiata R	1593	57%	95%	67%	40%
Posterior corona radiata L	760	82%	83%	64%	3%
Posterior corona radiata R	838	86%	87%	87%	20%
Superior corona radiata L	1264	62%	72%	27%	7%
Superior corona radiata R	1396	79%	63%	49%	34%
Internal capsule (anterior) L	805	42%	86%	31%	0%
Internal capsule (anterior) R	831	17%	3%	0%	0%
Internal capsule (posterior) L	866	54%	53%	34%	0%
Internal capsule (posterior) R	851	54%	18%	21%	2%
Internal capsule (retrolenticular) L	758	64%	72%	84%	0%
Internal capsule (retrolenticular) R	780	48%	79%	74%	56%
Posterior thalamic radiation L	1121	98%	98%	90%	20%
Posterior thalamic radiation R	1170	97%	98%	95%	64%
Tracts in brainstem					
Cerebellar peduncle (inferior) L	284	53%	0%	0%	0%
Cerebellar peduncle (inferior) R	281	58%	0%	0%	0%
Cerebellar peduncle (middle)	2786	66%	1%	0%	0%
Cerebellar penduncle (pontine crossing)	310	84%	0%	0%	0%
Superior cerebellar peduncle L	222	34%	0%	0%	0%
Superior cerebellar peduncle R	255	47%	0%	0%	0%
Cerebral peduncle L	646	72%	53%	35%	0%
Cerebral peduncle R	610	49%	54%	57%	0%
Corticospinal tract L	422	48%	10%	0%	0%
Corticospinal tract R	380	36%	0%	0%	0%
Medial lemniscus L	222	39%	0%	0%	0%
Medial lemniscus R	210	7%	0%	0%	0%

Table 7. The correlations between regions of reduced FA (as determined by TBSS analyses using TFCE) and individual cognitive measures in RRMS. See

Table 8 for details.

Fiber Bundles	Fiber Category	Skeletal size (Voxels)	FA reduction size	SDMT %	SDMT r	RAVLT %	RAVLT r	PASAT %	PASAT r
Superior longitudinal fasciculus	Association fibers	2868	1621	63%	0.498**	37%	0.349*	8%	0.242
External capsule	Association fibers	2749	1250	82%	0.579**	25%	0.348*	16%	**0.392***
Cingulum	Association fibers	1347	853	94%	0.598**	43%	0.363*	17%	0.297
Sagittal stratum	Association fibers	1024	838	97%	**0.708****	**86%**	**0.522****	**43%**	**0.455****
Fornix	Association fibers	797	768	**98%**	**0.618****	82%	0.420*	3%	0.283
Superior fronto-occipital fasciculus	Association fibers	126	118	15%	0.413*	0%	0.366*	0%	0.312
Corpus callosum	Commissural fibers	7470	6991	**98%**	0.569**	**85%**	0.427**	**41%**	0.322
Uncinate fasciculus	Commissural fibers	136	98	85%	0.397*	0%	0.237	0%	0.309
Corona radiata	Projection fibers	7520	5387	81%	0.554**	62%	0.431**	19%	0.284
Internal capsule	Projection fibers	4891	2266	56%	0.536**	46%	0.491**	9%	0.315
Posterior thalamic radiation	Projection fibers	2291	2229	**98%**	**0.689****	**93%**	**0.508****	**42%**	**0.392***
Cerebellar peduncle	Tracts in brainstem	4138	2603	0%	0.555**	0%	**0.529****	0%	0.311
Cerebral peduncle	Tracts in brainstem	1256	767	53%	0.427**	43%	0.408*	0%	0.281
Corticospinal tract	Tracts in brainstem	802	338	6%	0.379*	0%	0.303	0%	0.329
Medial lemniscus	Tracts in brainstem	432	102	0%	0.337*	0%	0.029	0%	0.077

Table 8. The correlations between grouped regions of reduced FA and individual cognitive measures in RRMS. Skeletal size is the number of voxels making up the tract, reduced FA size is the number of voxels within the tract demonstrating significant FA reduction (at $p < 0.01$). Percentages indicate the fraction of voxels in the tract with reduced FA (which also demonstrated significant correlation with cognitive scores), and r-values indicate the partial correlation coefficient for the association between the voxels with significant FA reduction for the entire tract and cognitive scores. Highest 3 values for each column are shown in **bold**. Statistical significance symbols: * indicates $p < 0.05$, and ** indicates $p < 0.01$.

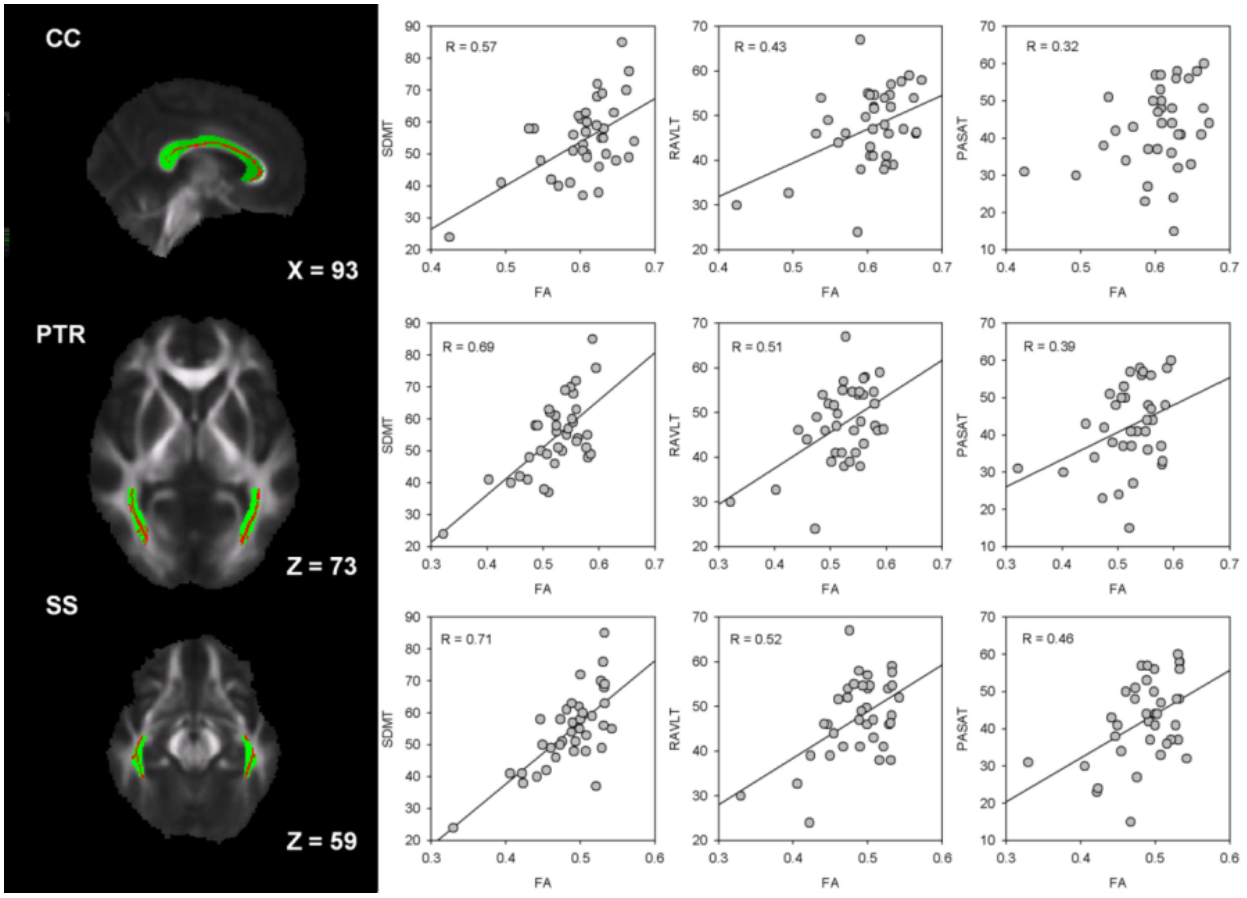

Figure 23. Examples of tract specific correlations between reduced FA and cognitive measures. Decreased FA correlates significantly with a decline in cognitive performance in the MS group within cognitively-relevant white fiber tracts. Left: Locations of cognitively-relevant fiber bundles with reduced FA (red, $p < 0.01$) including corpus callosum (CC), posterior-thalamic radiation (PTR), and sagittal stratum (SS), overlaid on JHU-ICBM-DTI-81 white matter atlas (green). Right: Scatter plots between mean reduced FA in corresponding fiber bundles, and each of the cognitive measures, where significant correlations ($p < 0.01$) were indicated by correlation line, and no line for non-significant correlations.

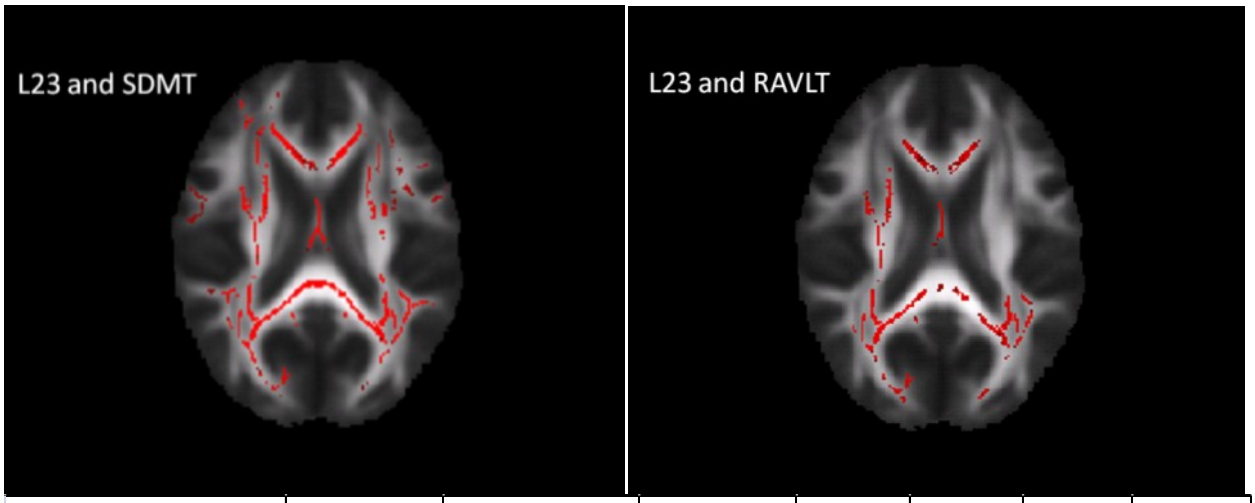

Fiber Bundles	Fiber Category	Skeletal size (Voxels)	FA_SDMT	FA_RAVLT	FA_PASAT	RD_SDMT	RD_RAVLT
Cerebellar peduncle	Tracts in brainstem	4138	0%	0%	0%	0%	0%
Cerebral peduncle	Tracts in brainstem	1256	33%	27%	0%	27%	25%
Cingulum	Association fibers	1347	60%	27%	11%	43%	15%
Corona radiata	Projection fibers	7520	58%	44%	13%	66%	39%
Corpus callosum	Commissural fibers	7470	92%	79%	38%	89%	70%
Corticospinal tract	Tracts in brainstem	802	3%	0%	0%	2%	0%
External capsule	Association fibers	2749	37%	9%	1%	32%	6%
Fornix	Association fibers	797	94%	79%	3%	94%	81%
Internal capsule	Projection fibers	4891	26%	21%	4%	26%	21%
Medial lemniscus	Tracts in brainstem	432	0%	0%	0%	0%	0%
Posterior thalamic radiation	Projection fibers	2291	96%	90%	41%	88%	73%
Sagittal stratum	Association fibers	1024	80%	70%	35%	76%	57%
Superior fronto-occipital fasciculus	Association fibers	126	14%	0%	0%	93%	44%
Superior longitudinal fasciculus	Association fibers	2868	36%	21%	5%	45%	20%
Uncinate fasciculus	Commissural fibers	136	61%	0%	0%	51%	0%

Figure 24. The association between cognitive measures and radial diffusivity (L23) in the TBSS skeleton in RRMS patients. The red voxels in the axial images (top figures) show those areas of increased radial diffusivity (L23) in the patients that also significantly correlate with SDMT and RAVLT. The TFCE method was used to correct for multiple comparisons, while treating age as a covariate ($p \leq 0.05$). The correlation is summarized in the bottom table. Skeletal size is the number of voxels making up the tract, reduced FA size (RA_thr99) is the number of voxels within the tract demonstrating significant FA reduction (at $p < 0.01$), the rest of the columns indicate the number of voxels in the tract with reduced FA/increased radial diffusivity, which also demonstrated significant correlation with cognitive scores. Values in bold show tracts where more correlating voxels were found using radial diffusivity than using FA.

6.3.6. T2 lesion load and NAWM changes

Local T2 lesion load varied considerably between anatomical regions, from < 1% in the corticospinal tract to 20% in the posterior thalamic radiation. Changes in skeletal FA correlated strongly with T2 lesion load, calculated locally within the same anatomical regions noted above. Similarly, mean FA within the NAWM only was found to correlate with local lesion load, with only minor changes in the correlation strengths compared to the skeletal FA correlations (see Table 9). Based on these findings, the DTI-cognitive test correlation analyses were repeated with the DTI data limited to NAWM only based on the lesion masks described above. As can be seen by comparing these results (Table 10) to the full skeleton results in Table 8.

Fiber Bundles	Region (# voxels)	T2LV	FA (Skeleton)	r-value	FA (NAWM)	r-value
Superior longitudinal fasciculus	13212	7%	0.46	-.762**	0.40	-.717**
External capsule	7929	1%	0.41	-.555**	0.36	-.632**
Cingulum	7484	1%	0.47	-0.16	0.38	-0.10
Sagittal stratum	4459	10%	0.48	-.638**	0.42	-.572**
Fornix	2908	5%	0.43	0.16	0.38	0.21
Superior fronto-occipital fasciculus	1014	7%	0.43	-.569**	0.38	-.641**
Corpus callosum	35291	8%	0.61	-.791**	0.53	-.775**
Uncinate fasciculus	756	2%	0.46	-0.28	0.38	-0.30
Corona radiata	36151	13%	0.42	-.806**	0.38	-.766**
Internal capsule	18646	3%	0.56	-.714**	0.50	-.761**
Posterior thalamic radiation	7950	20%	0.52	-.597**	0.47	-.525**
Cerebellar peduncle	21064	1%	0.48	0.22	0.41	0.21
Cerebral peduncle	4556	1%	0.63	0.01	0.55	0.01
Corticospinal tract	2732	0%	0.51	0.21	0.45	0.18
Medial lemniscus	1389	2%	0.55	0.13	0.49	0.09

Table 9. Correlations between mean FA and lesion load in RRMS. Region size is the number of voxels making up the entire white matter region, T2LV indicates the percentages of voxels having T2 hyperintensity within the region, FA skeleton is the mean FA value within the TBSS tract, and the corresponding r-values which were extracted from partial correlations between mean skeletal FA and T2 lesion volume. FA NAWM is the mean FA value for normal appearing white matters within the region, and the corresponding r-values extracted from partial correlations between mean NAWM FA and T2 lesion volume. ** $p < 0.01$.

Fiber Bundles	Fiber Category	SDMT	RAVLT	PASAT
Superior longitudinal fasciculus	Association fibers	.497**	.328	.206
External capsule	Association fibers	.594**	.380*	**.368***
Cingulum	Association fibers	**.596****	.350*	.309
Sagittal stratum	Association fibers	**.704****	**.540****	**.438****
Fornix	Association fibers	.590**	.385*	.255
Superior fronto-occipital fasciculus	Association fibers	.493**	.373*	.348*
Corpus callosum	Commissural fibers	.564**	.421*	.313
Uncinate fasciculus	Commissural fibers	.437**	.256	.327
Corona radiata	Projection fibers	.539**	.438**	.261
Internal capsule	Projection fibers	.584**	**.511****	.303
Posterior thalamic radiation	Projection fibers	**.662****	.501**	**.376***
Cerebellar peduncle	Tracts in brainstem	.576**	**.510****	.346*
Cerebral peduncle	Tracts in brainstem	.478**	.407*	.277
Corticospinal tract	Tracts in brainstem	.328	.295	.306
Medial lemniscus	Tracts in brainstem	.419*	.207	.107

Table 10. Correlations between NAWM-FA and individual cognitive measures in RRMS. r-values were extracted from partial correlations between mean FA in NAWM and each cognitive score. The highest values for each column are shown in bold. * $p<0.05$, ** $p<0.01$.

6.4. Discussion

DTI has provided a window to investigate CNS damage in MS. In this chapter, results of histogram analysis suggest that subtle measurable DTI abnormalities in the NAWM are present in MS. DTI using TBSS with additional analytical refinements show widespread reductions in FA consistent with damage across multiple white fiber tracts among individuals with RRMS relative to healthy controls, and that the FA reduction extended beyond lesion-prone tissue to include NAWM. Furthermore, FA strongly correlates with performance on the SDMT, a widely used cognitive measure in MS which assesses cognitive processing speed and visual working memory. Reductions in FA correspond to performance on the verbal memory test, but only a few areas correlate with the PASAT measure of verbal working memory. Taken together, the

findings demonstrate that extensive damage to CNS myelin in MS occurs across cognitively-relevant WM tracts, leading to a loss of neural communication in specific tracts that underlie cognitive function.

6.4.1. DTI methodological considerations

Pathological changes in MS have traditionally been followed using lesion imaging, demonstrating the utility of T2- and contrast-enhanced MRI for depiction of MS lesion noninvasively (*244, 245*). These techniques have also been used in some studies to examine associations with neuropsychological dysfunction; MS patients with cognitive impairment compared to those who are cognitively intact have greater lesion burden (*80, 246-248*). However, there was only a modest association between T2 lesion burden and neuropsychological test performance. This weak association between clinical and radiological findings may be due to the lack of pathological specificity of lesions, as T2 lesions do not discriminate between edema, demyelination and axonal loss (*249*). On the other hand, using more advanced quantitative MRI techniques such as magnetization transfer and MR spectroscopy (*226, 250, 251*), studies were able to detect pathological changes in normal appearing brain regions as well as strengthen the correlations between imaging abnormalities and cognitive deficits.

In contrast to lesion-based analysis, this chapter highlights the contribution of DTI based radiological changes within white matter fibers which would appear to be related to clinical disability. DTI provides both orientation and anisotropy information regarding white matter fiber tracts. This quantitative MRI technique has been used previously to investigate structural changes in MS (*93-95*). In order to define the white matter tract of interest, and to provide quantitative measures of DTI-based changes, most previous studies have used manual placement of a region-of-interest (ROI) (*252, 253*). However, ROI-based analysis suffers from high intra-

and inter-rater variability and proves very time consuming when numerous white matter tracts must be analyzed across many subjects. Moreover, it might be difficult to find the same anatomic markers to draw ROIs, thus making it difficult when comparing different subjects.

Histogram analysis is a more global analysis which can help to avoid the problem of poor correspondence between the brains of different subjects. Histogram features such as the mean value, the peak position, and the peak height are often used to quantify the global properties. When the histogram is normalized, the measures become independent of the size of the brain. Our results showed that it is possible to obtain histograms from lesion and NAWM separately. This allows the detection of subtle changes in the integrity of tissue, independent from lesion, thus providing additional global markers for monitoring the disease evolution.

Fiber tractography is a more sophisticated approach allowing the reconstruction of fiber bundles, still requiring the placement of ROIs as seeding points, based on prior knowledge of fiber anatomy, in order to define the point-of-origin of the white matter tract of interest. The reproducibility of such an approach thus also suffers from the need for manual ROI positioning. At present, fiber tractography is not robust nor is it fully automated for the analysis of all fiber tracts in the brain. In particular, in diseases such as MS where the existence of localized white matter lesions can lead to changes of small portions of a fiber, we have found that fiber tracking in patients is frequently unsuccessful and may produce severe overestimation of the disease pathology by missing complete fiber tracts.

VBM-based analysis is a fully automated, voxelwise technique enabling multi-subject analysis of DTI images by registering every subject's data to a common space. However, VBM-based analysis presents known limitations with registration and smoothing (*233, 254, 255*) particularly challenging for DTI where EPI-related distortion is common.

6.4.2. Advantages of DTI-TBSS with TFCE approach

To avoid these methodological deficiencies, we used the TBSS method, a newly developed analysis approach which complements VBM-based DTI analysis by projecting non-linear registered FA images onto an alignment-invariant tract representation (*233*). By establishing a "mean FA skeleton", representing the fiber bundle centers common to all subjects, TBSS minimizes the inter-subject variability and can provide better reliability compared to other techniques.

In fact, TBSS has been utilized in recent MS studies to gain insights into the underlying pathological mechanisms related to motor and cognitive disabilities (*113, 229, 234, 256-258*). Using TBSS analysis, we found significantly reduced fractional anisotropy in RRMS patients as compared to controls across the fiber skeleton. The FA reduction was seen in both lesion-prone and normal appearing white matter regions, providing evidence of white matter integrity changes that are not detected with conventional MRI techniques. However, in contrast to other studies in MS that have applied DTI with TBSS, we added a further refinement to the analysis by applying TFCE. These prior TBSS studies used cluster-based thresholding, an image thresholding technique to identify true signal from noise. Cluster-based thresholding is done with spatial smoothing and requires setting an arbitrary cluster-forming threshold. Here we used a recently introduced threshold free cluster enhancement technique that does not require arbitrary pre-smoothing of images and does not depend on an initial cluster forming threshold. In brief, all voxels in the raw statistic image can be represented by a distribution profile (or a histogram-like curve for voxels in the unthresholded statistic image). A TFCE value for a voxel is determined as the sum of all supporting section scores within the area underneath on the distribution curve. The number of supporting sections depend on the height (or signal intensity of the voxel) where

sections are divided into increments from zero to the signal height. The score of each section is simply its height (signal intensity) multiplied by its cluster extent (area of the contiguous cluster). The output value is therefore a weighted sum of the entire local clustered signal without the need for an arbitrary cluster-forming threshold. Since the image is passed through an algorithm which should enhance the intensity within cluster-like regions more than background regions, TFCE enhancement is able to discriminate between noise and spatially-extended signal. TFCE can be seen as a highly nonlinear smoothing kernel where each voxel is given a value that is dependent on the spatial neighborhood information in extended areas of signals. Therefore, if changes are diffuse and widespread as is the case with MS (*259*), TFCE will be more sensitive due to its ability to incorporate information from neighboring voxels from a potentially larger region. By combining TBSS analysis with TFCE technique, we were able to identify more widespread white matter FA reduction compared to previous TBSS-based MS studies using cluster-based thresholding (*113, 234*).

6.4.3. Association of cognitive dysfunction with demyelination

DTI also has the potential to differentiate the origin of tissue injury to determine whether only myelin or both myelin and axonal injury occurs (*260*). Diffusion anisotropy depends on the relative magnitude of axial diffusivity (the largest eigenvalue, which reflects diffusion parallel to the axon) versus radial diffusivity (the mean of second and third eigenvalues, representing diffusion perpendicular to the axon). The reductions in FA in both lesion (as shown in histogram analysis) and normal appearing white matter demonstrated in the MS relative to control subjects were primarily driven by increased radial diffusivity with no significant difference in axial diffusivity. Further, the cognitive measures correlated with radial but not axial diffusivity values. These findings are consistent with animal and *ex vivo* models of MS (*261, 262*), as well as other

MS-DTI studies (*229, 234, 263-265*), where reduced radial diffusivity was found with little or no change in axial diffusivity. These results suggest that damage in myelin across the cognitive-relevant functional pathways rather than only axonal loss in tracts underlies the cognitive impairment. However, pathologic studies have also demonstrated axonal transection and subsequent axonal loss in addition to demyelination in MS (*128, 266*). Moreover, there was a trend of, (though not statistically significant), increased axial diffusivity in our data, and there was a significant correlation between axial and radial diffusivity measures ($r = 0.763$, $p < 0.001$). Thus, our results with respect to radial diffusivity changes should be treated with some caution.

6.4.4. Relations between white matter tracts and clinical measures

Cognitive function was strongly correlated with FA in the association, commissural and projection fibers. Among the specific fiber bundles examined, the corpus callosum, the posterior thalamic radiation (including optic radiation), and the sagittal stratum (including the inferior longitudinal and frontal-occipital fasciculi) had the largest extent of FA reduction, and correlated most strongly with cognitive measures. Similar to our findings, others have linked MS associated corpus callosum damage to impaired cognitive performance (*264, 266-269*). While changes in the corpus callosum could involve loss of fiber integrity, disrupting the connection between different functional domains of the brain, diffusion abnormalities seen in the corpus callosum could also reflect degeneration of the connected gray matter (as shown in Chapter 5) causing secondary damage to the connected white matter tracts and loss in neuronal function. The association between impaired cognition and decreased FA in the posterior thalamic radiation, is consistent with the demonstrations of thalamic atrophy in MS and its association with memory impairment (*88, 270*). Both the sagittal stratum and the posterior thalamic radiation connect to the occipital lobe and disruption in the integrity of these pathways could contribute to the visual

perceptual deficits that frequently occur in MS, which may explain the strong correlations with SDMT, which has a prominent visual component. In all, these findings demonstrate a clear association between cognitive functioning and extensive DTI-implied pathology in WM tracts involved in cortical-cortical or cortical-subcortical pathways.

6.4.5. Validity of specific measure of cognitive function in MS

The assessment of cognitive functioning in MS is challenging, as only an extensive neuropsychological battery can detect the broad range of deficits present in these individuals. Yet prolonged testing is not feasible in many clinical settings. Therefore, a frequent research goal is to identify a single test or set of tests that are brief, sensitive and valid. Three cognitive measures were examined in this study, and in contrast to prior investigations, the extent of the association between WM changes and the specific cognitive functions was quantified. Our results indicate a progression of white matter involvement, with the most widespread association to the SDMT task, followed by RAVLT, and finally PASAT with the smallest degree of DTI-inferred white matter involvement. While the PASAT and SDMT are both frequently used in MS research (*18, 271*), only the PASAT is included as part of the widely used Multiple Sclerosis Functional Composite (MSFC) clinical outcome measure (*272*), though some have suggested perhaps the SDMT holds advantages over the PASAT (*225*). Our findings support the utility of both tests, but we found greater sensitivity with the SDMT, demonstrating much more widespread and stronger correlations to FA reductions. Others, analyzing the association between diffusion measures and the SDMT without regard for spatial dependencies, have also shown strong associations between MS associated CNS damage and this test (*265, 273, 274*). Based on our observations and those of others, the SDMT compared to the PASAT appears more sensitive to WM tract damage in MS.

Included in our cognitive assessment was the RAVLT, a measure of episodic verbal learning and memory that has not been investigated previously in DTI studies. Fiber tracts in the limbic system (*i.e.*, fornix and cingulum), are involved in establishing new learning and memory. We found significant associations between verbal memory assessed by RAVLT and reduced FA within the limbic system as well as in the white matter tracts providing connections from the limbic system to the rest of the brain (*e.g.,* superior longitudinal fasciculus). These findings further confirm prior studies that linked DTI changes in MS with performance on another memory task (the California Verbal Learning Test, CVLT) (*113, 275*). In an earlier study using fiber tractography, a significant correlation with memory performance and DTI measures of the fornix was identified (*275*); however, in contrast to our analysis where memory and white matter damage in the cingulum were linked, this earlier study using fiber tractography analysis did not identify a significant correlation between memory function and the cingulum nor between memory and the superior longitudinal fasciculus. In the TBSS study (*113*), CVLT performance correlated primarily with temporal and parietal tracts, similar to our observations using RAVLT. No DTI study to date (including the present one) has found an association between memory and the uncinate fasciculus, a tract thought to be relevant in emotional processing, learning and memory in other diseases (*276, 277*).

6.4.6. Normal appearing white matter in MS

Many studies in the last 20 years have confirmed involvement of so-called normal appearing white matter in the pathophysiology of MS (*106, 278-282*). A number of prior studies investigating the association between DTI-related measures and cognitive performance have also demonstrated the fact that there are regions of non-overlap of these associations with T2 lesions (*113, 234*) . To take these observations one step further, we performed quantitative, regional

comparisons to investigate the relationship between FA reductions and T2 lesion load. Correlations between FA reduction and T2 lesion load showed similar strengths when calculated within the NAWM-only as compared to those calculated across the entire TBSS skeleton. While these results would appear to highlight the importance of nearby T2 lesions in the loss of fiber integrity even in the NAWM, we cannot discount the possibility that patients with more severe lesion pathology are also plagued with more severe NAWM degeneration, although the pathological processes may be independent. Similarly, correlation analysis of NAWM FA reduction with the three cognitive measures all showed regions of strong association. These results would appear to support the opposing position; *i.e.*, the importance of DTI-derived white matter damage within the NAWM *independent* of T2 lesions. Nonetheless, we cannot discount the possibility that FA reductions within the NAWM, and their association with cognition, are derived from the nearby lesions. Future refinement of our regional analyses will allow some of these distinctions to be further refined and clarified.

6.4.7. Study Limitations and Considerations

Despite the robustness of the association between cognitive function and DTI measures in the MS group, there are a number of limitations to this study. There was an age difference between the subject groups. However, all analyses included adjustments for age, and repeated analyses without age correction did not significantly alter the TBSS results.

Our MS sample was a convenience sample, not chosen on the basis of cognitive impairment, and it is possible that a sample comprised of a greater number of cognitively impaired persons might have displayed stronger associations with MR measures. However, the current sample appeared fairly representative of the level of impairment typically displayed by persons with RRMS (*20*). . While only the RAVLT scores were significantly different between

the groups, we found that our SDMT data were being adversely affected by one outlier with an unusually good performance. With this subject removed, SMDT was also significantly different from controls ($p = 0.03$). Not all participants in the study were administered the RAVLT measure of verbal memory, and although we estimated RAVLT performance based on their performance on the SRT, another verbal memory measure (a substitution which we have used in other studies (*183*), it is possible that this process increased the variability for our measurements of this domain, minimizing the DTI-related associations. However, these nine patients were not clustered on either side of the patient group with respect to severity of their cognitive deficits, and thus any errors in the SRT substitution would not be expected to unfairly skew our results and affect our overall findings.

Similar to other TBSS studies, it is possible that registration misalignment to the standard template or atlas could have led to misclassification of the fiber tracts. Here, we used a popular template and atlas for our analysis, and we carefully examined the registration quality between the subjects' mean FA and the template FA, as well as the anatomical atlas. As mentioned, the interpretation of axial and radial diffusivity should also be taken with caution because axonal injury is often seen in multiple sclerosis (*128, 266*). Finally, although we had difficulty with fiber tractography with the tracts in the limbic system, tractography of such tracts should not be discouraged and they are likely to provide useful individual-based tract-specific information for cognitive studies. One explanation for such difficulty might be due to the large extent of atrophy in some subjects that could have introduced a partial volume effect from the CSF. DTI acquisition with CSF suppression (*283*), and increasing the resolution of DTI images (with longer acquisition time) would help to improve the results.

6.5. Summary

Our findings using a sensitive and reliable DTI approach (TBSS-DTI with TFCE) clearly indicate that in MS, the demyelination of the white matter tracts alters the structural integrity of the brain and underlies the cognitive impairment associated with the disease The combination of TBSS with TFCE is able to demonstrate widespread involvement with a number of white matter tracts with close to 90% of voxels with reduced FA compared to controls, and these disruptions have strong associations with domains of cognitive impairment often seen in MS. The TBSS findings clearly indicate the progression of SDMT > RAVLT > PASAT with respect to the degree of involvement of the normal appearing white matter within the domains probed by these tests. While there are strong correlations between lesion burden and FA reduction in most of the involved tracts, the associations between FA and SDMT remain significant even when restricted to NAWM; implicating the non-lesional tissue as playing an important role in the clinical outcome of the disease. Thus, the application of TBSS-DTI with TFCE can further enhance our understanding of the mechanisms underlying cognitive impairment in MS and could play a critical role in monitoring the clinical and cognitive effects of the disease.

Chapter 7

Metabolic Changes and Associations to Cognitive Function in MS

7.1. Introduction

Proton magnetic resonance spectroscopy (^{1}H-MRS) is a non-invasive technique that measures tissue metabolite concentrations *in vivo*. Changes in metabolite concentrations have been observed using MRS in lesions and normal appearing white matter (NAWM) in individuals with multiple sclerosis (MS) as described in Chapter 3. In particular, reduced concentration of N-acetyle-aspartate (NAA), a neuronal marker, has been found in lesions and NAWM in individuals with MS. These MRS detectable changes can occur in NAWM before they become visible lesions on conventional MRI (*138*). While conventional MRI is unable to discriminate between different types of pathology, MRS provides more sensitive measures to help distinguish metabolite abnormalities and improve the weak clinical associations with MRI.

As discussed in Chapter 5, recent attention in MS studies has turned from focusing on white matter pathology to understanding neuronal pathology in the gray matter (GM) of MS patients, particularly to explain cognitive symptoms. Although GM abnormalities in MS are thought to play an important role in the pathophysiology of clinical deficits, it has been difficult to visualize GM lesions and to provide sensitive assessment to reveal the true degree of GM pathological changes with conventional MRI, but could be visible using advanced MRI sequence such as DIR (Figure 5). While pathological studies suggest that GM pathology might be

different from that of WM (*54, 284, 285*), it is essential to be able to capture a more comprehensive picture of the range of tissue alterations in GM *in vivo*. Quantitative MRS studies have reported changes in metabolite concentrations in NAGM in MS. However, discrepancies exist in the current literature regarding metabolic abnormalities in GM. For example, reduced NAA concentrations in cortical GM of MS patients were found in some (*141, 151, 153*), but not all studies (*150*). Moreover, the current knowledge about pathological changes in individual GM structures is still limited. With respect to neurocognitive deficits, GM structures such as the hippocampus are of importance. Processes leading to abnormalities in functional structures could be complicated. Besides demyelination within these regions, inflammation, gliosis, and neurodegeneration can also occur. Therefore, it is important to identify spectroscopic abnormalities in these NAGM structures and how they are related to cognitive dysfunction.

In this chapter, I aimed to investigate changes in tissue-specific metabolite concentrations in lesions, NAWM, CGM, and hippocampus of relapsing remitting multiple sclerosis (RRMS) using MRS. The spectra quantification was carried out using LCModel (*286*). The relations between tissue specific metabolite changes and cognitive measures were also assessed.

7.2. Methods

7.2.1. Subjects and clinical assessments

Thirty-eight individuals with RRMS and 20 healthy controls participated in this study. Please refer to Chapter 4 for details on subject information, neurological and cognitive assessments.

7.2.2. MRS data acquisition

Single voxel spectroscopy data were acquired in control white matter (CTWM), normal appearing white matter (NAWM), non-enhancing lesion (NELES), cortical gray matter (CGM), and left hippocampus (LTHIP). As mentioned in Chapter 4, CTWM voxels were acquired primarily in the left frontal and parietal regions. Non-enhancing lesions were picked for those with a minimum of 6 mm diameter in one axis to minimize the partial volume effect. NAWM voxels were acquired on the contralateral side when possible; otherwise NAWM voxels were acquired as far away from the NELES (or any lesions) as possible. The average distance between NAWM voxels and any lesion was 2.48 $\pm$ 2.18 cm. CGM voxels were acquired predominately in the pre-central gyrus. LTHIP voxels were acquired with the major axis of the voxel located at the anterior-posterior axis of left hippocampus. Please refer to Chapter 4 for details on MRS data acquisition.

7.2.3. MRS data analysis

Metabolite concentrations in MRS spectra were quantified using the LCModel software package (*287*). The LCModel is a fully automatic method which analyzes an *in vivo* spectrum as a linear combination of model spectra of metabolite solutions *in vitro* and provides absolute quantification by reference to an external calibration standard. The reference model spectrum or basis set used was the Philips 3T gamma_press_te30_128mhz_144 basis set. The unsuppressed water signal was used as an internal reference. The final analysis was performed in the frequency domain (from 0.2 to 4.0ppm) with the raw (*i.e.*, free induction decay) data as an input; no filtering (e.g., Guassian smoothing) was applied to data prior to data entry into LCModel. The metabolite concentrations and ratios (relative to Cr+PCr) were extracted from the fitted spectra. Cr+PCr refers to creatine+phosphocreatine or tCr. The output from the LCModel also

provides global line width (FWHM) and SNR estimates. FWHM (full width at half-maximum) is a rough estimate of the linewidths of singlet resonances NAA, Cr, and Cho, and the SNR is defined as the ratio of the maximum in the spectrum minus baseline over the analysis window to twice the RMS residuals. Examples of LCModel output from white matter and hippocampal spectra are shown in Figure 25 and Figure 26, respectively.

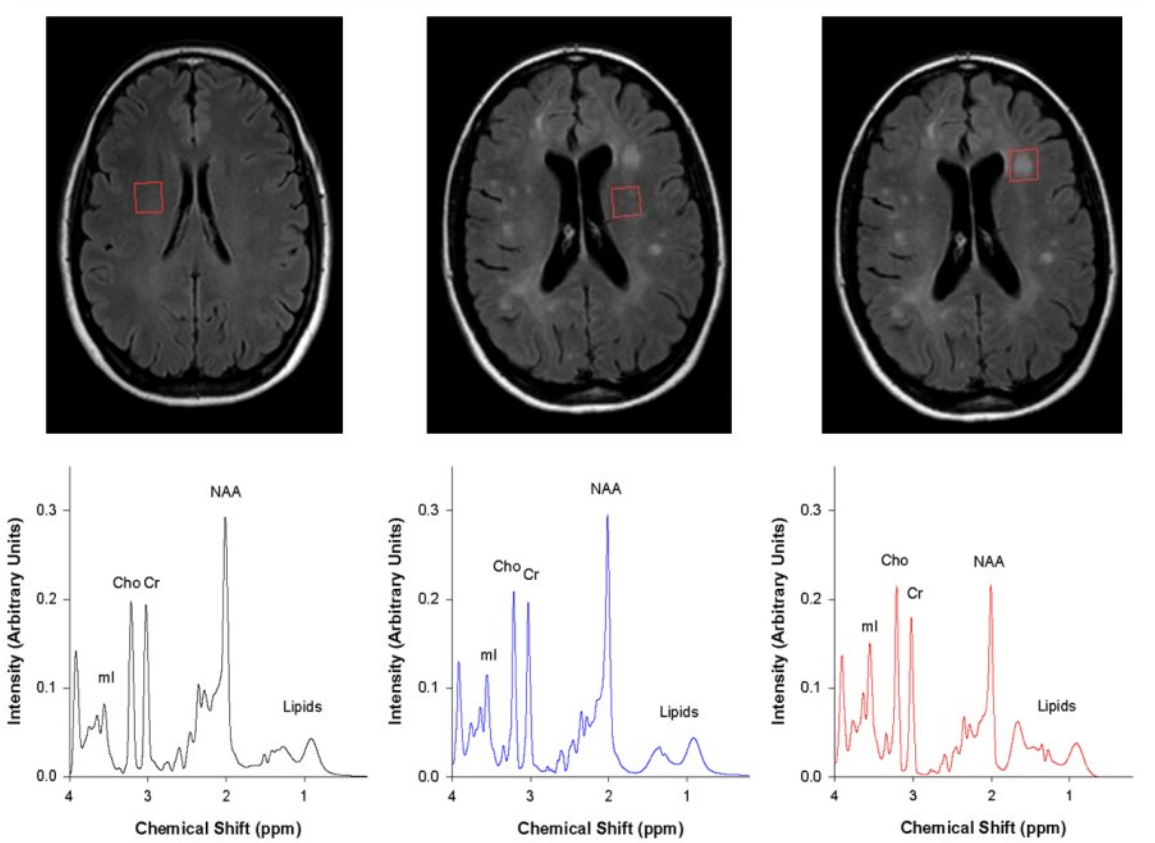

Figure 25. Example voxel planning and corresponding LCModel fitted spectra. Voxels were placed in CTWM (top-left), NAWM (top-middle), and NELES (top-right) on FLAIR images. The corresponding LCModel fitted spectra were then replotted on the bottom. Note the decreased level of NAA and increased level of Ins in the non-enhancing lesion compared to control and normal appearing white matter.

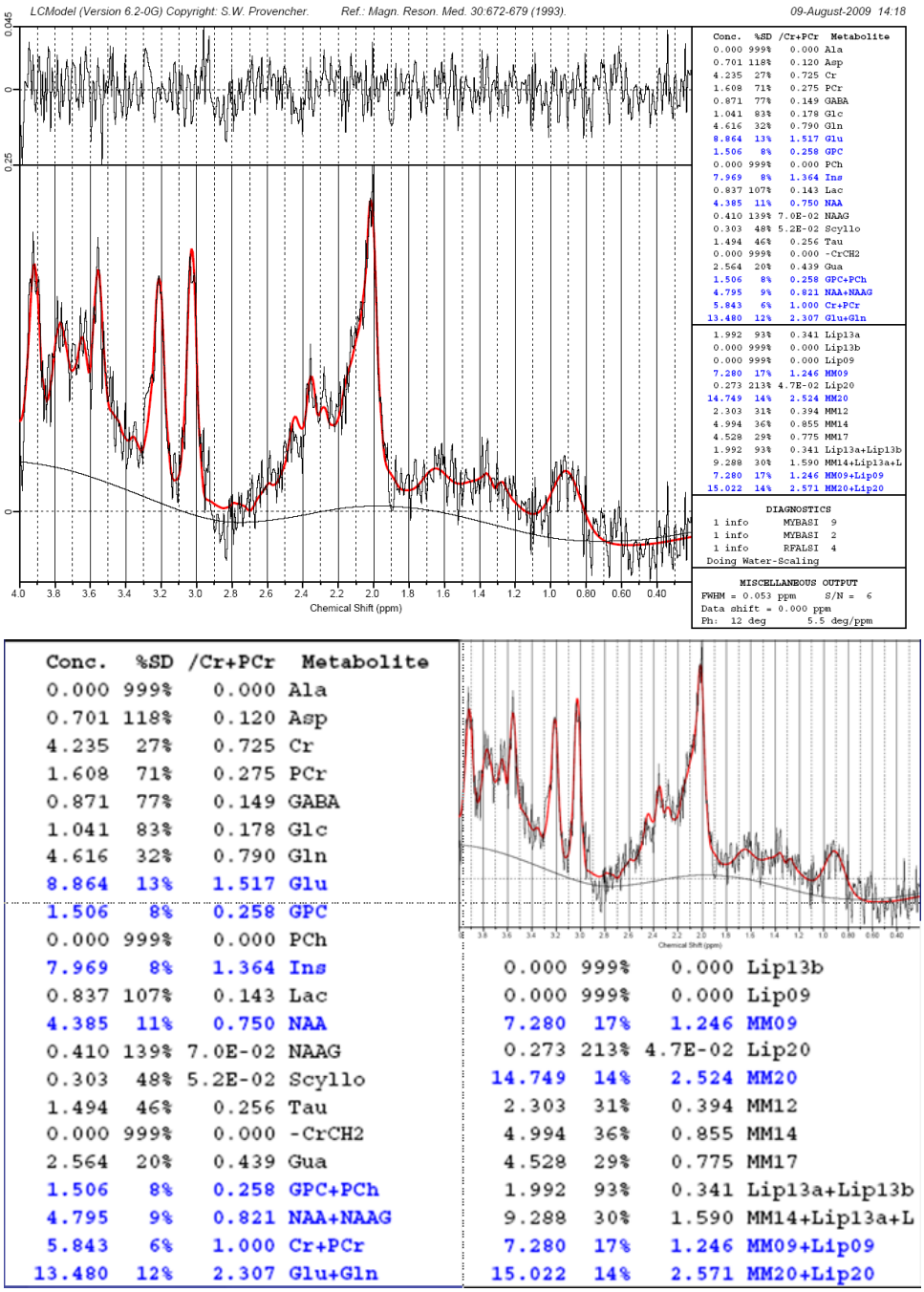

Figure 26. Demonstration of LCModel quantification of a hippocampus spectrum from a MS patient. Top: With the LCModel, the original spectrum (left) is first preprocessed including baseline fitting (black), then fitted (red) within the user-defined spectral interval (indicated by x-axis). The quality of fitting is indicated by the residues on top of the fitting window. The other outputs (right panel) from LCModel include the absolute concentration (also magnified), Noise assessment (also magnified), Concentration ratio with respect to Cr+pCr (also magnified), and Metabolite name, and in the miscellaneous output for quality assessment include FWHM, SNR, frequency shift and phase correction . In case of unsuccessful fitting, the LCModel also provides diagnostics or warning.

MRS data (metabolite concentration/ratios from LCModel) for both MS and healthy controls were further reduced based on the estimates of errors in metabolite quantification in the LCModel. This is expressed in percent standard deviation (%SD) of the estimated concentrations and represents the 95% confidence intervals of the estimated concentration values. Only metabolite concentrations with %SD < 20% were included in the analysis.

7.2.4. Statistics

One way ANOVA was used for comparison between CTWM, NAWM, and NELES. Significance levels for comparisons between MS and control subjects were calculated for LTHIP and GM with a two tailed *t* test when data were normally distributed, otherwise, the Mann-Whitney U test was used. The Pearson's correlation or the Spearman's rank correlation (if not normally distributed) was used to describe correlations between the metabolite ratio of metabolites with consistent LCModel results, cognitive scores (*i.e.*, SDMT, RAVLT, PASAT), and MRI measures from previous chapters (including GMF, WMF, BPF, T2LV, total cortical thickness, total Freesurfer hippocampal volume, FA, MD, AD, and RD) in the MS group. Only Glu+Gln (also referred to as Glx), GPC+PCh (also referred to as tCho), NAA+NAAG (also referred to as tNAA), Ins (known as myo-inisotol), and Lip09+MM09 were included in the analysis since these are the metabolites which gave consistent results (seen in > 50% of subjects; numbers of estimated metabolites in each voxel type as shown in Table 12 and Table 13). The GM spectra were excluded from correlation analysis due to small sample size. Statistical analyses were performed with SPSS v18.0. A p value of less than 0.05 was considered to be significant.

7.3. Results

7.3.1. Spectral Quality

The FHWM (full width half-maximum) is a measure of the linewidth of the spectrum (LC model calculates the FWHM from the water peak, but FWHM is expected to vary by less than 0.1 ppm over all metabolites (*286*)). The SNR is defined here as the ratio of the maximum peak in the spectrum (minus the baseline over the analysis window) to twice the RMS residuals. The mean of metabolite FWHM and SNR estimates are shown in Table 11. Overall, LTHIP spectra had slightly worse FWHM and SNR amongst regions studied. However, all LTHIP spectra FWHM and SNR were within the range suggested in the literature (*286*), and no single spectra had either FWHM that was two standard deviations higher than the mean FWHM or SNR that was two standard deviations lower than the mean SNR. No statistical differences in the SNR and FWHM were found between MS and controls. Since the FWHM appeared to be sufficient, and the signal to noise ratio was adequate for peak fitting of the major metabolites, it was not necessary to reject any data. It should also be noted that the poorer hippocampal spectral quality may lead to lower quantification precision.

	Subject Type	Voxel #	FWHM (ppm)	SNR
WM	***CTRL***	20	0.04 ± 0.01	9.35 ± 1.69
WM	***RRMS***	34	0.05 ± 0.01	8.82 ± 1.34
NELES	***RRMS***	31	0.05 ± 0.01	8.06 ± 1.50
LTHIP	***CTRL***	19	0.06 ± 0.01	5.89 ± 1.24
LTHIP	***RRMS***	34	0.07 ± 0.02	5.65 ± 1.25
GM	***CTRL***	5	0.05 ± 0.01	11.80 ± 1.79
GM	***RRMS***	7	0.04 ± 0.01	10.86 ± 1.95

Table 11. Spectral linewidth and signal-to-noise ratio of voxels examined. All voxels were included in the analysis based on their spectral quality as assessed by FWHM (full width half max) and SNR (signal-to-noise ratio). Amongst all voxels examined, the LTHIP spectra have poorer linewidth and SNR, which could have contributed to variations in metabolite estimation.

7.3.2. Metabolite Concentrations

There were a total of 35 combinations of metabolites included in the LCModel basis set. In this study, quantification estimates for metabolites and metabolite combinations were included only if their %SD was within 20%, and only those that were found frequently (in over 50% of subjects, details shown in Table 12 and Table 13) were included in the metabolite summary tables.

Table 12 (top) summarizes metabolite concentrations in white matter and lesions. Compared with the CTWM and NAWM, NELES had reduced levels of Glu, NAA, tNAA, and increased level of Ins; Glx concentration was also decreased in NELES compared with NAWM. Compared with CTWM, the only metabolite with a statistical difference to NAWM in MS patients was increased Ins.

Table 12 (bottom) summarized metabolite ratios in white matter and lesions when normalized to Cr+PCr. Compared with CTWM and NAWM, the same metabolite differences were found in the NELES, similar to the results without normalization. Compared with CTWM,

NAWM had decreased GPC and tNAA; the statistical difference in Ins seen with absolute concentrations disappeared when comparing ratios.

	CTWM		NAWM			NELES			
Metabolites	**mM ± SD**	**No.**	**mM ± SD**	**No.**	***p*-value***	**mM ± SD**	**No.**	***p*-value***	***p*-value****
Cr	4.15 ± 0.55	12	4.38 ± 0.55	16		4.40 ± 0.63	25		
Glu	6.00 ± 1.06	15	5.95 ± 0.70	28		5.12 ± 0.84	22	0.01	< 0.01
GPC	1.58 ± 0.17	18	1.53 ± 0.24	33		1.54 ± 0.26	30		
Ins	3.71 ± 0.78	20	4.20 ± 0.79	33	0.03	4.93 ± 1.01	30	< 0.01	< 0.01
NAA	6.09 ± 0.66	20	6.19 ± 0.57	34		5.15 ± 0.95	31	< 0.01	< 0.01
GPC+PCh	1.55 ± 0.19	20	1.52 ± 0.24	34		1.54 ± 0.26	31		
NAA+NAAG	7.49 ± 0.95	20	7.21 ± 0.68	34		6.13 ± 0.98	31	< 0.01	< 0.01
Cr+PCr	4.66 ± 0.49	20	5.02 ± 0.44	34		4.84 ± 0.51	31		
Glu+Gln	7.61 ± 2.01	19	8.19 ± 1.22	33		7.40 ± 1.34	28		0.02
MM09	5.13 ± 0.85	16	5.43 ± 1.29	20		5.13 ± 1.60	22		
MM09+Lip09	5.19 ± 0.89	19	6.06 ± 2.43	27		5.34 ± 1.73	25		

	CTWM		NAWM			NELES			
Metabolites	**Ratio ± SD**	**No.**	**Ratio ± SD**	**No.**	***p*-value***	**Ratio ± SD**	**No.**	***p*-value***	***p*-value****
Cr	0.90 ± 0.12	12	0.89 ± 0.09	16		0.89 ± 0.11	25		
Glu	1.28 ± 0.18	15	1.19 ± 0.15	28		1.04 ± 0.15	22	< 0.01	< 0.01
GPC	0.34 ± 0.03	18	0.31 ± 0.06	33	0.04	0.32 ± 0.05	30		
Ins	0.80 ± 0.18	20	0.85 ± 0.17	33		1.02 ± 0.22	30	< 0.01	< 0.01
NAA	1.32 ± 0.16	20	1.24 ± 0.13	34		1.07 ± 0.17	31	< 0.01	< 0.01
GPC+PCh	0.33 ± 0.04	20	0.31 ± 0.06	34		0.32 ± 0.05	31		
NAA+NAAG	1.62 ± 0.22	20	1.45 ± 0.20	34	0.01	1.27 ± 0.19	31	< 0.01	< 0.01
Cr+PCr									
Glu+Gln	1.63 ± 0.37	19	1.64 ± 0.21	33		1.51 ± 0.25	28		0.03
MM09	1.10 ± 0.21	16	1.09 ± 0.25	20		1.08 ± 0.40	22		
MM09+Lip09	1.12 ± 0.23	19	1.22 ± 0.48	27		1.11 ± 0.39	25		

Table 12. Group comparisons of metabolite concentration (top) and ratio (relative to total Cr, bottom) in CTWM, NAWM, and NELES. For each metabolite, only those had %SD > 20, and were frequently detectable (in at least 50% of total voxels) were included in the analysis. LCModel quantification provided evidence of changes in metabolites in NELES voxels (as indicated by decreased Glu, NAA and increased Ins) when compared to CTWM and NAWM. Metabolic changes were also observed in NAWM as indicated by increased Ins concentration, and decreased NAA+NAAG ratio. Symbols indicate statistical significance * vs. CTWM or ** vs. NAWM.

No statistically significance differences were found in the metabolite concentrations of LTHIP and GM when comparing MS spectra with control spectra. After normalizing metabolite

concentration to the tCr concentration, metabolite ratios were different between the two subject groups: decreased GPC and tCho ratios were found in LTHIP of MS subjects, and decreased Glu, GPC, tCho, and tNAA ratios were found in cortical GM of MS subjects. Results of LTHIP and cortical GM comparison are shown in Table 13.

	LTHIP					CGM				
	Control		RRMS			Control		RRMS		
Metabolites	mM ± SD	No.	mM ± SD	No.	*p*-value	mM ± SD	No.	mM ± SD	No.	*p*-value
Cr	5.32 ± 1.09	8	5.74 ± 0.92	14		N/A	2	N/A	1	
Glu	7.43 ± 0.95	14	7.68 ± 1.19	23		7.83 ± 1.07	5	7.04 ± 1.04	7	
GPC	1.70 ± 0.28	17	1.61 ± 0.23	29		1.31 ± 0.12	5	1.15 ± 0.13	7	
Ins	5.32 ± 0.63	17	5.92 ± 1.46	33		3.61 ± 0.42	5	3.76 ± 0.67	7	
NAA	5.22 ± 1.00	18	5.16 ± 1.01	29		7.40 ± 0.64	5	7.30 ± 0.30	7	
GPC+PCh	1.73 ± 0.28	19	1.62 ± 0.23	34		1.31 ± 0.12	5	1.15 ± 0.13	7	
NAA+NAAG	6.51 ± 0.90	19	6.51 ± 0.88	34		8.22 ± 0.60	5	7.86 ± 0.57	7	
Cr+PCr	5.76 0.82	19	5.93 0.80	34		5.35 0.19	5	5.93 0.57	7	
Glu+Gln	11.39 ± 2.15	17	11.67 ± 2.05	28		9.71 ± 0.97	5	9.75 ± 1.27	7	
MM09	5.63 ± 0.91	13	5.37 ± 0.87	18		6.02 ± 0.46	4	6.87 ± 0.90	6	
MM09+Lip09	5.66 ± 0.85	15	5.72 ± 1.15	24		6.51 ± 0.47	5	6.85 ± 0.86	7	

	LTHIP					CGM				
	Control		RRMS			Control		RRMS		
Metabolites	Ratio ± SD	No.	Ratio ± SD	No.	*p*-value	Ratio ± SD	No.	Ratio ± SD	No.	*p*-value
Cr	0.95 ± 0.14	8	0.97 ± 0.10	14		N/A	2	N/A	1	
Glu	1.28 ± 0.21	14	1.32 ± 0.21	23		1.47 ± 0.21	5	1.19 ± 0.20	7	0.05
GPC	0.30 ± 0.03	17	0.28 ± 0.04	29	0.05	0.25 ± 0.02	5	0.20 ± 0.04	7	0.02
Ins	0.91 ± 0.12	17	1.02 ± 0.32	33		0.68 ± 0.09	5	0.64 ± 0.14	7	
NAA	0.90 ± 0.17	18	0.87 ± 0.16	29		1.39 ± 0.16	5	1.24 ± 0.13	7	
GPC+PCh	0.30 ± 0.03	19	0.28 ± 0.04	34	0.03	0.25 ± 0.02	5	0.20 ± 0.04	7	0.02
NAA+NAAG	1.14 ± 0.17	19	1.11 ± 0.13	34		1.54 ± 0.16	5	1.33 ± 0.15	7	0.05
Cr+PCr										
Glu+Gln	1.97 ± 0.40	17	1.95 ± 0.35	28		1.82 ± 0.21	5	1.66 ± 0.27	7	
MM09	1.03 ± 0.25	13	0.92 ± 0.20	18		1.11 ± 0.06	4	1.20 ± 0.25	6	
MM09+Lip09	1.02 ± 0.23	15	0.97 ± 0.21	24		1.22 ± 0.11	5	1.18 ± 0.25	7	

Table 13. Group comparisons of metabolite concentration ratios in LTHIP and CGM. Changes of metabolic ratios quantified by the LCModel were observed in the gray matter of RRMS subjects. Decreased choline (GPC and GPC+PCh) ratios were found in LTHIP of RRMS, and decreased glutamate, choline, total choline, and total NAA ratios were found in cortical gray matter of RRMS subjects. Note that cortical GM had a smaller sample size.

7.3.3. MRS Correlations to Cognitive, Atrophy and DTI Measures

Of the five metabolites examined, no significant associations were found with cognitive measures. Correlations between metabolite ratios and measures of atrophy were significant for NAWM tNAA with BPF ($r = 0.442$, $p < 0.01$), WMF ($r = 0.436$, $p < 0.01$), GMF ($r = 0.364$, $p < 0.05$), T2LV ($r = -0.372$, $p < 0.05$), and total FreeSurfer hippocampal volume ($r = 0.346$, $p < 0.05$); for NAWM tCho with WMF ($r = 0.370$, $p< 0.05$); for NELES tCho with BPF ($r = 0.382$, $p < 0.05$); and for LTHIP Glx with BPF ($r = -0.449$, $p < 0.05$), WMF ($r = -0.560$, $p< 0.01$), and cortical thickness ($r = -0.404$, $p < 0.05$). Only tNAA in NAWM, and Glx in LTHIP correlated with DTI measures, where tNAA correlated with FA ($r = 0.430$, $p < 0.05$), MD ($r = -0.381$, $p < 0.05$), and RD ($r = -0.387$, $p < 0.05$), and Glx correlated with FA ($r = -0.402$, $p < 0.05$) and RD ($r = 0.389$, $p < 0.05$).

7.4. Discussion

In this chapter, we used proton MRS and provided evidence of metabolic dysfunction in lesions, NAWM, hippocampus and cortical GM in RRMS. The results also suggested that metabolite dysfunction may be closely related to MRI volumetrics and DTI measures, which could contribute to the cognitive impairment seen clinically.

7.4.1. Metabolites and Functions

Although this study does not provide histological and pathological measures directly, MRS metabolites have been linked to specific cell types and functions in previous studies, and alterations in such metabolites should reflect pathological dysfunctions. Of the metabolites assessed in this study using LCModel, tNAA, Ins, tCho, Glx, tCr, macromolecule and lipid at 0.9

ppm were present in the majority of subjects' spectra of all regions examined. N-acetylaspartate (NAA) is predominately found in neurons and may also be present in mature oligodendrocytes (*288*). MRS has estimated the NAA concentration to be lower in white matter than gray matter (*289*). N-acetylaspartyle-glutamate (NAAG) overlaps with NAA in the spectrum, and they are reported as the total NAA (tNAA) here. Myo-inositol (Ins) is often found in glial cells. Choline (Cho) is related to membrane turnover, and includes glycerol-phosphorylcholine (GPC) and phosphorylcholine (PCh). Glutamate (Glu) is a major excitatory neurotransmitter which overlaps with glutamine (Gln) to form the glutamate/glutamine complex (Glx); glutamate is also a key molecule in cellular metabolism. All of these metabolites are often mentioned in the MRS literature and are usually normalized to the total creatine (tCr) concentration. The tCr has two overlapping components: creatine (Cr) and phosphocreatine (PCr), which are essential in energy production in cells. As mentioned in Chapter 3, creatine concentration is relatively stable in the brain, and we did not find statistical significance difference between MS and controls in the tCr concentration in voxels of various regions, thus tCr was used as a normalization factor in the analysis. Lastly, macromolecule and lipid peak at 0.9 ppm (MM09+Lip09) were also observed in the majority of the spectra, which has not been well characterized, but was found elevated in acute MS lesions using a metabolite-nulling technique (*290, 291*).

7.4.2. Lesional and Normal Appearing White Matter Observations

In accordance with many previous studies, we found an overall decrease in tNAA (measured as both concentration and ratio) in lesional WM of patients with MS. The decrease in tNAA was primarily due to decrease in NAA, a neuronal marker, suggesting the presence of axonal metabolic dysfunction, and/or axonal loss, in the non-enhancing lesions. The tNAA ratio was also decreased in NAWM when compared with CTWM. Theoretically, a decrease in the

tNAA ratio could be due to either a decrease in tNAA concentration with no change in tCr, or an increase in tCr concentration with no change in tNAA. However, neither the tNAA nor the tCr concentration was statistically different between CTWM and NAWM in our data, suggesting that very marginal and subtle changes in the combination of tNAA and tCr may have contributed to the decreased tNAA ratio. Moreover, the changes in tNAA could be diluted where demyelination and axonal loss are occurring while coupled with partial remyelination in the NAWM of some patients.

Increased concentration of myo-inositol was detected in lesional and normal-appearing WM, and the Ins ratio was also increased in lesions. Several pathologic processes can lead to higher concentration of Ins, such as increase of activity or number of glial cells, or both (*278, 292*). We have found increased Ins together with decreased NAA, suggesting that the reduction in NAA may be caused by dilution effects as a result of neurons being more scarce and separated because of glial and astrocyte proliferation and infiltration. However, the increase in Ins is not necessary coupled with a decrease in NAA (*139*) or vice versa (*293*). The fact that our results showed increased Ins concentration in NAWM, but not NAA concentration, while Ins ratio was not statistically significant in NAWM, but the tNAA ratio was, suggests that the non-parallel behavior may be the result of normalizing with Cr. Altogether, our finding of increased Ins in lesions and NAWM suggests that gliosis might be important in MS pathology and further supports the use of Ins as a MS marker.

Another commonly detected metabolite in the spectra was glutamate and glutamine. Glu (measured as absolute concentration and ratio to tCr) was decreased in NELES, which may have reflected metabolic dysfunction and loss of neurons. However, a number of studies have attempted to estimate the metabolite differences of Glu, Gln or Glx, and have shown conflicting

results. Some studies showed elevated glutamate in acute lesions and NAWM (*144*), while others showed trends of decreased levels of Glx in NAWM in MS patients as compared to normal controls (*153, 280*). These conflicting results may be partially due to estimation differences in the quantification of the overlapping peaks of Glu/Gln.

No detectable changes in the concentrations of GPC or tGPC in either lesions or NAWM were found in this study, yet a mildly increased choline level has been observed in some studies in NAWM (*138, 139*), while other studies have found no change in choline levels (*294, 295*). However, a decreased GPC ratio was observed in NAWM in this study with borderline significance as a result of the statistics were performed as an exploratory investigation and were not corrected for multiple comparisons. Thus, this different finding should be interpreted with caution because a marginally higher level of tCr might lead to minor sensitivity in GPC/tCr values. Therefore, the role of choline in MS still remains uncertain and it could reflect a complex process with both demyelination and remyelination contributing to the total choline signal detected.

7.4.3. Cortical and Hippocampal Gray Matter Observations

From histopathology studies and findings from Chapter 4 in this study, there is no doubt that GM pathology is present in MS and may be quite extensive. Although no alterations in the absolute metabolite concentrations were found in both hippocampus and cortical GM, changes in metabolite ratios were found in both GM regions. Reduced GPC and tCho ratios were found in both hippocampus and CGM in MS patients. CGM also had decreased Glu and tNAA ratios in MS patients compared to controls.

As mentioned previously, reduction in GPC and tCho (mainly due to contribution from GPC) may indicate reduced cellular density or breakdown of cell membrane in GM. Unlike in

the NAWM, decreases in choline have been found in MS patients previously (*146*). The decrease in cell density, as suggested by decrease in choline found in both hippocampus and CGM, could result in net tissue atrophy and in the encroaching of the surrounding tissue, thus contributing to the overall reduction in GM volume. However, it should be noted that the significance level for the GPC ratio was borderline significant (*i.e.*, $p = 0.05$), thus this statistical difference might not be reproducible. Finally, it would be worthwhile to investigate if these results also apply to other GM regions, such the basal ganglia where maximum GM atrophy occurred as shown in Chapter 5.

Reduction in tNAA in CGM, like our findings in WM, may be related to cell loss and/or metabolic dysfunction. However, this reduction was not seen in the hippocampus in this study. Unlike in other gray matter structures such as the thalamus, NAA reduction in hippocampus has not been consistently shown in MS (*150*), which might be related to reduced spectral quality in the hippocampus where susceptibility effects are larger due to sources such as tissue inhomogeneity, the proximity to CSF, and a more complex cytoarchitecture. It could be that demyelination or axonal loss is less prevalent in the hippocampus of our RRMS patients than it is in other gray matter regions, and NAA reduction has not yet occurred in the hippocampus. This coincides with our results in Chapter 4 that hippocampal atrophy was not found but that atrophy was found in other GM regions. As mentioned before, the spectral quality of the hippocampus is poorer than in other GM regions, which may lead to lower quantification precision.

In the cortical GM, reduction in Glu was also found. As in the WM, the reduction may reflect reduced neurotransmitter activity, which could mark metabolic dysfunction. However, unlike our findings in WM, there is the absence of significant changes in Ins, which would suggest that glial loss might not be a major contributing factor in GM pathology in RRMS. It

should, however, be noted that a much smaller sample size of subjects with CGM MRS data were included as compared to other voxels, and one should not eliminate the possibility that we might find statistical significance by increasing the CGM sample size.

7.4.4. Metabolite Correlates with Other MR Measures

Amongst the four major metabolite components (all relative to tCr) examined, tNAA in the NAWM correlated with the majority of volumetric and DTI measures. Measurements of tNAA in the NAWM correlated positively with measures of whole brain, white matter, gray matter, and total hippocampal volume. In other words, the brain volume fraction decreases (or atrophy increases) with decreasing tNAA. Brain atrophy, an irreversible consequence of pathology, reflects loss of axons along with myelin and other tissue components. A tNAA measure complements atrophy findings in that it allows the assessment of total axonal damage, including loss of axon density and volume (which could lead to atrophy), or loss of myelin and axonal functionality (which reflects metabolic dysfunction that might not be associated with a related amount of atrophy). The latter is also supported by the significant correlations between tNAA in NAWM and radial diffusivity, an index for demyelination. Although NAWM tNAA also correlated with lesion burden and GM atrophy, this does not necessarily represent a causal relationship. In other words, a decrease of NAWM tNAA could be due to the Wallerian effect from lesional sites, or it could be independent from lesion pathology, and the pathological changes exist in parallel. As mentioned in earlier chapters, tissue damage in WM may or may not lead to pathological changes in GM.

Measurements of choline in the lesional and normal appearing white matter also correlated with volumetric measures, positively in this case, with choline levels increasing with decreasing tissue volume. Although choline reflects membrane turnover, which is associated

with demyelination, the increased choline can also reflect excess astrocytes and oligodendrocytes due to increased density of such cells (*296*). Moreover, volumetric measures could include non-neuronal tissue and inflammatory disease activity, which may be responsible for the positive relation between choline and tissue volume.

Lastly, Glx measurement in the hippocampus correlated negatively with atrophy and DTI measures. Because of neurotoxic potential of glutamate when it is altered (*297*), excess glutamate could contribute to axonal damage and brain atrophy as indicated. The association between MRS findings in GM and FA measures suggests that pathological changes in GM could be associated with white matter tissue integrity, as suggested in Chapter 6. Moreover, Glx is extremely difficult to quantify and is very susceptible to baseline errors and other effects, which may also contribute to the contradictory findings. Finally, we should allow for the possibility that the weak associations found in our study may be incidental.

7.4.5. Association between Metabolites and Cognitive Measures

In the exploratory correlation analysis, we did not find any significant correlation between measures of metabolites and the three cognitive measures. This is not surprising as using a single metabolite as a predictor for complex cognitive measures would be difficult. Indeed, many studies have not found metabolite correlates for cognitive impairment in MS (*298, 299*). However, when combined with other MR measures such as atrophy, one study using multiple regression models was able to account for larger variance in overall cognitive performance (*85*). In related work, our group developed a multiple regression model using only LCModel-derived metabolite concentrations that was not significantly correlated to the cognitive scores. On the other hand, it should be noted that our group has also developed a multivariate statistical model using raw NAWM spectra from a subset of the RRMS subjects used in this

study, which showed predictability of a combination of metabolites to the RAVLT score (*300*). The lack of correlation between cognitive measures and the metabolite alterations in RRMS in the present study does not necessarily lead to the conclusion that the predictive value of MRS findings is poor. MRS findings did correlate with other MR measures which are cognitively-relevant. Follow-up studies including conventional MRI and MRS can be helpful for further investigating the potential value of MRS in the prediction of neuropsychological disability in MS. Furthermore, it should be noted that our studies were exclusively limited to RRMS, a MS type with less severe cognitive deficits than other MS types, which might also explain the difficulty in demonstrating cognitive associations, though lower level of overall deficits were observed in the MS subjects as evidenced by the low EDSS.

7.4.6. Methodological and Analytical Considerations and Limitations

For MRS studies in general, it is difficult to select a pure tissue type with a reasonable voxel size to ensure good spectra quality without long acquisition time. The voxel placement criteria used here yielded voxels with minimal contamination from lesion (for non-lesion voxels), NAWM (for lesion and GM voxels), GM (for lesion and WM voxels), CSF (for all voxels), and non-brain tissue (for all voxels). In general, NAWM voxels had the largest proportions of a given tissue type to a given voxel (average 85%), whereas lesion voxels had the most partial volume effect amongst all voxels (average 40%). For hippocampus and CGM voxels, the tail of the hippocampus had a larger partial volume effect than the hippocampal head due to the structural complexity. CSF/lipid contamination was the hardest to minimize for CGM voxels.

The metabolite quantification technique is another consideration in all MRS studies. Here we used LCModel, the gold standard analytical technique in the MRS literature to date

(*287*). LCModel provides metabolite quantification in both absolute concentration and ratio relative to total creatine. While the concentration quantification gives values in mM based on a predefined basis set, it is difficult to calibrate against the actual values in the human brain *in vivo*. Since the concentration quantification may be different depending on the basis set and the parameters used, it might not be valid to directly compare results across centers. The use of ratio, on the other hand, may be less sensitive to the disease effects than the absolute quantification. However, the estimation error increases the number of metabolites used in the calculation; requiring the assumption that tCr is stable throughout tissue types, which is not consistent in MS studies.

Here, the correlations between variables were assumed to be linear. With the complexity of this disease, it may not be optimal to represent all these associations, and thus they should be reconsidered in future work. One additional consideration for correlation analysis with the amount of variables available was to explore other disease related parameters separately with Pearson correlations, rather than include them here and risk overparameterizing errors. When interpreting the results, one should note that with multiple comparisons, significance at a level of $p < 0.05$ may be due to chance alone.

Finally, this study used a single voxel approach rather than a multivoxel approach (example of a multivoxel approach is shown in Figure 27). We tried to achieve consistency in the hemispheric and lobal location of voxels for a particular type of tissue, though the voxel location, especially for NAWM and NELES voxels from an anatomical point of view, was different depending on lesion location. A comparison of spectra from different anatomical regions showed no statistical significance (although this could be due to small sample size for some regions). The variations in voxel locations could also contributed to the lack of

associations between MRS and cognition. Future studies should investigate whether or not an alteration of a metabolite was specific to the regions studied or was more generally throughout other regions within the same tissue type. Widespread abnormalities were observed in volumetric and DTI measurements, thus it is likely that the abnormalities we observed in the MRS study were more widespread.

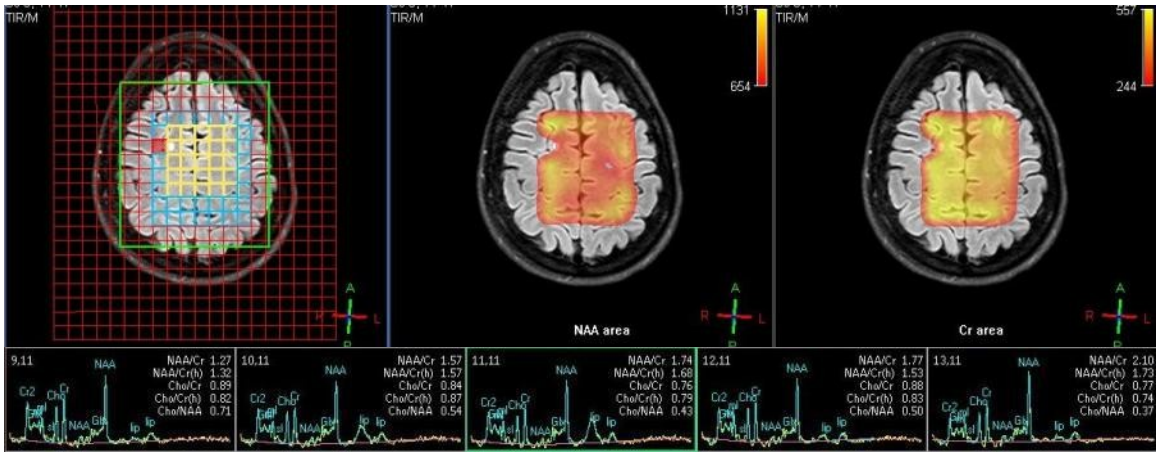

Figure 27. Example of multivoxel MRS. In multivoxel MRS, a grid of voxels is positioned on MRI image (left). Each voxel in the grid can be then processed (bottom panel) and metabolite maps (middle: NAA map; right: Cr map) can then be superimposed for visualization on corresponding MRI images. Bottom panel shows raw (white) and processed spectra (green) for selected voxels (top row of yellow boxes) from a RRMS patient.

7.5. Summary

In the present study, we have utilized MRS and provided a comprehensive non-invasive examination of metabolic alterations in the MS brain. Not only were we able to identify changes in metabolites underlying MS pathogenesis, we were able to pinpoint MS pathological differences in the normal appearing brain regions that were not detectable using conventional MRI. These changes in the normal appearing regions were also associated with volumetric and DTI measures, providing possible insight into mechanisms underlying changes in tissue integrity and metabolism. Although we were not able to find a MRS predictor for cognitive impairment

in MS, MRS still remains a valuable technique providing better sensitivity and specificity and should be used, perhaps together with other advanced techniques, in future studies.

Chapter 8

Summary and Future Directions

The mechanisms underlying disease progression in multiple sclerosis are still unclear. While conventional MR techniques have been used in the diagnosis and monitoring of this disease, the usefulness of conventional MRI is limited due to the lack of specificity and sensitivity to disease pathology. The lack of definite imaging biomarkers in MS also limits the development of therapeutic intervention that can eventually help treat the various symptoms of MS, including cognitive impairment. Here we have applied multi-modal MR imaging techniques to detect subtle changes that might reflect the underlying pathological mechanisms in brains of patients with relapsing-remitting multiple sclerosis. We have assessed the usefulness of using these MR techniques in predicting cognitive decline through correlational studies. The objectives of the present investigation were 1) to characterize volume loss in MS using advanced image analysis techniques, particularly in the gray matter regions, and its association to cognitive impairment; 2) to examine changes in MS tissue integrity using diffusion tensor imaging, and its correlation to cognition; 3) to investigate metabolic alterations in various regions of MS brain, and their association to cognition and other MR measures.

In brief, findings of this dissertation add to, and are consistent with, the observations in the MS literature, and we found that:

1) Significant gray matter atrophy occurs in MS brains, which corresponds to GM pathological observation, and may or may not accompanied by white matter atrophy;

2) Selective regional subcortical (basal ganglia) and cortical (frontal, parietal, and temporal) atrophy, quantified by FreeSurfer, correlated with cognitive dysfunction, suggest that these atrophy markers which may be useful to monitor disease course and assess efficacy of therapeutic interventions and treatment;

3) DTI parameters, such as FA and diffusivities, are sensitive markers to study white matter integrity both within and outside of WM lesions;

4) The TBSS-TFCE technique, allowing better detection of WM abnormalities, and indicates widespread association between reduced FA and cognitive impairment;

5) SDMT is a robust cognitive test in MS, with consistent association to atrophy and DTI indices;

6) MRS provided evidence of diffuse metabolic abnormalities in normal-appearing (white and gray matter) tissue in RRMS;

While as a result of this dissertation, more has been learned about underlying mechanisms for tissue damage that occurs in RRMS, we also recognize the limitations in sample characteristics, neuropsychological characteristics, and MRI methodology and analysis. Future studies should therefore improve upon current limitations, extend current studies to better understand the unexpected results, and generate new hypotheses based on our current exploratory findings. A few of the many possible future directions/improvements are:

1) A relatively small group of RRMS patients were included in this thesis, with factors such as education level, gender, handedness, IQ, ethnicity that were not controlled for. There was also an age difference between the RRMS patients and the healthy controls. Future work

could address this concern by extending the number of patients (and number of age-matched controls), as well as the number of time points. A larger cross-sectional study, controlling for various demographic characteristics, will likely reveal more statistical differences in MRI measures and stronger correlations between MRI metrics and clinical scores. On the other hand, if the changes in these measures are so subtle that they cannot be detected using small samples, it could be challenging to utilize these measures and apply them on an individual basis cross-sectionally. A longitudinal study could then be helpful in revealing changes in MRI metrics within individual patients as their disease progresses. Moreover, in order to continue building our understanding of the relations between cognitive impairment in general MS population and MR indices, the technique employed in this study should also be replicated in other MS subtypes.

2) Only a subset of cognitive domains was assessed at the present neuropsychological evaluation. In addition, only the RAVLT scores were significantly abnormal in MS patients out of the three tests used. It should be noted that the SDMT results were likely affected by an outlier in the MS group and once removed the difference on the mean SDMT scores between the MS and control groups reached significance. While all correlations were done within the MS group and the analyses were done for MRI metrics that were significantly different between the MS and the control group, we are aware that we included both cognitively-normal and mildly-impaired patients, thus the significant correlations between MRI findings and SDMT or PASAT should be interpreted with caution. Future studies could include more grounded cognitive measures for different and distinct cognitive domains with less overlap in testing. It should be also noted that a subgroup of MS patients included in this study were part of an on-going study that examines the influence of affective states (with or

without correlates to cognition) in MS. It should be also interesting to assess the relationship between cognition and emotional state in MS patients (e.g., depression and fatigue) to determine if the same MRI metrics can help to predict emotions in MS.

3) In terms of MRI acquisition and analysis, this dissertation suffers from methodological limitations similar to those reported in many other MRI studies.

    a. While we have demonstrated many regions of volume loss in our RRMS patients, we were not able to find significant atrophy in regions such as hippocampus that had been observed in other studies. As mentioned, the different methodology used could lead to variations in the quantitative results. In fact, there are many methods of examining structural brain ranging from manual to fully automated methods. Both manual and fully automated methods have benefits and limitations. While manual segmentation is viewed as the gold standard in many cases, it suffers from rater variability. The harmonization effort to standardize the definition of anatomic hippocampal boundaries will likely minimize technical differences in these measurement techniques in the future (*301*). It should be also considered that due to resource constraints, only one rater performed manual segmentation in one region. Perhaps future studies could involve multiple experienced raters to perform manual segmentation of other anatomical regions to validate findings using automated method. At the same time, future studies should also take advantage of the continuous development and validation of automated methods.

    b. We have demonstrated the usefulness of DTI in examining changes in tissue integrity. While we illustrated visually the relation between DTI and lesion, future work with

an improved analysis algorithm may involve looking at specific pathways transected by lesions using DTI tractography or combining VBM/Lesion methods with TBSS. TBSS results from this thesis can also help to generate tract/domain specific hypotheses for future DTI tractography. Improvement upon DTI acquisition with more gradient directions, higher image resolution, and implementing CSF suppression in the DTI sequence can help with the fiber tracking that was limited in the current study. Moreover, there are other DTI tools such as the FMRIB's diffusion toolbox for probabilistic tractography including crossing-fibre modeling, and DTIStudio's DifferoMap for atlas-based and voxel-based analyses that could be valuable alternatives to methods included in this thesis. Future studies can also utilize such methods to further the investigation of the spatial relation between NAWM DTI changes and the presence of T2 lesions.

c. Many other MRS acquisition and analysis techniques, besides the ones used in this thesis, are available and may be used to improve upon the current study. For example, future studies could expand upon the regions of interest for the MRS analysis across patients or generate within patient difference maps using the multivoxel approach. From our results, we observed changes in some lipid and macromolecule peaks, but were not able to reliably quantify other smaller lipid/macromolecular peaks. One could use metabolite-nulling techniques to separate these macromolecules and lipids from other metabolites, and modify the LCModel basis set to further investigate the spectral regions and determine if they are related to cognitive functions.

4) Using advanced MR techniques, we have shown changes in the normal appearing tissue that were not detectable using conventional MRI. Future studies should utilize the many other advanced MR sequences, such as magnetization transfer, perfusion imaging, and susceptibility weighted imaging, that could help detect more subtle MS-related parenchymal abnormalities and capture this "silent" pathology.

5) Although individually these techniques are each sensitive to brain alterations caused by disease, there is still a limited understanding of the specificity of these changes and how, or if, they are inter-related with one another. Certainly, in a complex and heterogeneous disease like MS, it is likely that no single pathological feature or method can implicate all changes. Therefore, future studies should also include additional MR techniques that complement each other, where multivariate analyses predicting cognitive outcomes would be a great extension of this dissertation work. For example, adding fMRI to the DTI study may provide complementary insights regarding tissue integrity and functional connectivity, and help determine if these factors may be associated with cognitive impairment in MS.

6) While we studied parenchymal changes in the MS brain, changes in the spinal cord should not be overlooked. Many methods used in this thesis can be also applied to study MS-related spinal cord damage. One could help understand the link between MR and pathology by conducting MRS experiments to compare metabolic profiles in the *in vivo* and *ex vivo* spinal cord CSF. However, it is likely that spinal cord damage might be more closely linked to motor disability than to cognitive impairment. Besides the spinal cord, MR techniques such as DTI can be also applied to optic neuritis, a disease with inflammation of the optic nerve that is usually caused by multiple sclerosis.

7) In this dissertation, we studied only adult MS, but pediatric MS is another major research area of interest. Pediatric MS may or may not share the same mechanisms as adult MS. Quantitative imaging techniques used in this thesis should also be applied to these children.

8) Last but not least, the ultimate goal of all MS studies is to find improved imaging biomarkers that can be used as clinical endpoints to help accelerate the development of a cure for MS. MS lesions still remain the most commonly accepted imaging biomarker in current MS clinical trials. We have shown lesion heterogeneity that might limit the use of lesions as a surrogate endpoint. While it would be worthwhile to continue monitoring the evolution of and treatment effects on the various lesions, including T2 lesions, T1 lesions, enhanced lesions and GM lesions, imaging markers from advanced MR techniques such as FA and atrophy also hold great potential.

In conclusion, this dissertation investigated advanced MR imaging techniques and novel acquisition methods to assess their capabilities and clinical applications in patients with MS. Despite the fact that additional research is required in order to better understand MS, this body of work advanced our knowledge in relating MR metrics to underlying disease processes, and improving characterization over and above that which is seen with conventional imaging. The results of this work may contribute towards developing future clinical metrics that comprehensively evaluate disease accumulation in patients, facilitating therapy development and monitoring, thus improving the quality of life for people who have MS. Finally, in this dissertation, we have developed and shown the value of quantitative MR imaging techniques and imaging processing tools as non-invasive methods for studying not only multiple sclerosis, but other disease of the human brain.

References

1. J. S. Burks, K. P. Johnson, *Multiple sclerosis : diagnosis, medical management, and rehabilitation*. (Demos, New York, 2000), pp. xviii, 598 p.
2. C. M. Poser, V. V. Brinar, Diagnostic criteria for multiple sclerosis: an historical review. *Clin Neurol Neurosurg* **106**, 147 (Jun, 2004).
3. G. R. Moore, Current concepts in the neuropathology and pathogenesis of multiple sclerosis. *The Canadian journal of neurological sciences. Le journal canadien des sciences neurologiques* **37 Suppl 2**, S5 (Sep, 2010).
4. J. J. Geurts, F. Barkhof, Grey matter pathology in multiple sclerosis. *Lancet Neurol* **7**, 841 (Sep, 2008).
5. D. H. Miller, A. J. Thompson, M. Filippi, Magnetic resonance studies of abnormalities in the normal appearing white matter and grey matter in multiple sclerosis. *Journal of Neurology* **250**, 1407 (Dec, 2003).
6. J. W. Peterson, L. Bo, S. Mork, A. Chang, B. D. Trapp, Transected neurites, apoptotic neurons, and reduced inflammation in cortical multiple sclerosis lesions. *Annals of Neurology* **50**, 389 (Sep, 2001).
7. D. Chard, D. Miller, Grey matter pathology in clinically early multiple sclerosis: Evidence from magnetic resonance imaging. *J Neurol Sci*, (Feb 5, 2009).
8. C. M. Poser *et al.*, New diagnostic criteria for multiple sclerosis: guidelines for research protocols. *Ann Neurol* **13**, 227 (Mar, 1983).
9. W. I. McDonald *et al.*, Recommended diagnostic criteria for multiple sclerosis: guidelines from the International Panel on the diagnosis of multiple sclerosis. *Ann Neurol* **50**, 121 (Jul, 2001).
10. C. H. Polman *et al.*, Diagnostic criteria for multiple sclerosis: 2005 Revisions to the "McDonald Criteria". *Annals of Neurology* **58**, 840 (Dec, 2005).
11. B. M. Keegan, J. H. Noseworthy, Multiple sclerosis. *Annu Rev Med* **53**, 285 (2002).
12. J. F. Kurtzke, Rating neurologic impairment in multiple sclerosis: an expanded disability status scale (EDSS). *Neurology* **33**, 1444 (Nov, 1983).
13. H. P. Hartung, A. Bar-Or, Y. Zoukos, What do we know about the mechanism of action of disease-modifying treatments in MS? *J Neurol* **251 Suppl 5**, v12 (Sep, 2004).
14. B. Sharrack, R. A. Hughes, Clinical scales for multiple sclerosis. *J Neurol Sci* **135**, 1 (Jan, 1996).
15. N. D. Chiaravalloti, J. DeLuca, Cognitive impairment in multiple sclerosis. *Lancet Neurol* **7**, 1139 (Dec, 2008).
16. M. Summers *et al.*, Cognitive impairment in multiple sclerosis can be predicted by imaging early in the disease. *J Neurol Neurosurg Psychiatry* **79**, 955 (Aug, 2008).
17. M. P. Amato *et al.*, The Rao's Brief Repeatable Battery and Stroop Test: normative values with age, education and gender corrections in an Italian population. *Mult Scler* **12**, 787 (Dec, 2006).
18. B. Brochet *et al.*, Should SDMT substitute for PASAT in MSFC? A 5-year longitudinal study. *Mult Scler* **14**, 1242 (Nov, 2008).
19. A. Achiron, Y. Barak, Cognitive impairment in probable multiple sclerosis. *J Neurol Neurosurg Psychiatry* **74**, 443 (Apr, 2003).

20. K. K. Zakzanis, Distinct neurocognitive profiles in multiple sclerosis subtypes. *Arch Clin Neuropsychol* **15**, 115 (Feb, 2000).
21. W. W. Beatty, R. L. Aupperle, Sex differences in cognitive impairment in multiple sclerosis. *Clin Neuropsychol* **16**, 472 (Dec, 2002).
22. S. M. Rao *et al.*, Cognitive dysfunction in multiple sclerosis. II. Impact on employment and social functioning. *Neurology* **41**, 692 (May, 1991).
23. I. S. Lobentanz *et al.*, Factors influencing quality of life in multiple sclerosis patients: disability, depressive mood, fatigue and sleep quality. *Acta Neurol Scand* **110**, 6 (Jul, 2004).
24. A. Feinstein, Mood disorders in multiple sclerosis and the effects on cognition. *J Neurol Sci* **245**, 63 (Jun 15, 2006).
25. C. Engel, B. Greim, U. K. Zettl, Diagnostics of cognitive dysfunctions in multiple sclerosis. *J Neurol* **254 Suppl 2**, II30 (May, 2007).
26. M. P. Amato, G. Ponziani, G. Siracusa, S. Sorbi, Cognitive dysfunction in early-onset multiple sclerosis: a reappraisal after 10 years. *Archives of Neurology* **58**, 1602 (Oct, 2001).
27. S. C. Huijbregts, N. F. Kalkers, L. M. de Sonneville, V. de Groot, C. H. Polman, Cognitive impairment and decline in different MS subtypes. *J Neurol Sci* **245**, 187 (Jun 15, 2006).
28. E. M. Haacke, *Magnetic resonance imaging : physical principles and sequence design*. (Wiley, New York, 1999), pp. xxvii, 914 p.
29. B. A. Hart *et al.*, Histopathological characterization of magnetic resonance imaging-detectable brain white matter lesions in a primate model of multiple sclerosis: a correlative study in the experimental autoimmune encephalomyelitis model in common marmosets (Callithrix jacchus). *The American journal of pathology* **153**, 649 (Aug, 1998).
30. R. Bakshi, Magnetic resonance imaging advances in multiple sclerosis. *J Neuroimaging* **15**, 5S (2005).
31. M. Inglese, R. I. Grossman, M. Filippi, Magnetic resonance imaging monitoring of multiple sclerosis lesion evolution. *Journal of Neuroimaging* **15**, 22S (2005).
32. R. Zivadinov, Can imaging techniques measure neuroprotection and remyelination in multiple sclerosis? *Neurology* **68**, S72 (May 29, 2007).
33. M. Filippi, F. Agosta, Imaging biomarkers in multiple sclerosis. *J Magn Reson Imaging* **31**, 770 (Apr, 2010).
34. B. Bielekova, R. Martin, Development of biomarkers in multiple sclerosis. *Brain* **127**, 1463 (Jul, 2004).
35. T. Moreau *et al.*, Preliminary Evidence From Magnetic-Resonance-Imaging For Reduction in Disease-Activity after Lymphocyte Depletion in Multiple-Sclerosis. *Lancet* **344**, 298 (Jul, 1994).
36. J. Newcombe *et al.*, Histopathology of multiple sclerosis lesions detected by magnetic resonance imaging in unfixed postmortem central nervous system tissue. *Brain* **114 (Pt 2)**, 1013 (Apr, 1991).
37. R. Zivadinov, T. P. Leist, Clinical-magnetic resonance imaging correlations in multiple sclerosis. *Journal of Neuroimaging* **15**, 10s (2005).
38. D. K. Li *et al.*, MRI T2 lesion burden in multiple sclerosis: a plateauing relationship with clinical disability. *Neurology* **66**, 1384 (May 9, 2006).

39. A. Bitsch *et al.*, A longitudinal MRI study of histopathologically defined hypointense multiple sclerosis lesions. *Annals of Neurology* **49**, 793 (Jun, 2001).
40. J. M. Stankiewicz *et al.*, Spinal cord lesions and clinical status in multiple sclerosis: A 1.5 T and 3 T MRI study. *Journal of the Neurological Sciences* **279**, 99 (2009).
41. A. Gass *et al.*, Characteristics of chronic MS lesions in the cerebrum, brainstem, spinal cord, and optic nerve on T1-weighted MRI. *Neurology* **50**, 548 (Feb, 1998).
42. F. Agosta, M. Filippi, MRI of spinal cord in multiple sclerosis. *Journal of neuroimaging : official journal of the American Society of Neuroimaging* **17 Suppl 1**, 46S (Apr, 2007).
43. D. H. Miller, R. I. Grossman, S. C. Reingold, H. F. McFarland, The role of magnetic resonance techniques in understanding and managing multiple sclerosis. *Brain* **121 (Pt 1)**, 3 (Jan, 1998).
44. D. H. Miller, F. Barkhof, J. A. Frank, G. J. M. Parker, A. J. Thompson, Measurement of atrophy in multiple sclerosis: pathological basis, methodological aspects and clinical relevance. *Brain* **125**, 1676 (Aug, 2002).
45. V. M. Anderson, N. C. Fox, D. H. Miller, Magnetic resonance imaging measures of brain atrophy in multiple sclerosis. *J Magn Reson Imaging* **23**, 605 (May, 2006).
46. R. A. Bermel, R. Bakshi, The measurement and clinical relevance of brain atrophy in multiple sclerosis. *Lancet Neurology* **5**, 158 (2006).
47. B. Turner, X. Lin, G. Calmon, N. Roberts, L. D. Blumhardt, Cerebral atrophy and disability in relapsing-remitting and secondary progressive multiple sclerosis over four years. *Mult Scler* **9**, 21 (Feb, 2003).
48. C. M. Dalton *et al.*, Progressive ventricular enlargement in patients with clinically isolated syndromes is associated with the early development of multiple sclerosis. *J Neurol Neurosurg Psychiatry* **73**, 141 (Aug, 2002).
49. N. F. Kalkers *et al.*, Longitudinal brain volume measurement in multiple sclerosis: rate of brain atrophy is independent of the disease subtype. *Arch Neurol* **59**, 1572 (Oct, 2002).
50. D. T. Chard *et al.*, Progressive grey matter atrophy in clinically early relapsing-remitting multiple sclerosis. *Multiple Sclerosis* **10**, 387 (2004).
51. C. M. Dalton *et al.*, Early development of multiple sclerosis is associated with progressive grey matter atrophy in patients presenting with clinically isolated syndromes. *Brain* **127**, 1101 (May, 2004).
52. N. De Stefano *et al.*, Evidence of axonal damage in the early stages of multiple sclerosis and its relevance to disability. *Archives of Neurology* **58**, 65 (Jan, 2001).
53. M. Tiberio *et al.*, Gray and white matter volume changes in early RRMS: a 2-year longitudinal study. *Neurology* **64**, 1001 (Mar 22, 2005).
54. A. Charil, M. Filippi, Inflammatory demyelination and neurodegeneration in early multiple sclerosis. *J Neurol Sci* **259**, 7 (Aug 15, 2007).
55. J. T. Chen *et al.*, Relating neocortical pathology to disability progression in multiple sclerosis using MRI. *Neuroimage* **23**, 1168 (Nov, 2004).
56. E. Fisher, J. C. Lee, K. Nakamura, R. A. Rudick, Gray matter atrophy in multiple sclerosis: A longitudinal study. *Annals of Neurology* **64**, 255 (2008).
57. M. Wylezinska *et al.*, Thalamic neurodegeneration in relapsing-remitting multiple sclerosis. *Neurology* **60**, 1949 (2003).
58. A. Cifelli *et al.*, Thalamic neurodegeneration in multiple sclerosis. *Annals of Neurology* **52**, 650 (Nov, 2002).

59. R. A. Bermel, M. D. Innus, C. W. Tjoa, R. Bakshi, Selective caudate atrophy in multiple sclerosis: a 3D MRI parcellation study. *Neuroreport* **14**, 335 (2003).
60. M. Sailer *et al.*, Focal thinning of the cerebral cortex in multiple sclerosis. *Brain* **126**, 1734 (Aug, 2003).
61. B. Audoin *et al.*, Localization of grey matter atrophy in early RRMS : A longitudinal study. *J Neurol* **253**, 1495 (Nov, 2006).
62. S. Mesaros *et al.*, Clinical and conventional MRI predictors of disability and brain atrophy accumulation in RRMS. A large scale, short-term follow-up study. *J Neurol* **255**, 1378 (Sep, 2008).
63. L. K. Fisniku *et al.*, Gray matter atrophy is related to long-term disability in multiple sclerosis. *Annals of Neurology* **64**, 247 (2008).
64. G. Tedeschi *et al.*, Correlation between fatigue and brain atrophy and lesion load in multiple sclerosis patients independent of disability. *J Neurol Sci* **263**, 15 (Dec 15, 2007).
65. J. Sepulcre *et al.*, Regional gray matter atrophy in early primary progressive multiple sclerosis: a voxel-based morphometry study. *Arch Neurol* **63**, 1175 (Aug, 2006).
66. M. P. Sanfilipo, R. H. B. Benedict, J. Sharma, B. Weinstock-Guttman, R. Bakshi, The relationship between whole brain volume and disability in multiple sclerosis: A comparison of normalized gray vs. white matter with misclassification correction. *Neuroimage* **26**, 1068 (Jul 15, 2005).
67. Y. Ge *et al.*, Brain atrophy in relapsing-remitting multiple sclerosis and secondary progressive multiple sclerosis: longitudinal quantitative analysis. *Radiology* **214**, 665 (Mar, 2000).
68. R. H. Benedict *et al.*, Prediction of neuropsychological impairment in multiple sclerosis: comparison of conventional magnetic resonance imaging measures of atrophy and lesion burden. *Arch Neurol* **61**, 226 (Feb, 2004).
69. R. Zivadinov *et al.*, MRI techniques and cognitive impairment in the early phase of relapsing-remitting multiple sclerosis. *Neuroradiology* **43**, 272 (Apr, 2001).
70. E. Fisher *et al.*, Eight-year follow-up study of brain atrophy in patients with MS. *Neurology* **59**, 1412 (Nov 12, 2002).
71. R. A. Rudick, E. Fisher, J. C. Lee, J. T. Duda, J. Simon, Brain atrophy in relapsing multiple sclerosis: relationship to relapses, EDSS, and treatment with interferon beta-1a. *Mult Scler* **6**, 365 (Dec, 2000).
72. M. Rovaris, G. Comi, M. Filippi, Can glatiramer acetate reduce brain atrophy development in multiple sclerosis? *J Neurol Sci* **233**, 139 (Jun 15, 2005).
73. P. D. Molyneux *et al.*, The effect of interferon beta-1b treatment on MRI measures of cerebral atrophy in secondary progressive multiple sclerosis. European Study Group on Interferon beta-1b in secondary progressive multiple sclerosis. *Brain* **123 (Pt 11)**, 2256 (Nov, 2000).
74. M. Filippi *et al.*, Interferon beta-1a for brain tissue loss in patients at presentation with syndromes suggestive of multiple sclerosis: a randomised, double-blind, placebo-controlled trial. *Lancet* **364**, 1489 (2004).
75. F. Klauschen, A. Goldman, V. Barra, A. Meyer-Lindenberg, A. Lundervold, Evaluation of Automated Brain MR Image Segmentation and Volumetry Methods. *Hum Brain Mapp* **30**, 1310 (Apr, 2009).
76. S. Sharma *et al.*, Evaluation of brain atrophy estimation algorithms using simulated ground-truth data. *Med Image Anal* **14**, 373 (Jun, 2010).

77. K. Nakamura, E. Fisher, Segmentation of brain magnetic resonance images for measurement of gray matter atrophy in multiple sclerosis patients. *Neuroimage* **44**, 769 (2009).
78. M. Blinkenberg *et al.*, Cortical cerebral metabolism correlates with MRI lesion load and cognitive dysfunction in MS. *Neurology* **54**, 558 (Feb 8, 2000).
79. S. D. Brass, R. H. Benedict, B. Weinstock-Guttman, F. Munschauer, R. Bakshi, Cognitive impairment is associated with subcortical magnetic resonance imaging grey matter T2 hypointensity in multiple sclerosis. *Mult Scler* **12**, 437 (Aug, 2006).
80. R. A. Sperling *et al.*, Regional magnetic resonance imaging lesion burden and cognitive function in multiple sclerosis: a longitudinal study. *Arch Neurol* **58**, 115 (Jan, 2001).
81. E. E. Smith *et al.*, Correlations between MRI white matter lesion location and executive function and episodic memory. *Neurology* **76**, 1492 (Apr 26, 2011).
82. M. P. Amato *et al.*, Cognitive impairment in early-onset multiple sclerosis. Pattern, predictors, and impact on everyday life in a 4-year follow-up. *Arch Neurol* **52**, 168 (Feb, 1995).
83. S. J. Camp *et al.*, Cognitive function in primary progressive and transitional progressive multiple sclerosis: a controlled study with MRI correlates. *Brain* **122 (Pt 7)**, 1341 (Jul, 1999).
84. R. Zivadinov *et al.*, A longitudinal study of brain atrophy and cognitive disturbances in the early phase of relapsing-remitting multiple sclerosis. *J Neurol Neurosur Ps* **70**, 773 (Jun, 2001).
85. C. Christodoulou *et al.*, Cognitive performance and MR markers of cerebral injury in cognitively impaired MS patients. *Neurology* **60**, 1793 (Jun 10, 2003).
86. R. H. Benedict *et al.*, Regional lobar atrophy predicts memory impairment in multiple sclerosis. *AJNR Am J Neuroradiol* **26**, 1824 (Aug, 2005).
87. K. Morgen *et al.*, Evidence for a direct association between cortical atrophy and cognitive impairment in relapsing-remitting MS. *Neuroimage* **30**, 891 (Apr 15, 2006).
88. M. K. Houtchens *et al.*, Thalamic atrophy and cognition in multiple sclerosis. *Neurology* **69**, 1213 (Sep 18, 2007).
89. N. L. Sicotte *et al.*, Regional hippocampal atrophy in multiple sclerosis. *Brain* **131**, 1134 (Apr, 2008).
90. M. P. Amato *et al.*, Neocortical volume decrease in relapsing-remitting MS patients with mild cognitive impairment. *Neurology* **63**, 89 (Jul 13, 2004).
91. R. H. Benedict *et al.*, Frontal cortex atrophy predicts cognitive impairment in multiple sclerosis. *J Neuropsychiatry Clin Neurosci* **14**, 44 (Winter, 2002).
92. J. Pelletier *et al.*, A longitudinal study of callosal atrophy and interhemispheric dysfunction in relapsing-remitting multiple sclerosis. *Arch Neurol* **58**, 105 (Jan, 2001).
93. Y. Ge, M. Law, R. I. Grossman, Applications of diffusion tensor MR imaging in multiple sclerosis. *Ann N Y Acad Sci* **1064**, 202 (Dec, 2005).
94. D. Goldberg-Zimring, A. U. Mewes, M. Maddah, S. K. Warfield, Diffusion tensor magnetic resonance imaging in multiple sclerosis. *Journal of neuroimaging : official journal of the American Society of Neuroimaging* **15**, 68S (2005).
95. M. Rovaris, M. Filippi, Diffusion tensor MRI in multiple sclerosis. *J Neuroimaging* **17 Suppl 1**, 27S (Apr, 2007).
96. P. J. Basser, C. Pierpaoli, Microstructural and physiological features of tissues elucidated by quantitative-diffusion-tensor MRI. *J Magn Reson B* **111**, 209 (Jun, 1996).

97. M. A. Horsfield, H. B. Larsson, D. K. Jones, A. Gass, Diffusion magnetic resonance imaging in multiple sclerosis. *Journal of neurology, neurosurgery, and psychiatry* **64 Suppl 1**, S80 (May, 1998).
98. D. Le Bihan *et al.*, Diffusion tensor imaging: concepts and applications. *J Magn Reson Imaging* **13**, 534 (Apr, 2001).
99. Q. Dong *et al.*, Clinical applications of diffusion tensor imaging. *Journal of Magnetic Resonance Imaging* **19**, 6 (2004).
100. P. C. Sundgren *et al.*, Diffusion tensor imaging of the brain: review of clinical applications. *Neuroradiology* **46**, 339 (2004).
101. R. Bammer *et al.*, Magnetic resonance diffusion tensor imaging for characterizing diffuse and focal white matter abnormalities in multiple sclerosis. *Magnetic resonance in medicine : official journal of the Society of Magnetic Resonance in Medicine / Society of Magnetic Resonance in Medicine* **44**, 583 (Oct, 2000).
102. S. Roychowdhury, J. A. Maldjian, R. I. Grossman, Multiple sclerosis: comparison of trace apparent diffusion coefficients with MR enhancement pattern of lesions. *AJNR. American journal of neuroradiology* **21**, 869 (May, 2000).
103. D. J. Werring, C. A. Clark, G. J. Barker, A. J. Thompson, D. H. Miller, Diffusion tensor imaging of lesions and normal-appearing white matter in multiple sclerosis. *Neurology* **52**, 1626 (May 12, 1999).
104. K. M. Hasan, R. K. Gupta, R. M. Santos, J. S. Wolinsky, P. A. Narayana, Diffusion tensor fractional anisotropy of the normal-appearing seven segments of the corpus callosum in healthy adults and relapsing-remitting multiple sclerosis patients. *J Magn Reson Imaging* **21**, 735 (Jun, 2005).
105. M. A. Rocca, M. Cercignani, G. Iannucci, G. Comi, M. Filippi, Weekly diffusion-weighted imaging of normal-appearing white matter in MS. *Neurology* **55**, 882 (2000).
106. D. J. Werring *et al.*, The pathogenesis of lesions and normal-appearing white matter changes in multiple sclerosis: a serial diffusion MRI study. *Brain* **123 (Pt 8)**, 1667 (Aug, 2000).
107. M. Cercignani, M. Bozzali, G. Iannucci, G. Comi, M. Filippi, Magnetisation transfer ratio and mean diffusivity of normal appearing white and grey matter from patients with multiple sclerosis. *J Neurol Neurosurg Psychiatry* **70**, 311 (Mar, 2001).
108. M. Rovaris *et al.*, Short-term accrual of gray matter pathology in patients with progressive multiple sclerosis: an in vivo study using diffusion tensor MRI. *Neuroimage* **24**, 1139 (Feb 15, 2005).
109. H. Vrenken *et al.*, Altered diffusion tensor in multiple sclerosis normal-appearing brain tissue: cortical diffusion changes seem related to clinical deterioration. *Journal of magnetic resonance imaging : JMRI* **23**, 628 (May, 2006).
110. C. S. Yu *et al.*, Histogram analysis of diffusion measures in clinically isolated syndromes and relapsing-remitting multiple sclerosis. *Eur J Radiol* **68**, 328 (Nov, 2008).
111. K. Schmierer *et al.*, Diffusion tensor imaging of post mortem multiple sclerosis brain. *Neuroimage* **35**, 467 (Apr 1, 2007).
112. B. Audoin *et al.*, Structure of WM bundles constituting the working memory system in early multiple sclerosis: a quantitative DTI tractography study. *Neuroimage* **36**, 1324 (Jul 15, 2007).
113. R. A. Dineen *et al.*, Disconnection as a mechanism for cognitive dysfunction in multiple sclerosis. *Brain* **132**, 239 (Jan, 2009).

114. X. Lin, C. R. Tench, P. S. Morgan, G. Niepel, C. S. Constantinescu, 'Importance sampling' in MS: Use of diffusion tensor tractography to quantify pathology related to specific impairment. *Journal of the Neurological Sciences* **237**, 13 (2005).
115. M. Wilson, C. R. Tench, P. S. Morgan, L. D. Blumhardt, Pyramidal tract mapping by diffusion tensor magnetic resonance imaging in multiple sclerosis: improving correlations with disability. *J Neurol Neurosur Ps* **74**, 203 (2003).
116. D. K. Shukla, C. C. Kaiser, G. T. Stebbins, D. L. Feinstein, Effects of pioglitazone on diffusion tensor imaging indices in multiple sclerosis patients. *Neurosci Lett* **472**, 153 (Mar 26, 2010).
117. R. J. Fox, Picturing multiple sclerosis: conventional and diffusion tensor imaging. *Semin Neurol* **28**, 453 (Sep, 2008).
118. C. Mainero *et al.*, Correlates of MS disability assessed in vivo using aggregates of MR quantities. *Neurology* **56**, 1331 (2001).
119. A. Pulizzi *et al.*, Determinants of disability in multiple sclerosis at various disease stages: a multiparametric magnetic resonance study. *Arch Neurol* **64**, 1163 (Aug, 2007).
120. A. Lin, B. D. Ross, K. Harris, W. Wong, Efficacy of proton magnetic resonance spectroscopy in neurological diagnosis and neurotherapeutic decision making. *NeuroRx* **2**, 197 (Apr, 2005).
121. D. L. Arnold, P. M. Matthews, G. Francis, J. Antel, Proton magnetic resonance spectroscopy of human brain in vivo in the evaluation of multiple sclerosis: assessment of the load of disease. *Magn Reson Med* **14**, 154 (Apr, 1990).
122. J. S. Wolinsky, P. A. Narayana, M. J. Fenstermacher, Proton magnetic resonance spectroscopy in multiple sclerosis. *Neurology* **40**, 1764 (Nov, 1990).
123. N. De Stefano, M. L. Bartolozzi, L. Guidi, M. L. Stromillo, A. Federico, Magnetic resonance spectroscopy as a measure of brain damage in multiple sclerosis. *J Neurol Sci* **233**, 203 (Jun 15, 2005).
124. C. A. Husted *et al.*, Biochemical-Alterations in Multiple-Sclerosis Lesions and Normal-Appearing White-Matter Detected by in-Vivo P-31 and H-1 Spectroscopic Imaging. *Annals of Neurology* **36**, 157 (Aug, 1994).
125. S. M. Leary *et al.*, 1H magnetic resonance spectroscopy of normal appearing white matter in primary progressive multiple sclerosis. *J Neurol* **246**, 1023 (Nov, 1999).
126. R. Sharma, P. A. Narayana, J. S. Wolinsky, Grey matter abnormalities in multiple sclerosis: proton magnetic resonance spectroscopic imaging. *Multiple Sclerosis* **7**, 221 (Aug, 2001).
127. A. Tourbah *et al.*, In vivo localized NMR proton spectroscopy of normal appearing white matter in patients with multiple sclerosis. *J Neuroradiol* **23**, 49 (Sep, 1996).
128. C. Bjartmar, B. D. Trapp, Axonal and neuronal degeneration in multiple sclerosis: mechanisms and functional consequences. *Current Opinion in Neurology* **14**, 271 (Jun, 2001).
129. E. Adalsteinsson *et al.*, Gray matter N-acetyl aspartate deficits in secondary progressive but not relapsing-remitting multiple sclerosis. *AJNR Am J Neuroradiol* **24**, 1941 (Nov-Dec, 2003).
130. N. De Stefano *et al.*, Brain damage as detected by magnetization transfer imaging is less pronounced in benign than in early relapsing multiple sclerosis. *Brain* **129**, 2008 (2006).
131. L. Fu *et al.*, Statistics for investigation of multimodal MR imaging data and an application to multiple sclerosis patients. *NMR Biomed* **9**, 339 (Dec, 1996).

132. M. Rovaris, G. Comi, M. Filippi, MRI markers of destructive pathology in multiple sclerosis-related cognitive dysfunction. *J Neurol Sci* **245**, 111 (Jun 15, 2006).
133. Z. Caramanos, S. Narayanan, D. L. Arnold, 1H-MRS quantification of tNA and tCr in patients with multiple sclerosis: a meta-analytic review. *Brain* **128**, 2483 (Nov, 2005).
134. F. Schubert *et al.*, Serial 1H-MRS in relapsing-remitting multiple sclerosis: effects of interferon-beta therapy on absolute metabolite concentrations. *Magnetic Resonance Materials in Physics Biology and Medicine* **14**, 213 (Jun, 2002).
135. J. Suhy *et al.*, 1H MRSI comparison of white matter and lesions in primary progressive and relapsing-remitting MS. *Mult Scler* **6**, 148 (Jun, 2000).
136. M. Tiberio *et al.*, Metabolite changes in early relapsing-remitting multiple sclerosis. A two year follow-up study. *J Neurol* **253**, 224 (Feb, 2006).
137. J. He *et al.*, Relapsing-remitting multiple sclerosis: Metabolic abnormality in nonenhancing lesions and normal-appearing white matter at MR imaging: Initial experience. *Radiology* **234**, 211 (Jan, 2005).
138. M. C. Tartaglia *et al.*, Choline is increased in pre-lesional normal appearing white matter in multiple sclerosis. *Journal of Neurology* **249**, 1382 (Oct, 2002).
139. H. Vrenken *et al.*, MR spectroscopic evidence for glial increase but not for neuro-axonal damage in MS normal-appearing white matter. *Magn Reson Med* **53**, 256 (Feb, 2005).
140. P. A. Narayana, T. J. Doyle, D. Lai, J. S. Wolinsky, Serial proton magnetic resonance spectroscopic imaging, contrast-enhanced magnetic resonance imaging, and quantitative lesion volumetry in multiple sclerosis. *Ann Neurol* **43**, 56 (Jan, 1998).
141. P. Kapeller *et al.*, Preliminary evidence for neuronal damage in cortical grey matter and normal appearing white matter in short duration relapsing-remitting multiple sclerosis: a quantitative MR spectroscopic imaging study. *J Neurol* **248**, 131 (Feb, 2001).
142. P. Kapeller *et al.*, Quantitative 1H MRS imaging 14 years after presenting with a clinically isolated syndrome suggestive of multiple sclerosis. *Mult Scler* **8**, 207 (May, 2002).
143. M. S. Fernando *et al.*, Comparison of the pathology of cerebral white matter with post-mortem magnetic resonance imaging (MRI) in the elderly brain. *Neuropathology and Applied Neurobiology* **30**, 385 (2004).
144. R. Srinivasan, N. Sailasuta, R. Hurd, S. Nelson, D. Pelletier, Evidence of elevated glutamate in multiple sclerosis using magnetic resonance spectroscopy at 3 T. *Brain* **128**, 1016 (May, 2005).
145. I. Mader, S. Rauer, P. Gall, U. Klose, (1)H MR spectroscopy of inflammation, infection and ischemia of the brain. *Eur J Radiol* **67**, 250 (Aug, 2008).
146. P. E. Sijens, J. P. Mostert, M. Oudkerk, J. De Keyser, (1)H MR spectroscopy of the brain in multiple sclerosis subtypes with analysis of the metabolite concentrations in gray and white matter: initial findings. *Eur Radiol* **16**, 489 (Feb, 2006).
147. J. J. Geurts *et al.*, Quantitative 1H-MRS of healthy human cortex, hippocampus, and thalamus: metabolite concentrations, quantification precision, and reproducibility. *J Magn Reson Imaging* **20**, 366 (Sep, 2004).
148. J. Oh, R. G. Henry, C. Genain, S. J. Nelson, D. Pelletier, Mechanisms of normal appearing corpus callosum injury related to pericallosal T1 lesions in multiple sclerosis using directional diffusion tensor and H-1 MRS imaging. *J Neurol Neurosur Ps* **75**, 1281 (2004).

149. Z. Caramanos, S. DiMaio, S. Narayanan, Y. Lapierre, D. L. Arnold, (1)H-MRSI evidence for cortical gray matter pathology that is independent of cerebral white matter lesion load in patients with secondary progressive multiple sclerosis. *J Neurol Sci* **282**, 72 (Jul 15, 2009).
150. J. J. Geurts *et al.*, MR spectroscopic evidence for thalamic and hippocampal, but not cortical, damage in multiple sclerosis. *Magnetic Resonance in Medicine* **55**, 478 (Mar, 2006).
151. P. Sarchielli *et al.*, Localized (1)H magnetic resonance spectroscopy in mainly cortical gray matter of patients with multiple sclerosis. *J Neurol* **249**, 902 (Jul, 2002).
152. L. N. Manganas *et al.*, Magnetic resonance spectroscopy identifies neural progenitor cells in the live human brain. *Science* **318**, 980 (Nov 9, 2007).
153. J. Sastre-Garriga *et al.*, Metabolite changes in normal-appearing gray and white matter are linked with disability in early primary progressive multiple sclerosis. *Arch Neurol* **62**, 569 (Apr, 2005).
154. J. L. Ruiz-Pena, P. Duque, G. Izquierdo, Optimization of treatment with interferon beta in multiple sclerosis. Usefulness of automatic system application criteria. *BMC Neurol* **8**, 3 (2008).
155. N. De Stefano *et al.*, Diffuse axonal and tissue injury in patients with multiple sclerosis with low cerebral lesion load and no disability. *Archives of Neurology* **59**, 1565 (Oct, 2002).
156. H. K. Mathiesen *et al.*, Correlation of global N-acetyl aspartate with cognitive impairment in multiple sclerosis. *Archives of Neurology* **63**, 533 (2006).
157. Y. Ge *et al.*, Neuronal cell injury precedes brain atrophy in multiple sclerosis. *Neurology* **62**, 624 (Feb 24, 2004).
158. L. Fu *et al.*, Imaging axonal damage of normal-appearing white matter in multiple sclerosis. *Brain* **121**, 103 (Jan, 1998).
159. M. Tintore, J. Sastre-Garriga, New treatment measurements for treatment effects on relapses and progression. *J Neurol Sci* **274**, 80 (Nov 15, 2008).
160. L. Vanhamme, T. Sundin, P. V. Hecke, S. V. Huffel, MR spectroscopy quantitation: a review of time-domain methods. *NMR Biomed* **14**, 233 (Jun, 2001).
161. S. Mierisova, M. Ala-Korpela, MR spectroscopy quantitation: a review of frequency domain methods. *NMR Biomed* **14**, 247 (Jun, 2001).
162. K. Schmierer *et al.*, Quantitative magnetic resonance of postmortem multiple sclerosis brain before and after fixation. *Magnetic Resonance in Medicine* **59**, 268 (2008).
163. K. Schmierer, F. Scaravilli, D. R. Altmann, G. J. Barker, D. H. Miller, Magnetization transfer ratio and myelin in postmortem multiple sclerosis brain. *Annals of Neurology* **56**, 407 (2004).
164. Z. Khaleeli, J. Sastre-Garriga, O. Ciccarelli, D. H. Miller, A. J. Thompson, Magnetisation transfer ratio in the normal appearing white matter predicts progression of disability over 1 year in early primary progressive multiple sclerosis. *J Neurol Neurosurg Psychiatry* **78**, 1076 (Oct, 2007).
165. G. R. Davies *et al.*, Emergence of thalamic magnetization transfer ratio abnormality in early relapsing-remitting multiple sclerosis. *Mult Scler* **11**, 276 (Jun, 2005).
166. M. A. van Buchem *et al.*, Correlation of volumetric magnetization transfer imaging with clinical data in MS. *Neurology* **50**, 1609 (Jun, 1998).

167. M. Filippi *et al.*, Magnetization transfer imaging to monitor the evolution of MS - A 1-year follow-up study. *Neurology* **55**, 940 (Oct 10, 2000).
168. B. Audoin *et al.*, Functional MRI study of PASAT in normal subjects. *MAGMA* **18**, 96 (May, 2005).
169. H. Vrenken *et al.*, Magnetization transfer ratio measurement in multiple sclerosis normal-appearing brain tissue: limited differences with controls but relationships with clinical and MR measures of disease. *Mult Scler* **13**, 708 (Jul, 2007).
170. M. V. Au Duong *et al.*, Altered functional connectivity related to white matter changes inside the working memory network at the very early stage of MS. *Journal of cerebral blood flow and metabolism : official journal of the International Society of Cerebral Blood Flow and Metabolism* **25**, 1245 (Oct, 2005).
171. N. Chiaravalloti *et al.*, Cerebral activation patterns during working memory performance in multiple sclerosis using FMRI. *J Clin Exp Neuropsychol* **27**, 33 (Jan, 2005).
172. M. Krause *et al.*, Prefrontal function associated with impaired emotion recognition in patients with multiple sclerosis. *Behav. Brain Res.* **205**, 280 (Dec, 2009).
173. B. Audoin *et al.*, Compensatory cortical activation observed by fMRI during a cognitive task at the earliest stage of MS. *Hum Brain Mapp* **20**, 51 (Oct, 2003).
174. C. Mainero *et al.*, fMRI evidence of brain reorganization during attention and memory tasks in multiple sclerosis. *Neuroimage* **21**, 858 (2004).
175. A. Cerasa *et al.*, Adaptive cortical changes and the functional correlates of visuo-motor integration in relapsing-remitting multiple sclerosis. *Brain Res Bull* **69**, 597 (May 31, 2006).
176. C. Mainero, P. Pantano, F. Caramia, C. Pozzilli, Brain reorganization during attention and memory tasks in multiple sclerosis: insights from functional MRI studies. *J Neurol Sci* **245**, 93 (Jun 15, 2006).
177. D. M. Mezzapesa, M. A. Rocca, M. Rodegher, G. Comi, M. Filippi, Functional cortical changes of the sensorimotor network are associated with clinical recovery in multiple sclerosis. *Hum Brain Mapp* **29**, 562 (May, 2008).
178. S. A. Helekar *et al.*, Functional brain network changes associated with maintenance of cognitive function in multiple sclerosis. *Front Hum Neurosci* **4**, 219 (2010).
179. S. M. Rao, C. F. S. G. o. t. N. M. S. Society. (Section of Neuropsychology, Medical College of Wisconsin, 1000 N. 92 St., Milwaukee, WI 53226, 1990).
180. A. Smith, *The Symbol Digit Modalities Test*. (Western Psychological Services, Los Angeles, 1973).
181. E. Strauss, E. M. S. Sherman, O. Spreen, *A compendium of neuropsychological tests: Administration, norms, and commentary*. (Oxford University Press, New York, ed. 3rd, 2006).
182. D. M. Gronwall, Paced auditory serial-addition task: a measure of recovery from concussion. *Percept Mot Skills* **44**, 367 (Apr, 1977).
183. W. F. Scherl *et al.*, Normative data for the selective reminding test: a random digit dialing sample. *Psychol Rep* **95**, 593 (Oct, 2004).
184. H. Buschke, P. A. Fuld, Evaluating storage, retention, and retrieval in disordered memory and learning. *Neurology* **24**, 1019 (Nov, 1974).
185. L. B. Krupp *et al.*, Multicenter randomized clinical trial of donepezil for memory impairment in multiple sclerosis. *Neurology* **76**, 1500 (Apr 26, 2011).

186. B. Fischl, A. M. Dale, Measuring the thickness of the human cerebral cortex from magnetic resonance images. *Proc. Natl. Acad. Sci. U. S. A.* **97**, 11050 (Sep 26, 2000).
187. B. Fischl *et al.*, Whole brain segmentation: automated labeling of neuroanatomical structures in the human brain. *Neuron* **33**, 341 (Jan 31, 2002).
188. J. Ashburner, K. J. Friston, Unified segmentation. *Neuroimage* **26**, 839 (Jul, 2005).
189. P. M. Thompson *et al.*, Cortical change in Alzheimer's disease detected with a disease-specific population-based brain atlas. *Cereb Cortex* **11**, 1 (Jan, 2001).
190. M. Sala *et al.*, Stress and hippocampal abnormalities in psychiatric disorders. *Eur. Neuropsychopharmacol.* **14**, 393 (Oct, 2004).
191. T. Zetzsche *et al.*, Hippocampal volume reduction and history of aggressive behaviour in patients with borderline personality disorder. *Psychiat Res-Neuroim* **154**, 157 (Feb, 2007).
192. C. Babiloni *et al.*, Hippocampal volume and cortical sources of EEG alpha rhythms in mild cognitive impairment and Alzheimer disease. *Neuroimage* **44**, 123 (Jan, 2009).
193. S. D. Roosendaal *et al.*, Structural and functional hippocampal changes in multiple sclerosis patients with intact memory function. *Radiology* **255**, 595 (May, 2010).
194. C. R. Jack, Jr., MRI-based hippocampal volume measurements in epilepsy. *Epilepsia* **35 Suppl 6**, S21 (1994).
195. G. Tao *et al.*, Deep gray matter atrophy in multiple sclerosis: A tensor based morphometry. *J Neurol Sci*, (Jan 23, 2009).
196. D. Horakova *et al.*, Gray matter atrophy and disability progression in patients with early relapsing-remitting multiple sclerosis A 5-year longitudinal study. *Journal of the Neurological Sciences* **282**, 112 (Jul, 2009).
197. A. Minagar, E. G. Toledo, J. S. Alexander, R. E. Kelley, Pathogenesis of brain and spinal cord atrophy in multiple sclerosis. *Journal of neuroimaging : official journal of the American Society of Neuroimaging* **14**, 5S (Jul, 2004).
198. W. Bruck, Inflammatory demyelination is not central to the pathogenesis of multiple sclerosis. *J Neurol* **252 Suppl 5**, v10 (Nov, 2005).
199. M. Calabrese *et al.*, Cortical lesions and atrophy associated with cognitive impairment in relapsing-remitting multiple sclerosis. *Arch Neurol* **66**, 1144 (Sep, 2009).
200. M. Calabrese *et al.*, Magnetic resonance evidence of cerebellar cortical pathology in multiple sclerosis. *J Neurol Neurosurg Psychiatry* **81**, 401 (Apr, 2010).
201. D. T. Chard *et al.*, Brain atrophy in clinically early relapsing-remitting multiple sclerosis. *Brain* **125**, 327 (Feb, 2002).
202. R. Antulov *et al.*, Regionally Distinct White Matter Lesions Do Not Contribute to Regional Gray Matter Atrophy in Patients with Multiple Sclerosis. *J Neuroimaging*, (Apr 13, 2010).
203. J. J. G. Geurts *et al.*, Intracortical lesions in multiple sclerosis: Improved detection with 3D double inversion-recovery MR imaging. *Radiology* **236**, 254 (Jul, 2005).
204. F. Nelson, A. Poonawalla, P. Hou, J. S. Wolinsky, P. A. Narayana, 3D MPRAGE improves classification of cortical lesions in multiple sclerosis. *Mult Scler* **14**, 1214 (Nov, 2008).
205. A. Akhondi-Asl, K. Jafari-Khouzani, K. Elisevich, H. Soltanian-Zadeh, Hippocampal volumetry for lateralization of temporal lobe epilepsy: automated versus manual methods. *Neuroimage* **54 Suppl 1**, S218 (Jan, 2011).

206. W. S. Tae, S. S. Kim, K. U. Lee, E. C. Nam, K. W. Kim, Validation of hippocampal volumes measured using a manual method and two automated methods (FreeSurfer and IBASPM) in chronic major depressive disorder. *Neuroradiology* **50**, 569 (Jul, 2008).
207. A. R. Khan, L. Wang, M. F. Beg, FreeSurfer-initiated fully-automated subcortical brain segmentation in MRI using large deformation diffeomorphic metric mapping. *Neuroimage* **41**, 735 (Jul, 2008).
208. R. M. Camicioli *et al.*, Posterior cingulate metabolic changes occur in Parkinson's disease patients without dementia. *Neurosci. Lett.* **354**, 177 (Jan 16, 2004).
209. J. H. Morra *et al.*, Automated 3D Mapping of Hippocampal Atrophy and Its Clinical Correlates in 400 Subjects with Alzheimer's Disease, Mild Cognitive Impairment, and Elderly Controls. *Hum Brain Mapp* **30**, 2766 (Sep, 2009).
210. J. J. Geurts *et al.*, Extensive hippocampal demyelination in multiple sclerosis. *J Neuropathol Exp Neurol* **66**, 819 (Sep, 2007).
211. V. Anderson *et al.*, Hippocampal atrophy in relapsing-remitting and primary progressive MS: a comparative study. *Mult Scler*, (Jul 14, 2010).
212. S. M. Gold *et al.*, Smaller Cornu Ammonis 2-3/Dentate Gyrus Volumes and Elevated Cortisol in Multiple Sclerosis Patients with Depressive Symptoms. *Biol Psychiatry*, (Jun 18, 2010).
213. D. P. Ramasamy *et al.*, Extent of cerebellum, subcortical and cortical atrophy in patients with MS: a case-control study. *J Neurol Sci* **282**, 47 (Jul 15, 2009).
214. M. Vercellino *et al.*, Demyelination, inflammation, and neurodegeneration in multiple sclerosis deep gray matter. *J Neuropathol Exp Neurol* **68**, 489 (May, 2009).
215. A. Prinster *et al.*, Grey matter loss in relapsing-remitting multiple sclerosis: A voxel-based morphometry study. *Neuroimage* **29**, 859 (Feb 1, 2006).
216. D. L. Masterman, J. L. Cummings, Frontal-subcortical circuits: the anatomic basis of executive, social and motivated behaviors. *J. Psychopharmacol.* **11**, 107 (1997).
217. U. Walter, S. Horowski, R. Benecke, U. K. Zettl, Transcranial brain sonography findings related to neuropsychological impairment in multiple sclerosis. *J Neurol* **254 Suppl 2**, II49 (May, 2007).
218. M. Calabrese *et al.*, Basal ganglia and frontal/parietal cortical atrophy is associated with fatigue in relapsing-remitting multiple sclerosis. *Mult Scler* **16**, 1220 (Oct, 2010).
219. M. Inglese *et al.*, Three-dimensional proton spectroscopy of deep gray matter nuclei in relapsing-remitting MS. *Neurology* **63**, 170 (Jul 13, 2004).
220. K. Morgen *et al.*, Distinct mechanisms of altered brain activation in patients with multiple sclerosis. *Neuroimage* **37**, 937 (Sep 1, 2007).
221. M. Calabrese *et al.*, Widespread cortical thinning characterizes patients with MS with mild cognitive impairment. *Neurology* **74**, 321 (Jan 26, 2010).
222. C. Smestad, L. Sandvik, N. I. Landro, E. G. Celius, Cognitive impairment after three decades of multiple sclerosis. *Eur J Neurol* **17**, 499 (Mar, 2010).
223. B. Grassiot, B. Desgranges, F. Eustache, G. Defer, Quantification and clinical relevance of brain atrophy in multiple sclerosis: a review. *J Neurol*, (Apr 8, 2009).
224. N. R. Temkin, R. K. Heaton, I. Grant, S. S. Dikmen, Detecting significant change in neuropsychological test performance: a comparison of four models. *Journal of the International Neuropsychological Society : JINS* **5**, 357 (May, 1999).

225. A. S. Drake *et al.*, Psychometrics and normative data for the Multiple Sclerosis Functional Composite: replacing the PASAT with the Symbol Digit Modalities Test. *Mult Scler* **16**, 228 (Feb, 2010).
226. X. Lin, C. R. Tench, P. S. Morgan, C. S. Constantinescu, Use of combined conventional and quantitative MRI to quantify pathology related to cognitive impairment in multiple sclerosis. *J Neurol Neurosurg Psychiatry* **79**, 437 (Apr, 2008).
227. K. J. Smith, W. I. McDonald, The pathophysiology of multiple sclerosis: the mechanisms underlying the production of symptoms and the natural history of the disease. *Philos. Trans. R. Soc. Lond. Ser. B-Biol. Sci.* **354**, 1649 (Oct, 1999).
228. R. H. Benedict, R. Zivadinov, Predicting neuropsychological abnormalities in multiple sclerosis. *J Neurol Sci* **245**, 67 (Jun 15, 2006).
229. K. C. Kern, J. Sarcona, M. Montag, B. S. Giesser, N. L. Sicotte, Corpus callosal diffusivity predicts motor impairment in relapsing-remitting multiple sclerosis: A TBSS and tractography study. *Neuroimage*, (Nov 4, 2010).
230. A. Ceccarelli *et al.*, Structural and functional magnetic resonance imaging correlates of motor network dysfunction in primary progressive multiple sclerosis. *Eur J Neurosci* **31**, 1273 (Apr, 2010).
231. A. C. Guo, J. R. MacFall, J. M. Provenzale, Multiple sclerosis: Diffusion tensor MR Imaging for evaluation of normal appearing white matter. *Radiology* **222**, 729 (Mar, 2002).
232. M. Filippi *et al.*, Changes in the normal appearing brain tissue and cognitive impairment in multiple sclerosis. *Journal of Neurology Neurosurgery and Psychiatry* **68**, 157 (Feb, 2000).
233. S. M. Smith *et al.*, Tract-based spatial statistics: voxelwise analysis of multi-subject diffusion data. *Neuroimage* **31**, 1487 (Jul 15, 2006).
234. S. D. Roosendaal *et al.*, Regional DTI differences in multiple sclerosis patients. *Neuroimage* **44**, 1397 (2009).
235. R. P. Woods, S. T. Grafton, C. J. Holmes, S. R. Cherry, J. C. Mazziotta, Automated image registration: I. General methods and intrasubject, intramodality validation. *J Comput Assist Tomogr* **22**, 139 (Jan-Feb, 1998).
236. H. Jiang, P. C. van Zijl, J. Kim, G. D. Pearlson, S. Mori, DtiStudio: resource program for diffusion tensor computation and fiber bundle tracking. *Comput Methods Programs Biomed* **81**, 106 (Feb, 2006).
237. S. Mori, P. C. van Zijl, Fiber tracking: principles and strategies - a technical review. *NMR Biomed* **15**, 468 (Nov-Dec, 2002).
238. M. F. Abdul-Rahman, A. Qiu, K. Sim, Regionally specific white matter disruptions of fornix and cingulum in schizophrenia. *PLoS One* **6**, e18652 (2011).
239. A. C. Bozoki, I. O. Korolev, N. C. Davis, L. A. Hoisington, K. L. Berger, Disruption of limbic white matter pathways in mild cognitive impairment and Alzheimer's disease: A DTI/FDG-PET Study. *Hum Brain Mapp*, (Jun 14, 2011).
240. J. Mazziotta *et al.*, A probabilistic atlas and reference system for the human brain: International Consortium for Brain Mapping (ICBM). *Philos Trans R Soc Lond B Biol Sci* **356**, 1293 (Aug 29, 2001).
241. T. E. Nichols, A. P. Holmes, Nonparametric permutation tests for functional neuroimaging: a primer with examples. *Hum Brain Mapp* **15**, 1 (Jan, 2002).

242. S. M. Smith, T. E. Nichols, Threshold-free cluster enhancement: addressing problems of smoothing, threshold dependence and localisation in cluster inference. *Neuroimage* **44**, 83 (Jan 1, 2009).
243. S. Mori *et al.*, Stereotaxic white matter atlas based on diffusion tensor imaging in an ICBM template. *Neuroimage* **40**, 570 (Apr 1, 2008).
244. R. Bakshi *et al.*, MRI in multiple sclerosis: current status and future prospects. *Lancet Neurology* **7**, 615 (Jul, 2008).
245. B. Bodini *et al.*, T2 lesion location really matters: a 10 year follow-up study in primary progressive multiple sclerosis. *J Neurol Neurosurg Psychiatry*, (Jul 13, 2010).
246. M. P. Amato *et al.*, Cognitive assessment and quantitative magnetic resonance metrics can help to identify benign multiple sclerosis. *Neurology* **71**, 632 (Aug 26, 2008).
247. J. C. Fulton *et al.*, MR lesion load and cognitive function in patients with relapsing-remitting multiple sclerosis. *AJNR Am J Neuroradiol* **20**, 1951 (Nov-Dec, 1999).
248. R. H. Lazeron *et al.*, Brain atrophy and lesion load as explaining parameters for cognitive impairment in multiple sclerosis. *Mult Scler* **11**, 524 (Oct, 2005).
249. W. Bruck *et al.*, Inflammatory central nervous system demyelination: correlation of magnetic resonance imaging findings with lesion pathology. *Annals of Neurology* **42**, 783 (Nov, 1997).
250. D. Cox *et al.*, The unique impact of changes in normal appearing brain tissue on cognitive dysfunction in secondary progressive multiple sclerosis patients. *Mult Scler* **10**, 626 (Dec, 2004).
251. W. Staffen *et al.*, Magnetic resonance spectroscopy of memory and frontal brain region in early multiple sclerosis. *J Neuropsychiatry Clin Neurosci* **17**, 357 (Summer, 2005).
252. H. Vrenken *et al.*, Diffusely abnormal white matter in progressive multiple sclerosis: in vivo quantitative MR imaging characterization and comparison between disease types. *AJNR Am J Neuroradiol* **31**, 541 (Mar, 2010).
253. F. Tovar-Moll *et al.*, Thalamic Involvement and Its Impact on Clinical Disability in Patients with Multiple Sclerosis: A Diffusion Tensor Imaging Study at 3T. *AJNR Am J Neuroradiol*, (Apr 15, 2009).
254. P. Mukherjee, S. W. Chung, J. I. Berman, C. P. Hess, R. G. Henry, Diffusion tensor MR imaging and fiber tractography: technical considerations. *AJNR Am J Neuroradiol* **29**, 843 (May, 2008).
255. W. Van Hecke *et al.*, On the construction of a ground truth framework for evaluating voxel-based diffusion tensor MRI analysis methods. *Neuroimage* **46**, 692 (Jul 1, 2009).
256. B. Bodini *et al.*, Exploring the Relationship Between White Matter and Gray Matter Damage in Early Primary Progressive Multiple Sclerosis: An In Vivo Study With TBSS and VBM. *Hum Brain Mapp* **30**, 2852 (Sep, 2009).
257. E. Raz *et al.*, Clinically Isolated Syndrome Suggestive of Multiple Sclerosis: Voxelwise Regional Investigation of White and Gray Matter. *Radiology* **254**, 227 (Jan, 2010).
258. E. Raz *et al.*, Gray- and white-matter changes 1 year after first clinical episode of multiple sclerosis: MR imaging. *Radiology* **257**, 448 (Nov, 2010).
259. M. Filippi, M. A. Rocca, MRI evidence for multiple sclerosis as a diffuse disease of the central nervous system. *J Neurol* **252 Suppl 5**, v16 (Nov, 2005).
260. S. K. Song *et al.*, Dysmyelination revealed through MRI as increased radial (but unchanged axial) diffusion of water. *Neuroimage* **17**, 1429 (Nov, 2002).

261. E. C. Klawiter *et al.*, Radial diffusivity predicts demyelination in ex vivo multiple sclerosis spinal cords. *Neuroimage*, (Jan 13, 2011).
262. S. K. Song *et al.*, Demyelination increases radial diffusivity in corpus callosum of mouse brain. *Neuroimage* **26**, 132 (May 15, 2005).
263. A. Giorgio *et al.*, Relationships of brain white matter microstructure with clinical and MR measures in relapsing-remitting multiple sclerosis. *J Magn Reson Imaging* **31**, 309 (Feb, 2010).
264. A. Ozturk *et al.*, MRI of the corpus callosum in multiple sclerosis: association with disability. *Mult Scler* **16**, 166 (Feb, 2010).
265. N. P. Warlop, E. Achten, E. Fieremans, J. Debruyne, G. Vingerhoets, Transverse diffusivity of cerebral parenchyma predicts visual tracking performance in relapsing-remitting multiple sclerosis. *Brain Cogn*, (Jul 1, 2009).
266. N. Evangelou *et al.*, Regional axonal loss in the corpus callosum correlates with cerebral white matter lesion volume and distribution in multiple sclerosis. *Brain* **123**, 1845 (Sep, 2000).
267. D. Lenzi *et al.*, Effect of corpus callosum damage on ipsilateral motor activation in patients with multiple sclerosis: a functional and anatomical study. *Hum Brain Mapp* **28**, 636 (Jul, 2007).
268. S. Mesaros *et al.*, Corpus Callosum Damage and Cognitive Dysfunction in Benign MS. *Hum Brain Mapp* **30**, 2656 (Aug, 2009).
269. T. Sigal, M. Shmuel, D. Mark, H. Gil, A. Anat, Diffusion Tensor Imaging of Corpus Callosum Integrity in Multiple Sclerosis: Correlation with Disease Variables. *J Neuroimaging*, (Dec 1, 2010).
270. R. H. Benedict, D. Ramasamy, F. Munschauer, B. Weinstock-Guttman, R. Zivadinov, Memory impairment in multiple sclerosis: correlation with deep grey matter and mesial temporal atrophy. *J Neurol Neurosurg Psychiatry* **80**, 201 (Feb, 2009).
271. M. S. Deloire *et al.*, How to detect cognitive dysfunction at early stages of multiple sclerosis? *Mult Scler* **12**, 445 (Aug, 2006).
272. R. A. Rudick, G. Cutter, S. Reingold, The multiple sclerosis functional composite: a new clinical outcome measure for multiple sderosis trials. *Multiple Sclerosis* **8**, 359 (Oct, 2002).
273. R. H. Benedict *et al.*, Diffusion-weighted imaging predicts cognitive impairment in multiple sclerosis. *Mult Scler* **13**, 722 (Jul, 2007).
274. M. Rovaris *et al.*, Cognitive dysfunction in patients with mildly disabling relapsing-remitting multiple sclerosis: an exploratory study with diffusion tensor MR imaging. *J Neurol Sci* **195**, 103 (Mar 30, 2002).
275. F. Fink *et al.*, The association between California Verbal Learning Test performance and fibre impairment in multiple sclerosis: evidence from diffusion tensor imaging. *Multiple Sclerosis* **16**, 332 (Mar, 2010).
276. B. Diehl *et al.*, Abnormalities in diffusion tensor imaging of the uncinate fasciculus relate to reduced memory in temporal lobe epilepsy. *Epilepsia* **49**, 1409 (Aug, 2008).
277. P. G. Nestor *et al.*, Neuropsychological correlates of diffusion tensor imaging in schizophrenia. *Neuropsychology* **18**, 629 (Oct, 2004).
278. I. V. Allen, S. McQuaid, M. Mirakhur, G. Nevin, Pathological abnormalities in the normal-appearing white matter in multiple sclerosis. *Neurological sciences : official*

journal of the Italian Neurological Society and of the Italian Society of Clinical Neurophysiology **22**, 141 (Apr, 2001).
279. S. Barbosa, L. D. Blumhardt, N. Roberts, T. Lock, R. H. Edwards, Magnetic resonance relaxation time mapping in multiple sclerosis: normal appearing white matter and the "invisible" lesion load. *Magnetic Resonance Imaging* **12**, 33 (1994).
280. D. T. Chard *et al.*, Brain metabolite changes in cortical grey and normal-appearing white matter in clinically early relapsing-remitting multiple sclerosis. *Brain* **125**, 2342 (Oct, 2002).
281. M. Filippi *et al.*, A magnetization transfer imaging study of normal-appearing white matter in multiple sclerosis. *Neurology* **45**, 478 (Mar, 1995).
282. A. Kutzelnigg *et al.*, Cortical demyelination and diffuse white matter injury in multiple sclerosis. *Brain* **128**, 2705 (Nov, 2005).
283. N. Malykhin, L. Concha, P. Seres, C. Beaulieu, N. J. Coupland, Diffusion tensor imaging tractography and reliability analysis for limbic and paralimbic white matter tracts. *Psychiatry Res.* **164**, 132 (Nov 30, 2008).
284. J. J. Geurts, P. K. Stys, A. Minagar, S. Amor, R. Zivadinov, Gray matter pathology in (chronic) MS: modern views on an early observation. *J Neurol Sci* **282**, 12 (Jul 15, 2009).
285. R. Zivadinov, A. Minagar, Evidence for gray matter pathology in multiple sclerosis: a neuroimaging approach. *J Neurol Sci* **282**, 1 (Jul 15, 2009).
286. S. W. Provencher, Estimation of metabolite concentrations from localized in vivo proton NMR spectra. *Magnetic resonance in medicine : official journal of the Society of Magnetic Resonance in Medicine / Society of Magnetic Resonance in Medicine* **30**, 672 (Dec, 1993).
287. S. W. Provencher, Automatic quantitation of localized in vivo 1H spectra with LCModel. *NMR Biomed* **14**, 260 (Jun, 2001).
288. J. Urenjak, S. R. Williams, D. G. Gadian, M. Noble, Specific expression of N-acetylaspartate in neurons, oligodendrocyte-type-2 astrocyte progenitors, and immature oligodendrocytes in vitro. *J. Neurochem.* **59**, 55 (Jul, 1992).
289. T. Michaelis, K. D. Merboldt, H. Bruhn, W. Hanicke, J. Frahm, Absolute concentrations of metabolites in the adult human brain in vivo: quantification of localized proton MR spectra. *Radiology* **187**, 219 (Apr, 1993).
290. I. Mader *et al.*, Proton MR spectroscopy with metabolite-nulling reveals elevated macromolecules in acute multiple sclerosis. *Brain : a journal of neurology* **124**, 953 (May, 2001).
291. U. Seeger, U. Klose, I. Mader, W. Grodd, T. Nagele, Parameterized evaluation of macromolecules and lipids in proton MR spectroscopy of brain diseases. *Magnetic resonance in medicine : official journal of the Society of Magnetic Resonance in Medicine / Society of Magnetic Resonance in Medicine* **49**, 19 (Jan, 2003).
292. A. Bitsch *et al.*, Inflammatory CNS demyelination: Histopathologic correlation with in vivo quantitative proton MR spectroscopy. *AJNR Am J Neuroradiol* **20**, 1619 (Oct, 1999).
293. M. P. Wattjes *et al.*, Axonal damage but no increased glial cell activity in the normal-appearing white matter of patients with clinically isolated syndromes suggestive of multiple sclerosis using high-field magnetic resonance spectroscopy. *AJNR. American journal of neuroradiology* **28**, 1517 (Sep, 2007).

294. P. Sarchielli *et al.*, Absolute quantification of brain metabolites by proton magnetic resonance spectroscopy in normal-appearing white matter of multiple sclerosis patients. *Brain* **122**, 513 (Mar, 1999).
295. M. P. Wattjes *et al.*, High field MR imaging and 1H-MR spectroscopy in clinically isolated syndromes suggestive of multiple sclerosis: correlation between metabolic alterations and diagnostic MR imaging criteria. *Journal of Neurology* **255**, 56 (Jan, 2008).
296. E. J. Vereyken, D. M. Fluitsma, M. J. Bolijn, C. D. Dijkstra, C. E. Teunissen, An in vitro model for de- and remyelination using lysophosphatidyl choline in rodent whole brain spheroid cultures. *Glia* **57**, 1326 (Sep, 2009).
297. D. Pitt, I. E. Nagelmeier, H. C. Wilson, C. S. Raine, Glutamate uptake by oligodendrocytes: Implications for excitotoxicity in multiple sclerosis. *Neurology* **61**, 1113 (Oct 28, 2003).
298. S. Penny, Z. Khaleeli, L. Cipolotti, A. Thompson, M. Ron, Early imaging predicts later cognitive impairment in primary progressive multiple sclerosis. *Neurology* **74**, 545 (Feb 16, 2010).
299. M. Summers *et al.*, Cognitive impairment in relapsing-remitting multiple sclerosis can be predicted by imaging performed several years earlier. *Mult Scler* **14**, 197 (Mar, 2008).
300. L. K. Vingara *et al.*, paper presented at the New York Academy of Sciences: Biomarkers of Brain Disease, Oxford, UK, 1/26/2009 2009.
301. C. R. Jack, Jr. *et al.*, Steps to standardization and validation of hippocampal volumetry as a biomarker in clinical trials and diagnostic criterion for Alzheimer's disease. *Alzheimers Dement* **7**, 474 (Jul, 2011).